Declassified and Approved For Release 2013/02/15 : CIA-RDP10-02196R000800020001-4 1X

*Russian Original Vol. 47, No. 1, July, 1979*

January, 1980

SATEAZ 47(1) 501-590 (1979)

LS, FILE

# SOVIET ATOMIC ENERGY

**АТОМНАЯ ЭНЕРГИЯ**
**(ATOMNAYA ÉNERGIYA)**

**TRANSLATED FROM RUSSIAN**

**CONSULTANTS BUREAU, NEW YORK**

Declassified and Approved For Release 2013/02/15 : CIA-RDP10-02196R000800020001-4

Declassified and Approved For Release 2013/02/15 : CIA-RDP10-02196R000800020001-4

# SOVIET ATOMIC ENERGY

*Soviet Atomic Energy* is a cover-to-cover translation of *Atomnaya Énergiya*, a publication of the Academy of Sciences of the USSR.

An agreement with the Copyright Agency of the USSR (VAAP) makes available both advance copies of the Russian journal and original glossy photographs and artwork. This serves to decrease the necessary time lag between publication of the original and publication of the translation and helps to improve the quality of the latter. The translation began with the first issue of the Russian journal.

**Editorial Board of** *Atomnaya Énergiya:*

**Editor:** O. D. Kazachkovskii

**Associate Editors:** N. A. Vlasov and N. N. Ponomarev-Stepnoi

**Secretary:** A. I. Artemov

I. N. Golovin
V. I. Il'ichev
V. E. Ivanov
V. F. Kalinin
P. L. Kirillov
Yu. I. Koryakin
A. K. Krasin
E. V. Kulov
B. N. Laskorin
V. V. Matveev
I. D. Morokhov
A. A. Naumov
A. S. Nikiforov
A. S. Shtan'
B. A. Sidorenko
M. F. Troyanov
E. I. Vorob'ev

Copyright © 1980, Plenum Publishing Corporation. *Soviet Atomic Energy* participates in the program of Copyright Clearance Center, Inc. The appearance of a code line at the bottom of the first page of an article in this journal indicates the copyright owner's consent that copies of the article may be made for personal or internal use. However, this consent is given on the condition that the copier pay the stated per-copy fee through the Copyright Clearance Center, Inc. for all copying not explicitly permitted by Sections 107 or 108 of the U.S. Copyright Law. It does not extend to other kinds of copying, such as copying for general distribution, for advertising or promotional purposes, for creating new collective works, or for resale; nor to the reprinting of figures, tables, and text excerpts.

Consultants Bureau journals appear about six months after the publication of the original Russian issue. For bibliographic accuracy, the English issue published by Consultants Bureau carries the same number and date as the original Russian from which it was translated. For example, a Russian issue published in December will appear in a Consultants Bureau English translation about the following June, but the translation issue will carry the December date. When ordering any volume or particular issue of a Consultants Bureau journal, please specify the date and, where applicable, the volume and issue numbers of the original Russian. The material you will receive will be a translation of that Russian volume or issue.

Subscription (2 volumes per year)

Vols. 46 & 47: $147.50 per volume (6 Issues)
Vols. 48 & 49: $167.50 per volume (6 Issues)

Single Issue: $50
Single Article: $7.50

Prices somewhat higher outside the United States.

*Soviet Atomic Energy* is abstracted or indexed in *Chemical Abstracts, Chemical Titles, Pollution Abstracts, Science Research Abstracts, Parts A and B, Safety Science Abstracts Journal, Current Contents, Energy Research Abstracts,* and *Engineering Index.*

**CONSULTANTS BUREAU, NEW YORK AND LONDON**

227 West 17th Street
New York, New York 10011

Published monthly. Second-class postage paid at Jamaica, New York 11431.

Declassified and Approved For Release 2013/02/15 : CIA-RDP10-02196R000800020001-4

Declassified and Approved For Release 2013/02/15 : CIA-RDP10-02196R000800020001-4

# SOVIET ATOMIC ENERGY

A translation of *Atomnaya Énergiya*

January, 1980

Volume 47, Number 1 July, 1979

## CONTENTS



Declassified and Approved For Release 2013/02/15 : CIA-RDP10-02196R000800020001-4

Declassified and Approved For Release 2013/02/15 : CIA-RDP10-02196R000800020001-4

# CONTENTS

(continued)



**The Russian press date (podpisano k pechati) of this issue was 6/27/1979. Publication therefore did not occur prior to this date, but must be assumed to have taken place reasonably soon thereafter.**

Declassified and Approved For Release 2013/02/15 : CIA-RDP10-02196R000800020001-4

Declassified and Approved For Release 2013/02/15 : CIA-RDP10-02196R000800020001-4

ARTICLES

# COMBINATION OF NUCLEAR-GEOPHYSICAL METHODS AND APPARATUS FOR INCREASING THE EFFICIENCY OF PROSPECTING, EXTRACTION, AND REPROCESSING OF NONRADIOACTIVE MINERAL RAW MATERIALS (BY THE EXAMPLE OF TIN ORES)

S. A. Baldin, S. N. Voloshchuk,
V. G. Egiazarov, L. V. Zernov,
I. A. Luchin, V. V. Matveev,
L. Ch. Pukhal'skii, and N. I. Chesnokov

UDC 550.835.08

A promising trend for the utilization of ionizing radiations in the national economy is the development of nuclear-physical methods and apparatus for solving the urgent problems of increasing the efficiency of prospecting, extraction, and reprocessing of mineral raw materials. The greatest successes in this field have been achieved with the high-speed analysis of uranium ores by a radiometric method, based on recording the natural $\gamma$ radiation with reference to a simple apparatus [1]. When solving similar problems for nonradioactive raw materials, use is made of the stimulated radiation induced in the substance by means of isotope sources, particle accelerators of various types, nuclear reactors, etc.

One of the most effective methods of analysis of a substance in applied problems is the roentgenoradiometric method (RRM), consisting in the excitation in the substance of x-ray characteristic emission with radioisotope sources and its subsequent recording by means of spectrometric equipment.

The energy spectrum of the induced radiation contains, together with the x-ray characteristic emission of the required element, the characteristic emission of other elements occurring in the composition of the ore, and also primary scattered radiation. Because of this, the necessary sensitivity and high measurement speed in the majority of cases can be attained only by using spectrometric instruments which are relatively complex in structure and composition, with devices for the automatic processing of the measurement results. This makes the use of nuclear-physics methods extremely difficult for the complex analysis of nonradioactive ores under production conditions, although several important problems at the present time have been successfully solved by these methods.

Nuclear-geophysical methods of logging, sampling uncrushed core samples and ores in the natural deposit, analysis of powdered samples, etc. have been developed and introduced, and in a number of cases methods for monitoring sorted ore, concentration products, pulps and solutions are being used. At the same time, automated methods and equipment for high-speed analysis and preliminary sorting in transportable tanks, separation into finely divided batches and lumps have almost been uninvestigated and unused, although on individual problems there are publications indicating the formulation of the problem, the results of laboratory investigations and certain positive experiments [2, 4].

In this present paper, the results of the development and introduction of a combination of nuclear-physical methods and equipment are recounted, which provide an effective solution for the production problems at all the principal stages of monitoring the mining-metallurgical production of tin. Taking into consideration the nuclear-physical characteristics of tin and the requirements for production, roentgenoradiometric [3] and $\gamma$-resonance methods of analysis [5] have been accepted mainly for the analytical monitoring of the complex. The latter is used in those cases when it is necessary to monitor the tin in the form of cassiterite or to carry out phase analysis on compounds of tin and iron.

Depending on the production problems to be solved, semiconductor detectors (SCD), scintillation and proportional counters are used, and also isotope sources of $^{241}Am$, $^{147}Pm$, and $^{119m}Sn$. The constitution of the equipment complex developed for monitoring in the different stages of the mining-metallurgical production process is shown in Fig. 1.

Translated from Atomnaya Énergiya, Vol. 47, No. 1, pp. 3-7, July, 1979. Original article submitted January 30, 1979.

0038-531X/79/4701-0501$07.50 © 1980 Plenum Publishing Corporation



Declassified and Approved For Release 2013/02/15 : CIA-RDP10-02196R000800020001-4

Declassified and Approved For Release 2013/02/15 : CIA-RDP10-02196R000800020001-4

TABLE 1. Averaged Indices of Lump Separation

| Technological sample | Total mass, tons | Coarseness grade, mm | Average yield of grade, % | Av. tin content (chem. anal.), % | Tailings | | | Concentrate | | | Conc. factor, rel. units |
|---|---|---|---|---|---|---|---|---|---|---|---|
| | | | | | yield from grade, % | yield from orig. ore, % | tin content, % | yield from grade, % | yield from orig. ore, % | tin content, % | |
| 1 | 69,6 | 63—100, | 13,6 | 0,138 | 51,0 | 6,8 | 0,071 | 50,0 | 6,8 | 0,185 | 1,45 |
| | | 100—200 | 17,4 | 0,176 | 44,0 | 7,7 | 0,060 | 56,0 | 9,7 | 0,267 | 1,52 |
| 2 | 48,0 | 63—100, | 14,4 | 0,096 | 85,0 | 12,2 | 0,055 | 15,0 | 2,2 | 0,328 | 3,4 |
| | | 100—200 | 18,0 | 0,130 | 79,0 | 14,2 | 0,072 | 21,0 | 3,8 | 0,348 | 2,7 |
| 3 | 7,74 | 20—32, | 8,5 | 0,174 | 63,0 | 5,4 | 0,100 | 37,0 | 3,1 | 0,310 | 1,72 |
| | | 32—63 | 15,6 | 0,220 | 81,0 | 12,6 | 0,070 | 19,0 | 3,0 | 0,860 | 3,9 |

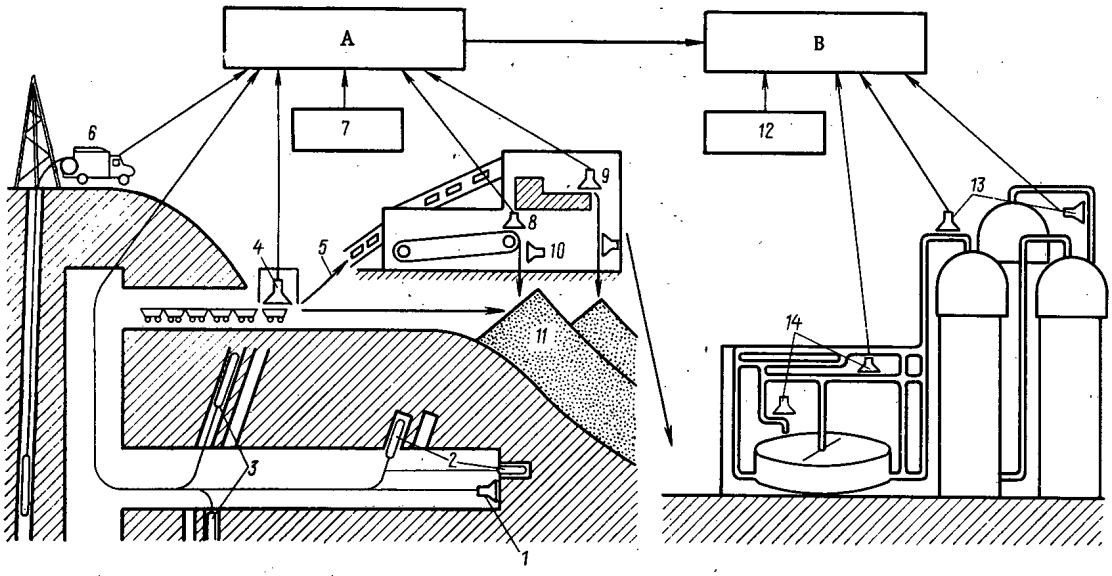


Fig. 1. Structure of the complex and monitoring functions: A) monitoring for prospecting, extraction, and sorting processes; B) control for treatment processes; 1) sampling; 2, 3) logging of shot holes and bores; 4) high-speed analysis at the ore-monitoring station; 5) sorting; 6) surface logging; 7) laboratory analysis of samples, core, and ores; 8, 9) batch and lump separation; 10) high-speed analysis of products; 11) tailings; 12) laboratory analysis of samples; 13, 14) continuous monitoring for metallurgy (solution monitoring) and concentration (pulp monitoring) processes, respectively.

In search and prospecting, the results of the roentgenoradiometric ore sampling at the site of the seam and of the uncrushed core sample, logging of the drillholes, roentgenoradiometric and $\gamma$-resonance analysis of the powdered samples (see Fig. 1: 1, 6, and 7) are used for the selection of promising sections and for obtaining the initial data for calculating the reserves.

At the stage of extraction and preliminary concentration of ores, by means of roentgenoradiometric ore sampling at the site of the seam and the uncrushed core sample, logging of shot holes and drillholes, high-speed analysis and sorting of the ores into transportable containers, preliminary concentration of the ores into finely divided batches and lumps, and analysis of the powdered samples by roentgenoradiometric and $\gamma$-resonance methods (see Fig. 1: 1-3, 6-9) are obtained starting data for calculating the reserves for detailed and operational prospecting, and optimization of the extraction process; prerequisites are established for the selective extraction and abandoning of substandard ores in the form of untouched blocks and rubbish, in order to reduce losses and depletion, and the extraction of the part of the shattered rock massif which is substandard in the content of tin.

In order to monitor and control the ore treatment process, the results of the roentgenoradiometric sampling of the ore on a conveyor belt are used, as are monitoring of the tin content in the solid phase of pulp and solutions in a continuous cycle, roentgenoradiometric and $\gamma$-resonance analysis of samples for tin and its accompanying components (see Fig. 1: 10, 12-14). The data obtained from the measurements allows the content of tin and accompanying elements to be determined in the ores and in the products of their treatment.



Declassified and Approved For Release 2013/02/15 : CIA-RDP10-02196R000800020001-4

Declassified and Approved For Release 2013/02/15 : CIA-RDP10-02196R000800020001-4

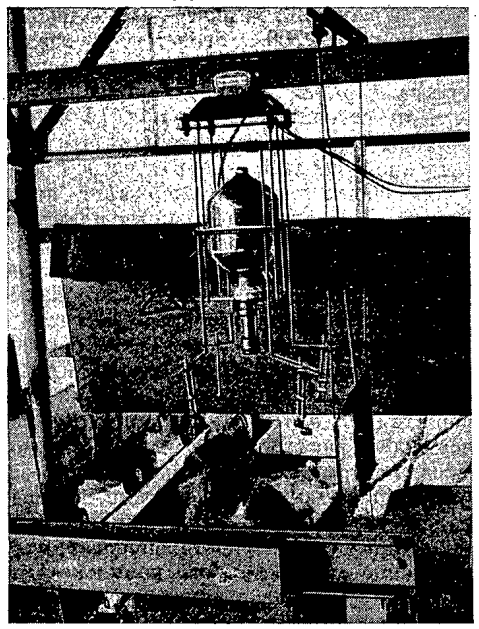

Fig. 2

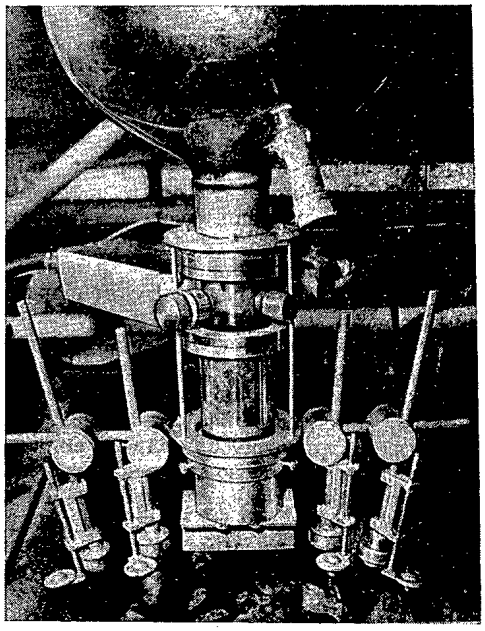

Fig. 3

Fig. 2. Irradiation and detection unit, with a semiconductor detector, at the ore-monitoring station.

Fig. 3. Irradiation and detection unit of a facility for the separation of ores with a semiconductor detector.

In the mining instruments for logging, sampling of the uncrushed core sample and ore at the site of the seam, scintillation detection units are used, with a thin sodium iodide crystal. The sensitivity threshold in the case of roentgenoradiometric sampling amounted to 0.05%, and in the case of logging – 0.07%. By comparing the results of the roentgenoradiometric sampling with the conventional furrow sampling, the mean-square error in determining the content of tin amounted to from ±32 (for a grade containing less than 0.1%) to ±13% (for a grade containing more than 0.5%). The relative mean-square error in the data from a comparison of logging with laboratory analyses of core samples is equal to ±30% for a grade containing less than 0.1%. It should be noted that the error of conventional geological sampling is ±40-60%. The sampling output amounts to not less than 20 m per shift, and the logging output is not less than 100 m per shift on the instrument. At the present time, using RRM, more than 30 km of the walls of mine workings can be sampled, and more than 10 km of drillholes bored from underground mine workings is logged.

In the facilities for high-speed analysis, sorting and separation of ores into transportable containers, finely divided batches and lumps, detection units are used with silicon semiconductor detectors (area of sensitive surface ~250 $mm^2$). The time for the roentgenoradiometric analysis of a single truck is 15-20 sec, and the output is more than 300 trucks per shift. More than 300,000 trucks have been analyzed in a production cycle on this facility. The cost of the high-speed analysis of the ore mass in the truck by the roentgenoradiometric method is ≈3 times less than the cost of handful sampling with a sharp increase of the measurement output, providing automation of sorting.

An irradiation unit and a detection facility with a cooled semiconductor detector and 4 isotope sources of $^{241}Am$ in shielded equipments with collimators is shown in Fig. 2.

Investigations conducted on the facility for separation into finely divided batches and lumps under production conditions have shown the feasibility in principle and technically of roentgenoradiometric concentration. It has been established that the content of tin in the lumps or batches is determined with an error of 30-40%, which is sufficient for the efficient separation of ores according to content, and the analytical sensitivity allows sorting to be carried out under batch and lump conditions with an output of 5-15 ton/h or more, depending on the coarseness of sorting of the material (Table 1).

The measurement section of the facility for ore separation is shown in Fig. 3, in which can be seen the lower part of the detection unit with the semiconductor detector and 4 isotope sources, positioned in pairs on



Declassified and Approved For Release 2013/02/15 : CIA-RDP10-02196R000800020001-4

Declassified and Approved For Release 2013/02/15 : CIA-RDP10-02196R000800020001-4

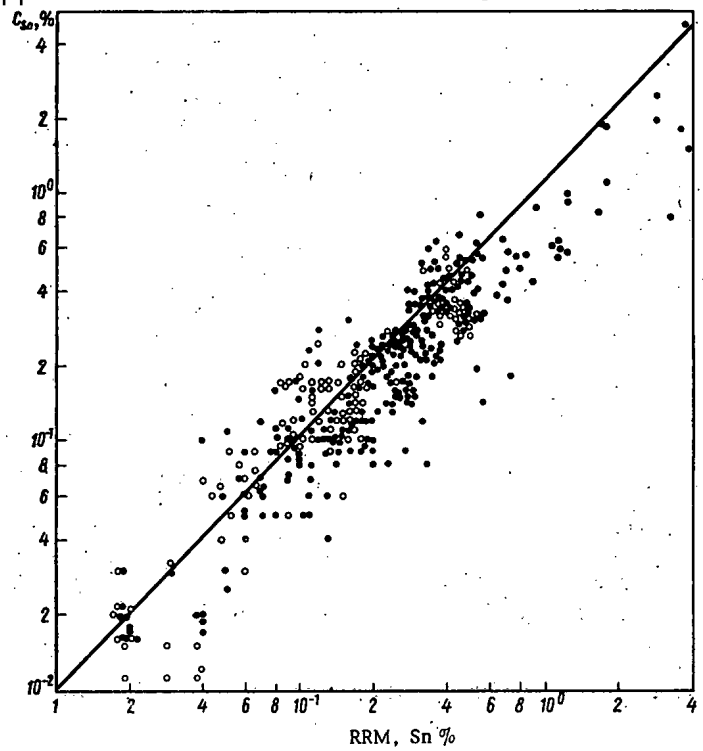


Fig. 4. Comparison of results of high-speed analysis of tin ores in trucks (roentgenoradiometric method) and bulk sampling ($C_{Sn}$, chemical analysis); ●) skarn ores; ○) shales.

both sides of the detector. Both facilities for the preliminary roentgenoradiometric concentration operate in the automatic regime and are equipped with processor-analyzers for processing the data by a specified algorithm and also monitoring and control devices with external slave mechanisms. It should be noted that facilities for the contactless automatic sorting and separation of ores, based on RRM, have been constructed and tried out under industrial conditions for the first time.

Roentgenoradiometric and x-ray absorption instruments and facilities for the continuous monitoring of concentration products (pulps and solutions) are based on the application of scintillation and semiconductor detector units. The sensitivity threshold for the analysis of pulps and solutions with a semiconductor detector is 0.001-0.003 wt.% and 5-10 mg/liter, respectively, and for solutions with scintillation detectors it is 70 mg/liter. The instruments and facilities provide data extraction into external equipments (digital printout, pen recorder) and to the production process monitoring and control system.

The laboratory instruments developed for the analysis of powdered ore samples and their treated products include instruments for determining the content of the total tin and tin oxide (in the form of cassiterite) by roentgenoradiometric and $\gamma$-resonance methods, instruments based on semiconductor spectrometers for determining the content of tin and accompanying elements by the roentgenoradiometric method, and instruments for the phase analysis of tin and iron in ores and processed products by the $\gamma$-resonance method. The accuracy of the analyses of powdered samples is not inferior to, and in some cases even exceeds, the accuracy of chemical analysis. The sensitivity threshold is 0.005-0.02% of the total tin and tin in the form of cassiterite.

The mean-square relative deviations of the results of analysis by the $\gamma$-resonance method of the tin content in the form of cassiterite from the results of chemical analysis are given below:

| Grade of tin content, % | No. of determinations | Deviation, % |
|---|---|---|
| 0.05 | 454 | ± 58.4 |
| 0.05-0.1 | 405 | ± 27.3 |
| 0.1-0.25 | 447 | ± 16.2 |
| 0.25-1 | 229 | ± 11.2 |
| 1 | 88 | ± 5.2 |



Declassified and Approved For Release 2013/02/15 : CIA-RDP10-02196R000800020001-4

Declassified and Approved For Release 2013/02/15 : CIA-RDP10-02196R000800020001-4

TABLE 2. Distribution of a Mined-Ore Mass According to Range of Content of Tin, Based on High-Speed Analysis of Ores in Trucks by the Roentgenoradiometric Method, %

| Range of tin content | Average content | Yield of ore | Yield of tin | Range of tin content | Average content | Yield of ore | Yield of tin |
|---|---|---|---|---|---|---|---|
| 0—0,10 | 0,04 | 33,5 | 7,6 | 0,30—0,40 | 0,34 | 8,8 | 17,0 |
| 0,10—0,15 | 0,12 | 18,3 | 12,9 | 0,40—0,60 | 0,51 | 6,8 | 19,7 |
| 0,15—0,30 | 0,21 | 37,4 | 39,3 | 0,60 | 0,89 | 0,9 | 4,5 |

The results of comparisons for other types of analyses of powdered samples on tin and incidental components also have shown the high accuracy and sensitivity of roentgenoradiometric analyses. In all, ≈ 300,000 samples have been analyzed. The output of the analyses is 100-120 analyses per instrument per shift.

It is well known that the roentgenoradiometric method has a low penetration depth, not exceeding a few millimeters, because of which the most important problem of the investigations was to estimate the representability and accuracy of the results of the analyses in the case of logging, sampling at the site of the deposit, and especially in the high-speed analyses in the transportable containers. Comparison of the results of the determination of the tin in a surface seam of ore loaded into a truck by the roentgenoradiometric method and by total sampling with chemical analysis of selected samples (> 500 trucks with different tin contents) showed that there is a direct correlation dependence between them. For a tin content of < 0.1 and > 0.1%, the correlation coefficient amounted to 0.71 and 0.82 with a relative mean-square error for both content grades of ≈ ±30% (Fig. 4). Similar data were obtained when comparing the results on representative bulk investigations of roentgenoradiometric sampling at the site of the deposit and logging with furrow sampling and sampling of drillhole core samples by conventional methods. Thus, according to the content of tin determined by the roentgenoradiometric method in a surface seam, the tin content in the volume investigated can be judged quite accurately, which confirms the calculations by the Materon–de Wies formula, and which showed the feasibility of replacing bulk elements with linear or area equivalents of these samples with preservation of the statistical representation of sampling [6].

The application of the combination of nuclear-geophysical methods and equipment provides an important economic effect, due to the replacement of conventional methods of analysis and sampling by nuclear-geophysical methods and the change of technology of prospecting, extraction and processing of tin ores. Thus, the cost of the nuclear-geophysical analysis of powdered samples is a factor of 6-8 less than that of chemical analysis, and the cost of nuclear-geophysical sampling at the site of the deposit is a factor of 5-6 less than furrow sampling, etc. Already at the present time the effect of using the instruments of the complex in production has amounted to about 1 million rubles.

The use of logging of drillholes and shot holes and sampling at the site of the deposit allows the greater part of drilling with sampling of the core to be replaced by more productive and cheaper coreless drilling, the volume of the shattered rock mass to be reduced because of the part of the substandard ores remaining in the depths in the form of untouched blocks, and prerequisites to be created for selective extraction and reduction of depletion and losses. The introduction into the technology of extraction, of high-speed analysis and sorting of ores in transport containers, preliminary concentration into finely divided batches and lumps will allow 20-40% of the waste tailings with a tin content of 0.06-0.08% to be separated, which will make it possible to reduce the volume and to increase the content of tin in the ore directed to further processing by a factor of 1.2-1.5. For example, during the development of one of the experimental units, using nuclear-geophysical methods, 5.6% of the ore with a tin content of ~0.08% remained in the depths in the form of untouched blocks; according to the data of high-speed analysis of the ores in trucks with a limiting content of 0.1%, 33% of the tailings was separated with a tin content of 0.04%; the concentration factor in this case amounted to 1.37 (Table 2); and with a limiting content of 0.15%, 51.8% of the tailings was separated with a tin content of 0.07% and a concentration factor of 1.61.

The preliminary concentration of ores into finely divided batches and lumps allows the tin content in ore directed to further processing to be increased additionally, and its volume to be reduced. As investigations have shown, in the case of lump sorting of ores with a size of 32-200 mm by the roentgenoradiometric method,



Declassified and Approved For Release 2013/02/15 : CIA-RDP10-02196R000800020001-4

Declassified and Approved For Release 2013/02/15 : CIA-RDP10-02196R000800020001-4

15-25% of the tailings (from the original ore sent for concentration) is separated with a tin content of 0.05-0.08%. Technicoeconomic calculations and the results of industrial operation of a complex show that the total effect of its introduction amounts to 2-3 rubles per ton of ore.

Conclusions. A combination of nuclear-geophysical methods and equipment has been developed, tested, and introduced into commercial operation, for searching, prospecting, extracting, and processing lean tin ores, encompassing the whole production cycle. The introduction of the complex significantly increases the technicoeconomical production indices as a whole, allows the use of a more productive extraction technology, ore processing, and the creation of automated production control systems. The use, in the complex, of equipment with semiconductor detectors in conjunction with analyzer-processors has allowed for the first time in the practice of the mining and concentration industry the creation of automatic roentgenoradiometric facilities for contactless high-speed analysis, sorting and preliminary concentration of lean tin ores into transport containers, finely divided batches and lumps. The design of the complex, the flow-sheet–technological principles of equipment construction and the methods of measurement provide the capability for using it to solve similar problems for other types of nonradioactive raw materials, such as molybdenum, tungsten, zinc, copper, and other ores, including complex ores.

## LITERATURE CITED

1. L. Ch. Pukhal'skii and M. V. Shumilin, Prospecting and Sampling of Uranium Deposits [in Russian], Nedra, Moscow (1977).
2. A. P. Ochkur et al., Gamma Methods in Ore Geology [in Russian], Nedra, Leningrad (1976).
3. E. P. Leman et al., Nuclear Geophysics in Ore Geology [in Russian], NPO Geofizika, Leningrad (1977).
4. A. P. Tatarnikov, Nuclear-Physics Methods of Concentration of Minerals [in Russian], Atomizdat, Moscow (1974).
5. V. I. Gol'danskii et al., Gamma-Resonance Methods and Instruments for Phase Analysis of Mineral Raw Materials [in Russian], Atomizdat, Moscow (1974).
6. É. Karl'e, Procedure for the Quantitative Assessment of Uranium Deposits [in Russian], Atomizdat, Moscow (1961).

# ALGORITHM FOR THE EXTREMAL CONTROL OF THE ENERGY DISTRIBUTION IN A POWER REACTOR

I. Ya. Emel'yanov, V. V. Postnikov, and G. V. Yurkin

UDC 621.039.562

It is necessary in the development and operation of large-capacity power reactors to equip them with automatic systems for the control of the energy distribution (ED) in the active zone which are based on digital computers.

For the extremal control of the ED, i.e., for the control of the ED with a search for the optimal values of a goal function, programs were used which are based on implementation of different "classical" optimization schemes [1-3]: Wiener's theory, dynamic programming, the maximum principle of Pontryagin, and others. However, these methods are complicated with respect to instrumentation (they require a large memory and a lot of computer time), they are calculated for a single extremum determination, and in addition they can lead to errors due to inadequacy of the process in the reactor and the model of it used in the control algorithms [1].

Thus, e.g., in order to calculate a single control cycle in experiments on an HBWR, 5 min of computer time, 7K of operator memory, and 240K of disk memory (K represents 1024 machine words) are necessary. The difference between the actual process and a linear model of it was eliminated by the introduction of a large number of artificial variables [2].

Translated from Atomnaya Énergiya, Vol. 47, No. 1, pp. 8-12, July, 1979. Original article submitted February 2, 1978.

 0038-531X/79/4701-0506$07.50 © 1980 Plenum Publishing Corporation

Declassified and Approved For Release 2013/02/15 : CIA-RDP10-02196R000800020001-4

Declassified and Approved For Release 2013/02/15 : CIA-RDP10-02196R000800020001-4

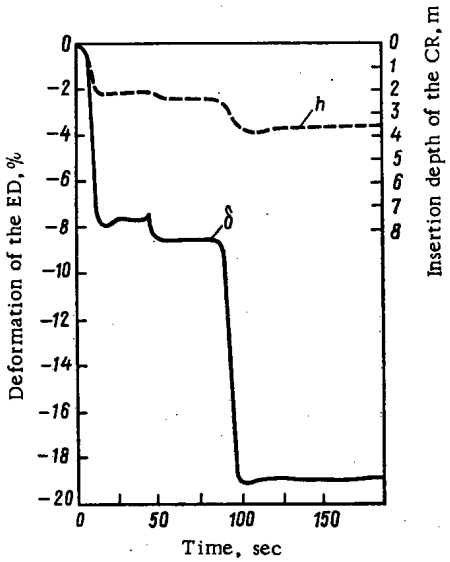


Fig. 1

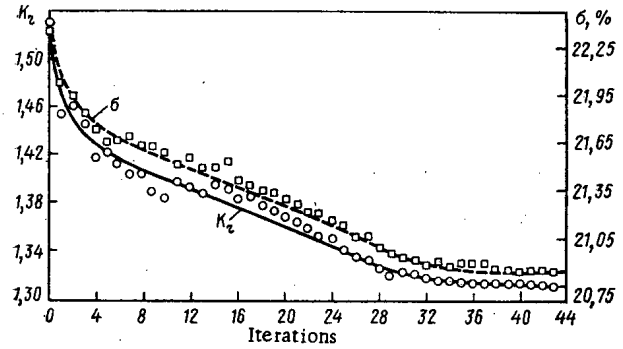


Fig. 2

Fig. 1. Deformation of the ED in the 30-56 cell (–) at constant average power of the RBMK-1000 reactor of the LAÉS, and the position of the CR in the 24-57 cell (---).

Fig. 2. Dependence of $K_r$ (○) and $\sigma$ (□) on the number of iterations of CR control ($\beta(k) = 4$).

The solution of the problem with the application of a reactor model improved by the method of dynamic programming [3] required an operator memory of ~40,000 words, 130,000 words on a magnetic drum, and ~500 sec of computer time (on a computer of the HITAC 5020E type); in the opinion of the authors, $10^4$ times more machine time would be required for the usual method of dynamic programming [3]. Therefore, the question of choosing the most acceptable method of controlling the ED has not been conclusively resolved. On the one hand practical testing and a sufficient number of experiments are necessary to accomplish this, and on the other hand a comparison of the different methods in a specific class of problems is necessary.

The most important characteristics of the algorithms are their complexity, the convergence rate, stability to noise, computation time, and so on. The difficulties of implementing general optimization schemes associated with the processing of information of large volume and dimensionality have led to the appearance of a different kind of iterative heuristic procedures based on a step-by-step (pulse) search for the optimum and capable of finding the extremum of a goal function with simultaneous refinement of the algorithm parameters [4]. The heuristic side of step-by-step search methods has been investigated in [5]; however, it has seldom been discussed with application to the problems of the optimal control of the ED.

It is advisable in this connection to discuss the extremal control of the ED with the help of a step-by-step search of the extremum with a combination of test and working steps and in combination with a number of heuristic methods of self-adjustment of the parameters. Heuristic and logical methods of self-adjustment, which recall the procedure implementable by an operator behind a control panel, minimize the machine time costs for solution of the problem.

## STATEMENT OF THE PROBLEM AND A DESCRIPTION OF AN ALGORITHM FOR ITS SOLUTION

The problem of extremal control as a method of automatic optimization [6] consists of the minimization or maximization of some goal function whose value depends on controllable and uncontrollable parameters of an object.

One can select as the goal function the nonuniformity coefficient of the ED with respect to the reactor radius:

$$K_r = \max [W(\mathbf{r}, \rho)/SW_0(\mathbf{r})]; \quad (1)$$

$$S = \frac{\int_v W(\mathbf{r}, \rho)\, dv}{\int W(\mathbf{r})\, dv}$$



Declassified and Approved For Release 2013/02/15 : CIA-RDP10-02196R000800020001-4

Declassified and Approved For Release 2013/02/15 : CIA-RDP10-02196R000800020001-4

where $W(\mathbf{r}, \rho)$ is the actual ED, which depends on the position of the control rods (CR), and $W_0(\mathbf{r})$ is the specified ED.

Each component of the vector $\rho$ is of the form

$$\rho_j = \gamma_j \rho_{1j}, \tag{2}$$

and

$$0 \leqslant \rho_j \leqslant 1, \tag{3}$$

where $\rho_{1j}$ is the unit vector of the insertion of the j-th CR with an amplitude equal to unit (the minimum technically attainable) displacement of the CR, which comprises the fraction C of the total effectiveness of the rod, and $\gamma_j$ is the number of unit displacements of the CR corresponding to a given position.

We will assume that a step-by-step search for the extremum can be accomplished with a reactor control system under the conditions

$$n = \text{const}, \quad \alpha_j = \text{const}; \tag{4}$$

$$n = \text{var}, \quad \alpha_j = \text{const}; \tag{5}$$

$$n = \text{const}, \quad \alpha_j = \text{var}; \tag{6}$$

$$n = \text{var}, \quad \alpha_j = \text{var}, \tag{7}$$

where n is the number of movable CR and $\alpha_j$ is the number of unit displacements of the j-th CR accomplished in a control step.

Let us also introduce a restriction on the deviation of the reactivity $\delta\rho$ at each step associated with the movement of a CR:

$$\delta\rho = \left| \sum_{j=1}^{n} \Delta\rho_j \right| \leqslant \varepsilon, \tag{8}$$

where $\Delta\rho_j = \alpha_j C$.

Finally, we will point out that the control problem is the attainment of

$$\min \{\max [W(\mathbf{r}, \rho)/SW_0(\mathbf{r})]\}. \tag{9}$$

We will discuss simultaneously with the goal function (1) in the process of a step-by-step extremum search the parameter $\sigma$, which reflects the quality of the equalizing of $K_r(\mathbf{r})$:

$$\sigma^2(\rho) = \frac{1}{V} \int_v \left[ \frac{W(\mathbf{r}, \rho)}{SW_0(\mathbf{r})} - 1 \right]^2 dV. \tag{10}$$

Let us consider one of the possible methods of solving the problem for the control system conditions (5), using the methodology of a step-by-step extremum search [4]. In this case the problem reduces to a search for the direction of movement of the rods $\rho_{1j}$ and the intensity of ED control, ensuring a decrease of the goal function (1) at each step.

We will introduce the parameter $\beta$, which characterizes the strength of ED control, i.e., reflects n and $\Delta\rho_j$:

$$\beta = \sum_{j=1}^{n} \alpha_j \tag{11}$$

We will divide the active zone into I arbitrary regions, at the center of each of which the j-th CR is located.

The iterative procedure of solution reduces to the following.

1. In the k-th state of the reactor preceding the (k + 1)-th movement of the CR, there is in each j-th zone a reactor cell with a maximum ratio of the actual and specified ED:

$$K_j^{(k)\max} = \frac{W_j^{(k)}}{SW_{cj}}. \tag{12}$$



Declassified and Approved For Release 2013/02/15 : CIA-RDP10-02196R000800020001-4

Declassified and Approved For Release 2013/02/15 : CIA-RDP10-02196R000800020001-4

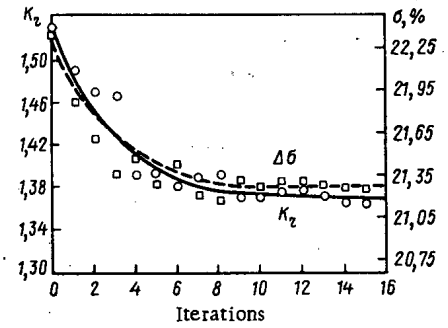


Fig. 3

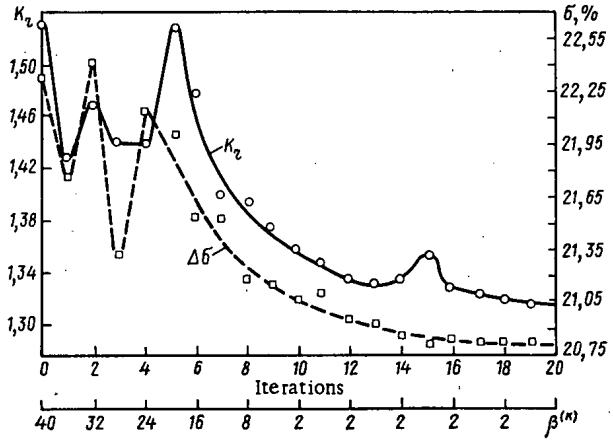


Fig. 4

Fig. 3. Variation of $K_r$ (○) and σ (□) in connection with CR control ($\beta^{(k)} = 10$).

Fig. 4. Variations of $K_r$ (○) and σ (□) in the case of ED control with a variable number of CR at each step specified according to a heuristic law.

2. The instantaneous unbalance of reactivity $\Delta\rho^{(k)}$ measured from the deviation of the position of the rods of the automatic controller and caused both by $\delta\rho$ and by other processes, e.g., depletion, poisoning, etc., is determined in the k-th state.

3. The insertion and extraction of each CR by the identical number of unit steps ($\alpha$) is accomplished in $n^{(k)}_{max}$ zones with maximum values $K_j^{(k)\,max}$ and $\rho_j < 1 - \alpha C$ and also in $n^{(k)}_{min}$ zones with minimum $K_j^{(k)max}$ and $\rho_j > \alpha C$. At the same time $n^{(k)}_{min}$ and $n^{(k)}_{max}$ satisfy the relationships

$$n^{(k)}_{max} - n^{(k)}_{min} = \text{int}\left(\frac{\Delta\rho^{(k)}}{\alpha C}\right); \tag{13}$$

$$n^{(k)}_{max} + n^{(k)}_{min} = n^{(k)} = \frac{\beta^{(k)}}{\alpha}; \tag{14}$$

$$1 < \beta^{(k)} < \beta^{(k)}_{ss}. \tag{15}$$

where $\beta^{(k)}_{ss}$ is the maximum value of $\beta^{(k)}$ for which convergence of the process based on (8) and (9) is ensured, and $\alpha$ is selected from the condition $\varepsilon < \alpha C$.

In the case in which both the ED and the reactor power $N_p$ are controlled according to the algorithm in question, one should use $(\Delta N_p / N)\beta_{eff}$ as $\Delta p^{(k)}$ in (13), where $\beta_{eff}$ is the effective fraction of delayed neutrons and $\Delta N_p$ is the unbalance of the actual and specified powers.

It is natural that the values $n^{(k)}_{max}$ and $n^{(k)}_{min}$ should depend on $\beta^{(k)}$, which are selected in the range (15) on the basis of safety conditions and the necessary convergence rate of the control process, and which are subject to attrition of the maximum values of $\Delta\rho^{(k)}$, and so on.

4. The iterations are continued until Eq. (9) attains a value which is a minimum for a given reactor state.

## NUMERICAL IMPLEMENTATION ON A COMPUTER

On the basis of the method expounded a program applicable to a type BÉSM-6 computer has been developed according to which investigations have been conducted in the conditions of controlling the ED for different actual states of the RBMK-1000 reactor of the LAÉS [7].

The results of a two-dimensional physical calculation of the static states of the reactor were used as the operator for the identification of the ED in the active zone [8]. One should note that experiments on the investigation of the spatial-temporal characteristics of the RBMK-1000 reactor of the first unit of the LAÉS during the power start-up period have permitted investigating the reaction of the ED to the introduction of local perturbations.



Declassified and Approved For Release 2013/02/15 : CIA-RDP10-02196R000800020001-4

Declassified and Approved For Release 2013/02/15 : CIA-RDP10-02196R000800020001-4

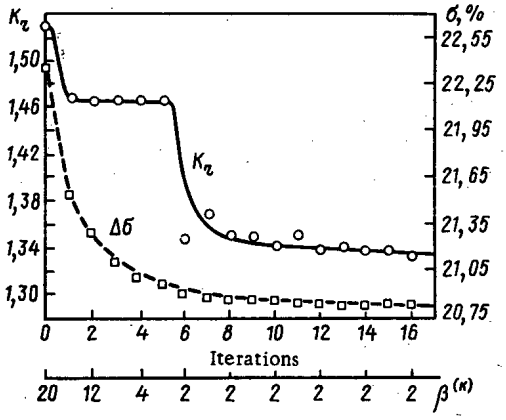


Fig. 5. Variation of $K_r$ (○) and σ (□) as a function of the number of iterations of ED control with self-adjustment of the number of CR.

The nature of the transitional processes at an individual point of the active zone is illustrated by the data of Fig. 1, in which the variation of the ED in a test on the movement of an individual CR is presented.

An analysis of the experimental investigations of the spatial-temporal characteristics of the ED of the RBMK-1000 reactor shows that a static ED is established practically immediately after each movement (see Fig. 1). The ED varies by no more than 3-5% in time intervals no shorter than a minute, which we will call "adiabatic intervals" in the following.

Conditions (4) and (5) are used in the program upon a single-step movement of the CR ($\alpha = 1$) with a variation of the number n of simultaneously moved CR from 2 to 40, and $C = 1/12$ was adopted in all cases. We note that in practice the minimum movements of the CR are several times less, which permits improving the equalization of the ED by the method under discussion.

The reactivity is corrected upon the oscillation of the reactivity of the reactor associated with movement of the CR; however, it was not necessary to do this in the calculations, since the equality $n_{max}^{(k)} = n_{min}^{(k)}$ was satisfied in all iterations.

Since the quality of ED control was evaluated from the nonuniformity coefficient (1), $W_0(r)$ was taken to be constant over the entire reactor.

The iterative process (setting the CR into motion) was concluded if

$$|\sigma^{(k-5)} + \sigma^{(k-4)} + \sigma^{(k-3)} - \sigma^{(k-2)} - \sigma^{(k-1)} - \sigma^{(k)}| \leqslant \delta, \tag{16}$$

where δ was adopted in the range 0.0010-0.0015.

Under actual conditions in a reactor the control process should resume at the $l$-th cycle after cessation according to the condition (16) if

$$\sigma \geqslant \frac{1}{3}(\sigma^{(k-2)} + \sigma^{(k-1)} + \sigma^{(k)}) + \Delta, \tag{17}$$

where Δ is specified on the basis of the assumed size of the oscillations of $\min(K_r)$.

In the case of control of the reactor power according to the algorithm in question the process should resume also with the yield $\Delta N_p^{k+l}$ from the limits specified.

The following positions were investigated in this method.

1. An evaluation of the nature of the convergence of the iterative process for different parameters $\beta^{(k)}$.

2. The determination of the effectiveness of the controller in the region of the extremum for a step-by-step variation of the parameter $\beta^{(k)}$.

3. A search for the self-adjustment law of $\beta^{(k)}$ which minimizes the time costs for a search in connection with movement of the system to an optimal state.

To estimate the time costs for the search, control was initially conducted under the conditions nearest to the procedure carried out by an operator ($3 \geq \beta^{(k)} \geq 1$).

The data of one of these calculations for the actual state of the RBMK-1000 of the second unit of the LAÉS, which are presented in Fig. 2, show that the search process for a constant and small $\beta_k$ which for a



Declassified and Approved For Release 2013/02/15 : CIA-RDP10-02196R000800020001-4

Declassified and Approved For Release 2013/02/15 : CIA-RDP10-02196R000800020001-4

selected $\alpha = 1$ is equal to the number of CR simultaneously moving in each (k + 1)-th activation reduces for $\sigma$ and $K_r$ approximately to a linear law with respect to k. However, the convergence rate is small, which indicated the necessity of increasing the controlling action $\beta^{(k)}$.

The control calculations, one of which is illustrated by the data of Fig. 3, have shown that an increase in the number of simultaneously moved CR leads to an acceleration of the search. The amplitude of the oscillations near the extremum increases somewhat, but the asymptotic values of $K_r$ and $\sigma^{(k)}$ exceed the analogous values for Fig. 2.

A reduction in the time costs for the search upon an increase in the number of CR simultaneously moving in each iteration indicated the necessity of investigating the nature of the control over a wide range of variations of $\beta^{(k)}$. To this end, a series of calculations was conducted with variable values of $\beta^{(k)}$ specified according to different heuristic laws.

Data from one of these calculations in which the number of simultaneously moved CR in each activation was specified according to the heuristic law indicated in Fig. 4 are presented in Fig. 4. It is noted that for $\beta^k > 20$ significant oscillations of $K_r$ and $\sigma^k$ are observed whose amplitudes in some cases exceeded the initial values, which indicated unstable convergence or even divergence of the process. Control of the ED for $\beta^k \geq 20$ with a gradual decrease of the number of simultaneously moved CR to two resulted in a smooth and rapid convergence of the process to minimum values of the goal function.

Analysis of the calculations with respect to extremal control of the ED upon a variation of $\beta^k$ over a wide range of values has shown that for the adopted two-dimensional reactor model control of the ED in connection with simultaneous movement of $> 20$ CR in each activation ($\beta^k > 20$, $\alpha_j = 1$, $C = 1/12$) does not result in convergence of the process, but the process diverges in a number of cases; stable convergence is observed for $\beta^{(k)} \leq 20$, which delimits the maximum strength of the control action upon a search for the self-adjustment law $\beta^{(k)}$ as a function of the quality index ($\sigma^{(k)}$).

It is found that in the model used for the RBMK-1000 reactor the greatest rate of searching for the goal is achieved if the self-adjustment law (with $\alpha_j = 1$) is represented in the form

$$\beta^{(k)} = \begin{cases} 20 & \text{for } \sigma^{(k)} \geqslant \sigma_{max} \quad (18) \\ 18\dfrac{\sigma^{(k)} - \sigma_{min}}{\sigma_{max}\sigma_{min}} + 2 & \text{for } \sigma_{min} < \sigma^{(k)} < \sigma_{max} \quad (19) \\ 2 & \text{for } \sigma^{(k)} \leqslant \sigma_{min} \quad (20) \end{cases}$$

At the same time $\sigma_{min}$ for the reactor state considered was 0.2075, and $\sigma_{max}$ was 0.2225.

It is evidently advisable in real algorithms on a reactor to use the value $\sigma_{min}$ obtained upon a previous cessation of the control process according to the condition (16).

The results of one of these calculations with the use of conditions (18)-(20) are given in Fig. 5 in the form of the dependence of $K_r$ and $\sigma^{(k)}$ on the number of activations of the rods, analysis of which shows that the CR which have not changed their initial position amount to 75% of the total number, and those which have changed by 0.5, 1, and 1.5 amount to 12, 7, and 6%, respectively. The operator reserve of reactivity remained unchanged.

The computational-time costs to carry out a single iteration were determined practically completely by the reactor model, i.e., by the time of the physical calculation (3 min on a BÉSM-6), which exceeds by $\approx 1000$ times the computational time according to the extremal control program.

The investigations conducted have shown that:

1) the extremal control algorithm presented provides for convergence of the process in the reactor model used for the simultaneous movement of no more than 20 CR with an identical step C equal to 1/12;

2) self-adjustment of the controlling action by means of the variation of the simultaneously moved CR permits obtaining optimal ED with minimal time costs;

3) a reactor model is not obligatory in practice in connection with the implementation of the proposed method of ED control, since in this case a reactor equipped with an ED control system in the active zone based on inertialess detectors can be used directly.

If at each iteration the interrogation, recall, and solution adoption times on the computer are less than 1 sec (which is completely realistic for computers used in atomic electric-power stations), the control process



Declassified and Approved For Release 2013/02/15 : CIA-RDP10-02196R000800020001-4

Declassified and Approved For Release 2013/02/15 : CIA-RDP10-02196R000800020001-4

is concluded within the limits of the adiabatic range. It is evident that self-adjustment of the control action by means of a variation of the number of steps with a constant number of movable CR $n \geq 2$ (6) would result in worse results with respect to $\sigma_{min}$ than would (5) in view of the finiteness of C.

One can expect that the greatest effectiveness of self-adjustment of the controller can be achieved with the simultaneous variation of the number and steps of the movable CR.

The extremal control algorithm can be applied when a model of the reactor is present in the control system, which evidently permits reducing the number of movements of the CR upon approaching the goal and ensuring prediction of the optimal ED.

The possibility of implementation of the algorithm described for the control of the ED with and without the use of a reactor model, simplicity, and rapid action under conditions of a deficit of operative memory permits recommending it for the development of operational programs for the digital-computer units.

In conclusion, the authors thank V. S. Lavrukhin for the experimental data which he made available on measurements of transition processes carried out on an RBMK-1000 reactor.

## LITERATURE CITED

1. W. Lipinski and A. Vacroux, IEEE Trans., NS-17, No. 1, 510 (1970).
2. R. Grumbach and B. Blomsnes, in: Proc. of a Symp. Prague 22-26, IAEA, Vienna, January 1973, p. 303.
3. K. Oguri and Y. Ebizuka, J. Nucl. Sci. Tech., 12, No. 7, 391 (1975).
4. J. Macdonald and B. Koen, Nucl. Sci. Eng., 56, 142 (1975).
5. N. Nielsen, Artificial Intellect [Russian translation], Mir, Moscow (1973).
6. V. V. Kazakevich and A. V. Rodov, Systems of Automatic Optimization [in Russian], Énergiya, Moscow (1977).
7. A. P. Aleksandrov et al., At. Energ., 37, No. 2, 99 (1974).
8. S. S. Gorodkov, Preprint IAÉ-2294, Moscow (1973).

# SOME PECULIARITIES OF THE STRUCTURE OF THE FLOW IN THE CASE OF CRITICAL DISCHARGE CONDITIONS OF BOILING WATER THROUGH CYLINDRICAL CHANNELS

V. S. Aleshin

UDC 621.1.013

A lot of attention has been devoted in recent years to the investigation of the discharge of saturated and underheated water prior to the saturation temperature. This is caused by the necessity of determining the flow rate in connection with the solution of a number of engineering problems, and in particular in connection with the discussion of emergency situations associated with flows in the coolant loop of atomic electric power plants.

The processes taking place in the discharge channel have not yet been studied sufficiently. The suggested flow models and the description of its structure are contradictory. This complicates the development of the methods of calculating the flow rate of a mixture, the discharge rates, and other characteristics of the flows under discussion. Obtaining new test data which reveal the physics of the processes in the discharge channel is extremely necessary.

Numerous curves of the static pressure and the flow temperature, which are measured by a special probe along the axis of a cylindrical channel with sharp entrance edges, have been obtained on an experimental setup whose description was given earlier*; the initial pressure $P_i$ at the channel entrance was varied from 2.45 to 9.6 MPa, underheating up to the saturation temperature $\Delta t_{uh}$ was varied from 0 to 60°C and $l/d$ was varied from 0.5 to 9.55. A number of these curves were considered in the paper cited. Here we will dwell on a more detailed analysis of them.

* V. S. Aleshin et al., At. Energ., 38, No. 6, 375 (1975).

Translated from Atomnaya Énergiya, Vol. 47, No. 1, pp. 12-15, July, 1979. Original article submitted July 4, 1978.



0038-531X/79/4701-0512$07.50 © 1980 Plenum Publishing Corporation

Declassified and Approved For Release 2013/02/15 : CIA-RDP10-02196R000800020001-4

Declassified and Approved For Release 2013/02/15 : CIA-RDP10-02196R000800020001-4

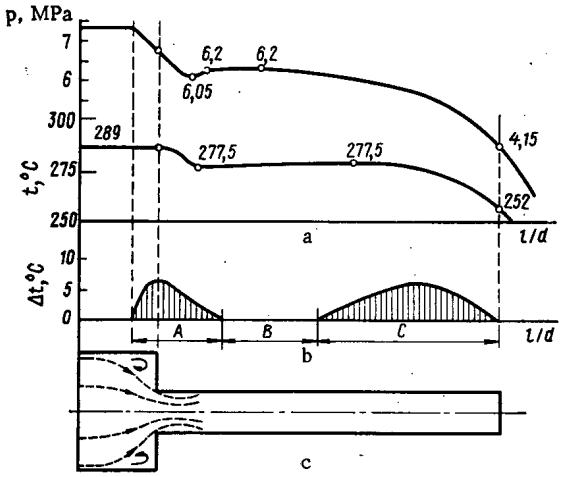


Fig. 1

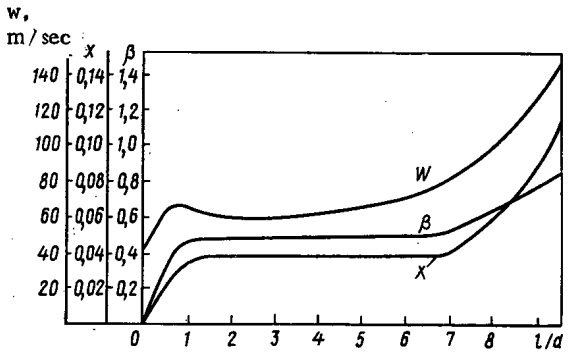


Fig. 2

Fig. 1. Variation of p, t, and $\Delta t_{sh}$ along the channel length: a) curves of the static pressure and temperature of the flow; b) variation of the amount of superheating of the fluid $\Delta t_{sh} = t - t_s$; and c) discharge channel.

Fig. 2. Variation along the channel length of the velocity w of the mixture and mass x and volume $\beta$ discharge vapor content for $P_1 = 7.35$ MPa, $\Delta t_{uh} = 0°C$; $l/d = 9.55$.

In Fig. 1a are given the curves of the static pressure and temperature upon the discharge of saturated water through a channel with diameter d = 9.53 mm, $l/d = 9.55$, and an initial pressure of 7.35 MPa. Superheating of water in the discharge channel $\Delta t_{sh} = t - t_s$ (where t is the flow temperature and $t_s$ is the saturation temperature at a given pressure) obtained from these curves is shown in Fig. 1b.

It follows from Fig. 1b that three characteristic sections occur along the channel length (Fig. 1c): the initial section A in the region of the entrance edge at which the fluid is in a superheated metastable state; a middle section B – one of stabilized parameters in which the liquid and the vapor are in a state close to thermodynamic equilibrium; and an end section C in the region of the exit edge, in which the flow is characterized by appreciable nonuniformity.

In the initial section the flow pressure begins to decrease right until the entrance to the discharge channel and reaches a minimum at some distance from the sharp entry edges, and then it increases somewhat. This "dip" in the pressure is caused by compression of the stream, as in the case of purely hydraulic discharge conditions from cylindrical channels with sharp entry edges.

A reduction in the flow temperature occurs with some delay, which causes superheating of the liquid to some maximum value. The greatest superheating and variation of the $\Delta t_{sh}$ curve along the channel length depend on the initial parameters of the liquid (pressure and underheating $\Delta t_{uh}$) and on the channel length ($l/d$). Superheating of the liquid decreases practically to zero towards the end of the section.

Thus complicated hydrodynamic and thermal processes accompanied by superheating of the liquid and its partial evaporation prior to attainment of thermodynamic equilibrium occur in section A in the flow of a boiling liquid. The appearance of incipient gas bubbles should evidently be expected first of all in the zone of local pressure decrease and formation of intense ring vortices between the compressed flow and the channel walls.

Vapor condensation is possible in the initial section in connection with a certain "dip" and a subsequent increase in the pressure together with vapor formation, which complicates yet more the mechanism of heat and mass exchange between phases.

The variation of the flow pressure in section B of stabilized parameters is determined by hydraulic drag, but the temperature practically corresponds to the saturation temperature. The length of this section depends on the total length of the channel and the degree of underheating of the liquid up to the saturation temperature, since the length of the initial section increases as $\Delta t_{uh}$ increases.

The division of the channel into three sections and the isolation of a section of stabilized parameters permits a sounder approach both to the calculation of pressure losses to drag and to the calculation of the pressure differential at the entry and exit edges caused by the acceleration of the flow in connection with a variation in its density.



Declassified and Approved For Release 2013/02/15 : CIA-RDP10-02196R000800020001-4

Declassified and Approved For Release 2013/02/15 : CIA-RDP10-02196R000800020001-4

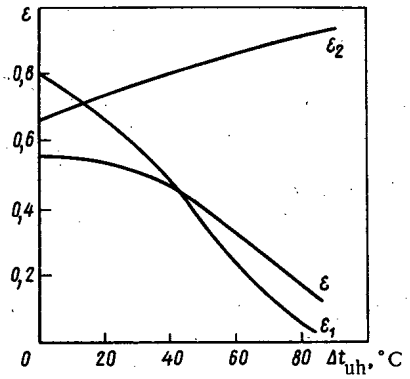


Fig. 3

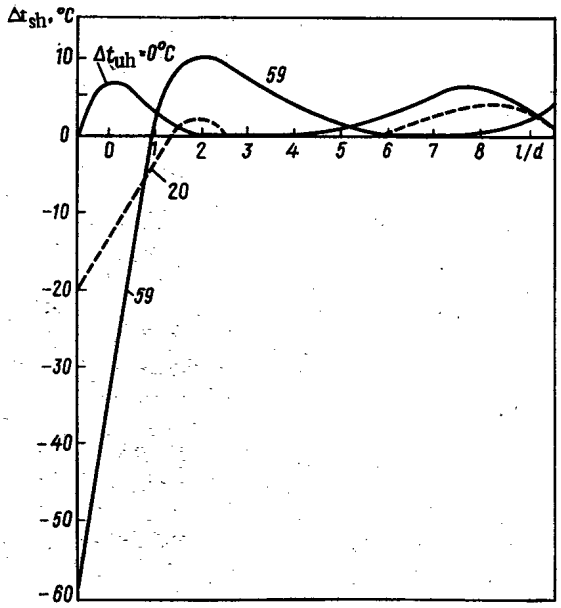


Fig. 4

Fig. 3. Dependence of the pressure differentials at the entry edge $\varepsilon_1 = P_i/P_1$ and the exit edge $\varepsilon_2 = P_2/P_i$ on the initial underheating $\Delta t_{uh}$ ($\varepsilon_1 \cdot \varepsilon_2 = \varepsilon = P_2/P_1$, and $P_i$ is the pressure in the section of stabilized parameters).

Fig. 4. Variation of $\Delta t_{sh} = t - t_s$ along the channel length for various initial $\Delta t_{uh}$ with $P_1 = 7.35$ MPa and $l/d = 9.55$.

The liquid is also in a metastable state at the exit edge (section C) in connection with the pressure drop, as is established by the analysis of numerous curves. Superheating of the liquid increases at first to a definite maximum, and then towards the exit edge it decreases practically to zero, and an equilibrium two-phase flow emerges from the channel.

The values of the flow velocity w, the mass x, and volume $\beta$ of the discharge vapor contents along the channel length obtained from the pressure and temperature curves are given in Fig. 2. The flow was considered as a quasiequilibrium one in connection with the determination of w, x, and $\beta$, and the channel was divided into 12 sections equal in length.

The temporal characteristics of the metastable state of the liquid at the entry and exit edges of the discharge channel were determined from the calculated values obtained for the variation of the specific volume of the mixture and the flow velocity along the channel length (averaged over the sections) and also from the measured mass discharge rate of the mixture.

The calculations show that the time $\tau_1$ during which superheating of the liquid at the entry edge increases to a maximum amounts to $\approx (3.5\text{-}4) \cdot 10^{-4}$ sec. The time $\tau_2$ of the decrease of $\Delta t_{sh}$ from the greatest value to zero is equal to $(2.5 \cdot 3) \cdot 10^{-4}$ sec. For other initial pressures and underheating to saturation, $\tau_1$ and $\tau_2$ differ somewhat from the values given, but evidently the mechanism of bubble boiling in the discharge channel is characterized by definite stability and a weak dependence on the initial parameters.

The increase of $\Delta t_{sh}$ in section C occurs during $\tau_3 = (3.0\text{-}3.5) \cdot 10^{-4}$ sec, and then the temperature of the liquid decreases to the saturation temperature at the critical pressure towards the exit edge in a time $\tau_4 = (1.5\text{-}2.8) \cdot 10^{-4}$ sec. According to the data obtained, $\tau_1 > \tau_3$ evidently for the time necessary for the passage of the first phase of bubble boiling – the formation of incipient bubbles (nuclei) of gas, and $\tau_4 < \tau_2$ due to intensification of heat and mass exchange between phases at the exit edge by virtue of large agitation of the flow.

It is known that critical discharge occurs in the case of large pressure gradients. The fraction of the pressure drop at the entry edge $\varepsilon_1 = P_i/P_1$ and at the exit edge $\varepsilon_2 = P_2/P_i$ depends appreciably on the initial underheating of water up to saturation temperature (Fig. 3). When $\Delta t_{uh} = 0°C$, a large fraction of the pressure differential occurs at the exit section, and a large fraction of the acting differential occurs at the entry section. If the liquid does not boil in the channel, the entire pressure differential acts at the entry edge.



Declassified and Approved For Release 2013/02/15 : CIA-RDP10-02196R000800020001-4

Declassified and Approved For Release 2013/02/15 : CIA-RDP10-02196R000800020001-4

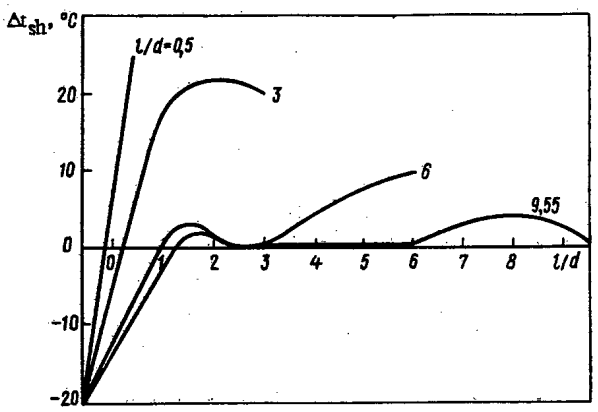


Fig. 5. Dependence of $\Delta t_{sh}$ on the length of the discharge channel for $P_1 = 7.35$ MPa and $\Delta t_{uh} = 20°C$.

The nature of the variation of the pressure differential presented in Fig. 3 permits explaining the unusual conditions of the liquid flow for an initial underheating of $\Delta t_{uh} \approx 15$–$20°C$ and different initial pressures. For this underheating of the liquid at the entry edge the pressure falls to the saturation pressure $P_s$ corresponding to the initial temperature. Therefore, no superheating of the liquid or steam formation is observed at section A. Saturated water flows along the channel right up to the exit section C, and the entire process of steam formation turns out to be referred to the exit section. It is not excluded that for a specific channel length the process of steam formation can be extended over the entire channel length in the case of a small superheating of the liquid.

We note that in the entry section some superheating of the liquid is observed in the zone of the pressure "dip" for $\Delta t_{uh} \approx 15$–$20°C$, which can be accompanied by steam formation and subsequent condensation of the steam upon an increase in the pressure. However, taking into account the fact that the liquid is in a metastable superheated state by 2–4°C for a very short time, it is not excluded that steam formation does not generally occur.

The effect of the degree of initial underheating of the liquid at the channel entrance on the variation of $\Delta t_{sh} = t - t_s$ along the channel length is shown in Fig. 4; $P_1 = 7.35$ MPa, $l/d = 9.55$, and $\Delta t_{uh} = 0$, 20, and 59°C. For $\Delta t_{uh} = 0°C$ the maximum superheating is ~7°C, for $\Delta t_{uh} = 59°C$ the maximum superheating is equal to 10°C,* and for $\Delta t_{uh} \approx 20°C$ superheating is practically equal to zero. It is natural that as $\Delta t_{uh}$ increases the maximum of the superheating is shifted into the interior of the channel and section A extends over it. This situation is associated with an increase in the flow velocity and a small change in the time necessary for completion of the steam-formation process.

The second section B is also shifted along the liquid flow as $\Delta t_{uh}$ increases, and for $\Delta t_{uh} = 59°C$ it is shifted so much towards the exit edge that the flow at the exit section in a channel with $l/d = 9.55$ turns out to be in metastable equilibrium. This fact indicates that with the given initial parameters a channel with $l/d = 9.55$ turns out to be "short," i.e., the processes of phase transitions are not completed towards the exit section, and thermodynamic equilibrium is not established in the flow between phases. Thus depending on the initial pressure and the degree of underheating of the liquid up to the saturation temperature, one and the same channel can be long or short. Evidently, one can explain with this fact how the boundary between long and short channels varies, according to the data of different investigators, from $l/d = 6$–$8$ to $l/d = 16$–$18$.

The variation of $\Delta t_{sh} = t - t_s$ for an initial pressure $P_1 = 7.35$ MPa and $\Delta t_{uh} = 20°C$ is given in Fig. 5 as a function of the channel length. The steam formation process is completed towards the exit section only for $l/d = 9.55$ and more with the indicated initial parameters. For $l/d < 9$ the flow at the channel exit is in the metastable state. The more the liquid is superheated, the shorter the channel. As follows from Fig. 5, the dependence $\Delta t_{sh} = f(l/d)$ is close to a linear one for short channels.

The mass discharge rate of the mixture upon the discharge of boiling water through short channels depends appreciably on $l/d$. Thus, as $l/d$ decreases from 9.55 to 3.0, the mass flow rate increases by ≈ 20%. At the same time the flow rate remains practically constant (it decreases by ~2% due to some increase in the hydraulic drags) in the case of discharge through long channels (when the steam formation process is completed towards the exit edge) upon an increase of $l/d$ from 9.55 to 18.4.

* The actual value of $\Delta t_{sh}$ will be somewhat higher, since in a metastable two-phase flow a thermocouple shows a temperature lower than the actual temperature of the superheated liquid.



Declassified and Approved For Release 2013/02/15 : CIA-RDP10-02196R000800020001-4

Declassified and Approved For Release 2013/02/15 : CIA-RDP10-02196R000800020001-4

# DEPENDENCE OF THE EJECTION COEFFICIENT OF URANIUM ON THE FLUX OF THERMAL NEUTRONS

G. P. Ivanov, V. A. Bessonov,
N. A. Grinevich, V. A. Popovichev,
and E. A. Borisov

UDC 539.211:546.79

The passage of fission fragments through thin layers of matter is accompanied by sputtering of the material of the layer [1]. The study of this phenomenon of ejection is theoretical, and it attracts the attention of investigators [3] in a series of articles [2].

One should emphasize that for the determination of the mean ejection coefficient, i.e., for the determination of the number of uranium atoms knocked loose by a single fission fragment crossing the surface of a uranium-containing layer, one and the same procedure has been employed previously, which is based on the analysis of the composition and amount of fissionable material of the emitter deposited on the collector after irradiation of the assembly by a flux of thermal neutrons in a nuclear reactor. This "static" procedure has significant inadequacies, since it does not permit obtaining information on the intermediate states of the emitter and the deposit on the collector, and it also does not offer the possibility of tracing the dynamics of the sputtering process, and in particular the phenomenon of reejection [4] upon irradiation by a flux of neutrons and the action of the fission fragments. The new procedure applied for investigating the phenomenon of ejection has permitted eliminating the deficiencies mentioned and appreciably increases the accuracy of the measurements. The emitter in a prepared device can be moved over the collector during irradiation (Fig. 1). One can choose the exposure time of the emitter over any section of the collector from fractions of a second to several hours. The unit containing the emitter and collector was placed, as before, into a quartz cell and pumped down to a vacuum of $10^{-4}$ mm Hg, while simultaneously being heated up to 200°C, and then it was irradiated in a channel of the VVRTs reactor, with the emitter moved into place over the collector according to a specified program. After the irradiation the collector was removed from the unit, and the amount of deposited $^{235}U$ was determined from the $\alpha$ activity or with the help of more sensitive solid-state track detectors (SSTD) [5, 6], which permit recording simultaneously the distribution of $^{235}U$ on the collector [6].

The material collected on the collector is distributed in such a dynamic experiment along the path of motion of the emitter. The amount of uranium on each section of the collector was determined, and knowing the flux of neutrons for a given position of the emitter–collector unit, it is possible to calculate the differential ejection coefficient as well as the integrated ejection coefficient normally obtained in the static experiments.

The experiments permitted analyzing the effect of the neutron flux on the sputtering of the surface of a uranous-uranic oxide sample by determining the uranium content on the collectors by means of the separate tracks detected by SSTD. Conglomerates of material containing from $10^8$ to $10^{11}$ atoms of $^{235}U$ are also detected [6].

The ejection coefficient was calculated in the case of analysis of the collector by $\alpha$ activity according to a formula derived on the assumption that the yield of $\alpha$ particles and fission fragments from dense layers of uranium-containing materials is described by one and the same law:

$$K = A_c/A_e F_1 \sigma \Gamma, \quad (1)$$

where K is the observed ejection coefficient, $A_c$ and $A_e$ are the counting rate of $\alpha$ particles from the collector and the emitter, respectively, which are located in identical geometrical conditions with respect to the $\alpha$-particle detector, $\sigma$ is the fission cross section of $^{235}U$ by thermal neutrons, $F_1$ is the flux of thermal neutrons upon irradiation of the emitter–collector unit, and $\Gamma$ is a geometrical factor of the emitter–collector unit, i.e., the fraction of the radiation from the emitter incident on the collector.

Translated from Atomnaya Énergiya, Vol. 47, No. 1, pp. 15-18, July, 1979. Original article submitted December 24, 1976; revised November 17, 1978.



0038-531X/79/4701-0516$07.50 © 1980 Plenum Publishing Corporation

Declassified and Approved For Release 2013/02/15 : CIA-RDP10-02196R000800020001-4

Declassified and Approved For Release 2013/02/15 : CIA-RDP10-02196R000800020001-4

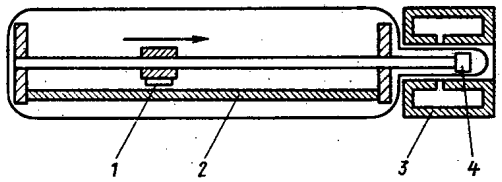


Fig. 1

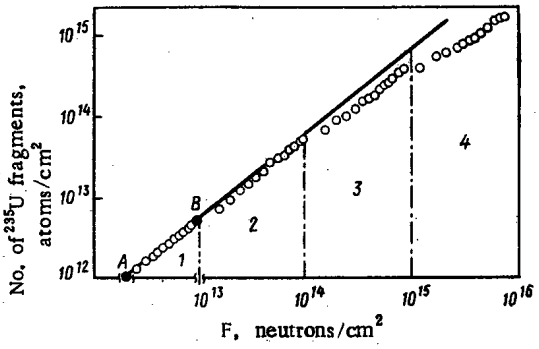


Fig. 2

Fig. 1. Equipment for the investigation of sputtering of material under the action of fission fragments: 1) emitter; 2) collector; 3) electromagnet; and 4) core.

Fig. 2. Dependence of the number of $^{235}$U atoms sputtered in the dynamic test from 1 cm$^2$ of the surface of an emitter made out of uranous-uranic oxide on the flux of thermal neutrons without conglomerate sputtering taken into account (○ – experiment).

In the case of analysis by the SSTD method the observed ejection coefficient can be calculated according to the following formula, which can be derived if the number of uranium atoms deposited on the collector is expressed in terms of the number of tracks by SSTD upon secondary irradiation of the collector–emitter unit:

$$K = S_{tot} a / S_{fv} \varepsilon F_1 F_2 \sigma^2 P_e \mu_0 \Gamma, \quad (2)$$

where $S_{tot}$ is the total area of the collector field, $S_{fv}$ is the area of the field of view when counting the tracks on the detector with a microscope, $a$ is the mean number of tracks in the field of view, $F_2$ is the flux of thermal neutrons upon irradiation of the collector in contact with the SSTD, $P_e$ is the number of $^{235}$U atoms in the emitter, $\mu_0$ is the fraction of fission fragments knocked out of the emitter in the direction of the collector, and $\varepsilon$ is the efficiency of recording the fission fragments with SSTD (in this case $\varepsilon = 0.4$).

Thin layers of uranous-uranic oxide enriched in $^{235}$U (thickness of the layer ~ 4 mg/cm$^2$) were used as the emitters. For this purpose layers of a dilute alcohol solution of uranyl nitrate with collodion were deposited on an aluminum substrate. After drying in air the substrate was baked in a muffle furnace at a temperature of 500°C, which ensures conversion of uranyl nitrate into $U_3O_8$. These operations were repeated before a mechanically strong film of uranous-uranic oxide was obtained on the substrate with a nonuniformity of ~ 10% in the thickness.

Prior to the dynamic test the dependence of the ejection coefficient of such emitters on the flux density of thermal neutrons was investigated under static conditions in a channel of the VVRTs reactor at a neutron flux of $10^{16}$ neutrons/cm$^2$. The error in the determination of the ejection coefficient reached 100% in these tests; however, one can assume that the ejection coefficient remains constant at a flux density up to $5 \cdot 10^{12}$ neutrons/cm$^2$·sec, and increases appreciably at $5 \cdot 10^{13}$ neutrons/cm$^2$·sec, which can be explained by the heating up of the emitter as a result of significant heat liberation. At $F \approx 10^{16}$ neutrons/cm$^2$ and a flux density of thermal neutrons of (3.5, 35, 70, 175, 525, and 5000)·$10^{10}$ neutrons/cm$^2$·sec the ejection coefficient is equal to 130, 200, 100, 120, 180, and 480 atoms/fragment, respectively. Taking account of this fact, dynamic tests were carried out at a flux density of $1.8 \cdot 10^{12}$ neutrons/cm$^2$·sec, i.e., in the region in which the effect of the flux density on the ejection coefficient is absent.

The dependence of the number of $^{235}$U atoms sputtered out of the emitter in the dynamic test on the neutron flux is given in Fig. 2. The relative error of the individual experimental points does not exceed 10%. It is necessary in connection with the determination of the absolute flux of neutrons on the emitter and the cumulative number of sputtered atoms to also take into account the flux obtained by the emitter at points A and B ($1.2 \cdot 10^{14}$ and $1.8 \cdot 10^{14}$ neutrons/cm$^2$).

In the range from 0 to $8 \cdot 10^{14}$ neutrons/cm$^2$ (sections 1 and 2) the number of sputtered atoms depends linearly on the neutron flux (the standard deviation from the linear relation is less than 2%). In section 3 the arrangement of the experimental points indicates a decrease in the ejection coefficient. We note that the question is still the observed ejection coefficient obtained from the experimental data without corrections for secondary phenomena. An especially abrupt departure of the experimental points from the straight line is observed in section 4, which is partially related to reejection.



Declassified and Approved For Release 2013/02/15 : CIA-RDP10-02196R000800020001-4

Declassified and Approved For Release 2013/02/15 : CIA-RDP10-02196R000800020001-4

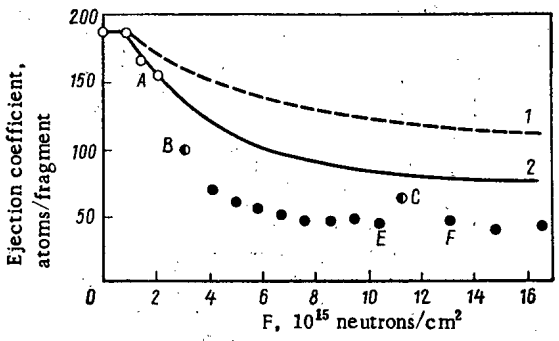


Fig. 3. Dependences of the integrated (---) and true differential (——) ejection coefficient on the thermal neutron flux (without conglomerate sputtering taken into account) obtained with corrections for reejection and calculated in a dynamic test with emitter exposures ≤ 100 (○), 500 (◐), and 1000 sec (●).

The conditions for deposition of atoms onto the collector can be expressed by the equation

$$dn_c/dt = \Gamma K_t j - R, \tag{3}$$

where $n_c$ is the number of atoms deposited on the collector, t is the time, $K_t$ is the true ejection coefficient, j is the number of fragments which leave the emitter per unit time, and R is the number of atoms which leave the collector per unit time as a result of reejection. The geometrical factor in the dynamic experiment was taken equal to 0.34. One can represent the quantity R in the form

$$R = j\Gamma\sigma_r n_c/S_e = \Phi\sigma_r n_c, \tag{4}$$

where $S_e$ is the area of the emitter, $\Phi = j\Gamma/S_e$ is the flux of fission fragments penetrating the collector (i.e., the number of fission fragments passing through 1 cm$^2$ of the collector surface in 1 sec), and $\sigma_r$ is the interaction cross section, which in this case can be called the reejection coefficient averaged over the energy of the fission fragments.

With the initial conditions $n_c = 0$ at $t' = 0$ we obtain from Eqs. (3) and (4)

$$\rho_c = n_c/S_e = (K_t/\sigma_r)\left[1 - \exp\left(-\frac{j}{S_e}\sigma_r \Gamma t\right)\right], \tag{5}$$

where $\rho_c$ is the surface area of the atoms on the collector (for equal areas of the emitter and collector).

The dependence of the observed ejection coefficient on the neutron flux is presented in Fig. 3 for the emitter. At points B and C the exposure is equal to 500 sec (the neutron flux is $0.9 \cdot 10^{15}$ neutrons/cm$^2$, and the flux density of fragments through the sample surface is $\sim 2.2 \cdot 10^{12}$ fragments/cm$^2$ · sec). At points following point B the exposure is 1000 sec (the neutron flux is $1.8 \cdot 10^{15}$ neutrons/cm$^2$). Identical ejection coefficients at points E and F and an increase of the ejection coefficient at point C, where the exposure was two times less, indicate that the accumulation of material on the collector is accompanied by reejection. Analysis of the results from the dynamic test with the use of the equation permits calculating $\sigma_r$ of reejection, which for an emitter (uranous-uranic oxide on an aluminum substrate)–collector (aluminum) system amounts to $\sim 10^{-12}$ cm$^2$.

The reejection cross section can be interpreted as a "hot" spot with area $\sigma_r$ formed upon the intersection of the collector surface with a fission fragment. At the same time atoms located in the spot zone leave the collector surface, acquiring a sufficiently high energy. Consequently, in tests with an aluminum collector the diameter of the "hot" zone formed by each fission fragment which penetrated the collector is ~120 Å. Naturally, the removal of atoms collected on the collector as a result of the bombardment of its surface by fission fragments should depend significantly both on the nature of the bond of the deposited atoms and particles with the collector surface and on the dimensions of the "hot" zone generated.

The results of tests on the sputtering of uranous-uranic oxide upon irradiation to a thermal neutron flux of $\sim 10^{17}$ neutrons/cm$^2$ permitted determining that the reejection coefficient is 4.5 times greater when a palladium collector is used than when an aluminum collector is used.

Knowing the reejection cross section, it is possible to calculate for the dynamic test the true ejection coefficients. It is evident that up to point A (100-sec exposure) the true and observed ejection coefficients coincide (see curve 2 of Fig. 3). The true differential ejection coefficient remains constant up to a neutron flux of $\sim 8 \cdot 10^{14}$ neutrons/cm$^2$ (the integrated flux of fission fragments through the emitter surface is $\sim 2 \cdot 10^{12}$



Declassified and Approved For Release 2013/02/15 : CIA-RDP10-02196R000800020001-4

Declassified and Approved For Release 2013/02/15 : CIA-RDP10-02196R000800020001-4

fragments/cm$^2$) and is equal to 190 atoms/fragment. Then it decreases sharply at first and then slowly to 80-100 atoms/fragment in the case of an integrated flux of $5 \cdot 10^{13}$ fragments/cm$^2$. The most probable cause for the decrease of the true ejection coefficient is evidently the processing of the emitter surface by fission fragments. If one assumes that a fission fragment passing through the emitter surface forms a "hot spot" $\sim 10^{-12}$ cm$^2$ in size, then for a neutron flux of $\sim 10^{15}$ neutrons/cm$^2$ and a corresponding integrated flux of fission fragments ($3 \cdot 10^{12}$ fragments/cm$^2$) the entire surface of the emitter is completely processed by fission fragments. A decrease in the true ejection coefficient by a factor of 2-3 was observed precisely in this case. One should note that further irradiation of a uranous-uranic oxide sample is accompanied by a decrease in the integrated ejection coefficient to 15 atoms/fragment for a neutron flux of $10^{18}$ neutrons/cm$^2$ (the integrated flux of fragments is $\sim 3 \cdot 10^{15}$ fragments/cm$^2$), which is in good agreement with the published data [7]. One can assume that not only the initial state of the emitter surface but also the alteration of this state upon the action of reactor radiation and fission fragments exert an effect on the sputtering process of uranous-uranic oxide at a comparatively large neutron flux. In addition, the nature of conglomerate sputtering of materials under the action of fission fragments and neutrons with an energy of 14 MeV which has been discovered [6, 8, 9], which should be reflected in the ejection coefficient, can change upon the transition to a large flux.

## LITERATURE CITED


1. S. T. Konobeevskii, The Action of Radiation on Materials [in Russian], Atomizdat, Moscow (1967).
2. V. I. Gol'danskii et al., Izotopy v SSSR, No. 12, 17 (1963).
3. V. A. Bessonov, At. Energ., 37, No. 1, 52 (1974).
4. M. Rogers and J. Adam, J. Nucl. Mater., 6, No. 2, 182 (1962).
5. R. Fleischer, P. Price, and R. Walker, Science, 149, No. 3862, 383 (1965).
6. V. A. Bessonov et al., At. Energ., 40, No. 5, 395 (1976).
7. G. Nilsson; J. Nucl. Mater., 20, No. 1, 215, 231 (1966).
8. M. Kaminski and S. Das, J. Nucl. Mater., 53, No. 1, 162 (1974).
9. J. Biersack, D. Fink, and P. Mertens, J. Nucl. Mater., 53, No. 1, 194 (1974).


# EFFECT OF IRRADIATION ON THE ULTIMATE FRACTURE STRENGTH OF THE ALLOY Zr-2.5% Nb


O. A. Shat-skaya, E. Yu. Rivkin, A. M. Vasnin, V. V. Klyushin, A. V. Kozlov, V. M. Nalesnik, and M. E. Rodin


UDC 669.296+621.039.531+621.791.72

Embrittlement of zirconium alloys by the action of irradiation and hydrogenation [1] attracts particular attention in view of the fact that such alloys are used to fabricate fuel-channel tubes which should possess the necessary resistance to brittle fracture.

In order to investigate the changes in the strength characteristics of zirconium alloys in the course of operation, a test fuel channel was extracted from the reactor of the first unit at the Beloyarsk Atomic Power Plant after 1100 effective days of service; the channel consisted of a tube made of the alloy Zr-2.5% Nb with an external diameter of 63 mm and a wall thickness of 4 mm. The parameters of its irradiation are given in Table 1. Specimens for the investigations were cut from segments with coordinates 0.2-0.5 m, 3.2-3.5 m, and 6.5-6.8 m along the length of the extracted fuel-channel tube.

The mechanical properties were determined by testing rings 6 mm wide at 293 and 573°K. In all cases, ductile fracture was preceded by considerable deformation and a change in the shape of the sample. The instantaneous strength $\sigma_b$ was found from the rupturing load while the yield point $\sigma_{0.2}$ and the relative elongation $\delta$ were found from the diagram of the force vs grip displacement. According to the data of Table 2, irradiation increases the instantaneous strength and the yield point and decreases the relative elongation.

For the toughness tests notched samples measuring 55 × 10 × 4 mm oriented in the longitudinal direction were cut from the fuel-channel tube. A notch 2 mm deep with a radius ~0.1 mm at the tip was aligned

Translated from Atomnaya Énergiya, Vol. 47, No. 1, pp. 18-21, July, 1979. Original article submitted July 17, 1978.

0038-531X/79/4701-0519$07.50 © 1980 Plenum Publishing Corporation



Declassified and Approved For Release 2013/02/15 : CIA-RDP10-02196R000800020001-4

Declassified and Approved For Release 2013/02/15 : CIA-RDP10-02196R000800020001-4

TABLE 1. Principal Characteristics of Conditions of Irradiation of Fuel Channel ($E \geq 0.2$ MeV)

| Coordinates of segments from bottom of reactor core, m | Neutron flux, neutrons/ $cm^2 \cdot sec$ | Fluence, neutrons/ $cm^2$ | Surface temp., °K | |
|---|---|---|---|---|
| | | | internal | external |
| 0—0,45 | $1,5 \cdot 10^{13}$ | $1,6 \cdot 10^{21}$ | 579 | 582 |
| 0,45—1,22 | $2,3 \cdot 10^{13}$ | $2,4 \cdot 10^{21}$ | 585 | 589 |
| 1,22—1,99 | $3,0 \cdot 10^{13}$ | $3,0 \cdot 10^{21}$ | 592 | 597 |
| 1,99—2,74 | $3,4 \cdot 10^{13}$ | $3,4 \cdot 10^{21}$ | 595 | 602 |
| 2,74—3,51 | $3,7 \cdot 10^{13}$ | $3,8 \cdot 10^{21}$ | 596 | 605 |
| 3,51—4,26 | $3,7 \cdot 10^{13}$ | $3,8 \cdot 10^{21}$ | 596 | 605 |
| 4,26—5,06 | $3,2 \cdot 10^{13}$ | $3,2 \cdot 10^{21}$ | 596 | 603 |
| 5,06—5,86 | $1,8 \cdot 10^{12}$ | $1,8 \cdot 10^{21}$ | 596 | 601 |
| 5,86—6,56 | $2,2 \cdot 10^{11}$ | $2,3 \cdot 10^{20}$ | 596 | 599 |
| 6,56—7,11 | $2,3 \cdot 10^{10}$ | $2,8 \cdot 10^{29}$ | 596 | 598 |

TABLE 2. Mechanical Properties of Tube Material

| Coordinates of segment of tube, m | Fluence, neutrons/ $cm^2$ | Operating temperature, °K | Temp. of test, °K | | | | | |
|---|---|---|---|---|---|---|---|---|
| | | | 293 | | | 573 | | |
| | | | $\sigma_b$, MPa | $\sigma_{0.2}$, MPa | $\delta$, % | $\sigma_b$, MPa | $\sigma_{0.2}$, MPa | $\delta$, % |
| — | initial state | | 490 | 400 | 20 | 343 | 304 | 19 |
| 0,2—0,5 | $(1,6—2) \cdot 10^{21}$ | 579—583 | 637 | 540 | 14 | 470 | 432 | 11 |
| 3,2—3,5 | $3,8 \cdot 10^{21}$ | 596—605 | 608 | 530 | 12 | 460 | 412 | 11 |
| 6,5—6,8 | $(3,2—8,2) \cdot 10^{19}$ | 596—599 | 560 | 440 | 15 | 440 | 382 | 16 |

in the direction of the height of the sample (10 mm). The tests, which were carried out on a pendulum hammer of the KMD-30 type over the temperature range 293-573°K, permitted the following conclusions:

Irradiation does not change the toughness obtained for the material in the initial state. This usefully distinguishes the annealed alloy Zr-2.5% Nb from the same alloy subjected to threefold treatment (tempering, cold deformation, annealing), for which the shift of the critical temperature of brittleness may reach 100-150°K at a fluence of $(2-5) \cdot 10^{20}$ neutrons/$cm^2$;

the toughness does not depend on the fluence in the range from $3.2 \cdot 10^{19}$ to $4.8 \cdot 10^{21}$ neutrons/$cm^2$.

A quantitative estimate of the resistance to brittle fracture can be made within the framework of fracture mechanics, using the critical crack opening $\delta_c$. In order to determine this characteristic we cut annular and longitudinal samples from the tube. The notches cut in these samples were oriented so that the conditions of crack development along the tube axis and in the tangential direction would be reproduced. The radius at the tip of the notch was less than 0.1 mm. In the course of the tests the samples were set up on supports, and sensors recorded the diagram of the force vs the crack opening. For the critical opening we took the value of the crack opening at the instant that maximum load was reached. Tests were also carried out in the range of temperatures from 293 to 573°K. The relations obtained for the longitudinal samples are given in Fig. 1, in which, for comparison, we also give the data for the alloy Zr–2.5% Nb subjected to threefold treatment [2]. The annular samples were tested only at 293°K (Fig. 2). It follows from Figs. 1 and 2 that irradiation markedly reduces the critical crack opening at 293°K. At 573°K irradiation up to $(1.5-2) \cdot 10^{21}$ neutrons/$cm^2$ reduces the critical crack opening substantially more than at 293°K, but with an increase in the fluence to $3.8 \cdot 10^{21}$ neutrons/$cm^2$ this difference practically disappears. According to Fig. 2, at 293°K there is no further reduction of the critical crack opening in longitudinal samples at a fluence of more than $(3.2-8.2) \cdot 10^{19}$ neutrons/$cm^2$ and the same is true for annular samples at a fluence of more than $(1.5-2) \cdot 10^{21}$ neutrons/$cm^2$. It follows from Fig. 2 that the resistance to crack motion in the axial direction of the tube is higher than in the tangential direction. The same data were obtained in tests of the original samples [3]. It turned out that the ratio between the critical crack openings for longitudinal and annular samples of the material in the initial state is also maintained on the horizontal segment of the dependence of this characteristic on the fluence. When a fluence of $1.6 \cdot 10^{19}$ neutrons/$cm^2$ has been reached, the critical crack opening in the metal of the seam differs from that measured for the same metal in the initial state (curves 2 and 3 in Fig. 1). Comparison of the data obtained with the results of investigations by B. Pickles [2] shows that as in the initial state (in particular), so after irradiation of annealed Zr–2.5% Nb alloy the critical crack opening is greater than in the alloy subjected to threefold treatment.

The results of the investigations permit an estimate to be made of the ultimate fracture strength of fuel-channel tubes, i.e., permit the relation between the acting stresses and the size of possible defects to be determined. Let us consider local defects (pores, inclusions, short cracks) and extended defects (long hairline cracks, scratch marks, cracks). Development of defects of the first type can lead to the formation of through cracks in the tube to a length of no more than twice the tube wall thickness and the purpose of the calculations comes down to finding their critical length; complete rupture of the tube may occur after this critical value is reached. In this case the fracture strength is characterized by the critical opening of a crack oriented in the axial direction. The development of defects of the second type may occur over the entire length of a crack in the radial direction. In this case, the purpose of the calculations comes down to determining the critical depth of a surface defect; complete rupture of the tube may occur before this depth is reached.



Declassified and Approved For Release 2013/02/15 : CIA-RDP10-02196R000800020001-4

Declassified and Approved For Release 2013/02/15 : CIA-RDP10-02196R000800020001-4

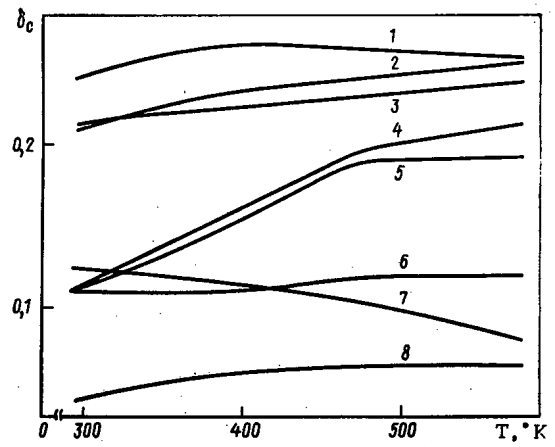


Fig. 1

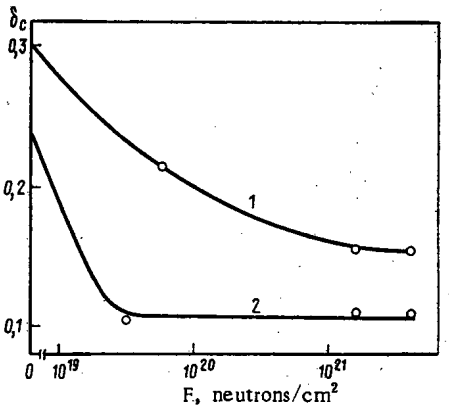


Fig. 2

Fig. 1. Dependence of critical crack opening on temperature: 1, 2) basic metal and metal of seam, without irradiation; 3) metal of seam under irradiation with fluence of $(1\text{-}1.5)\cdot10^{19}$ neutrons/cm$^2$; 4, 5, 6) basic metal under irradiation with fluence of $(3.2\text{-}8.2)\cdot10^{19}$, $(1.6\text{-}2)\cdot10^{21}$, and $3.8\cdot10^{21}$ neutrons/cm$^2$, respectively; 7, 8) data for initial and irradiated state [2].

Fig. 2. Dependence of critical crack opening on neutron fluence: 1) annular and 2) longitudinal specimens.

The following formula [4] can be used to calculate tubes of zirconium alloys with through defects:

$$\delta_c = (8\sigma_{0,2}l/E\pi)M^2 \ln \sec(\pi\sigma/2\sigma_{0,2}),$$

where E is the modulus of elasticity, $l$ is the half-length of a through crack, $M^2 = 1 + 1.61l^2/Rt$ is a correction for the tube curvature, R and t are the mean radius and the wall thickness of the tube, $\sigma$ is the tangential stress in the tube. Calculations were carried out for tubes in the initial and irradiated (fluence $3.8\cdot10^{21}$ neutrons/cm$^2$) states at 293 and 573°K. The values of $\delta_c$ were taken from the results of tests of annular samples in accordance with Fig. 2, and those of $\sigma_{0,2}$, from the data in Table 2. As follows from Fig. 3, in the case of short cracks irradiation increases the value of the rupture stress (as the result of the rise in the yield point under irradiation) whereas in the case of long cracks irradiation somewhat reduces the stress. With a working stress level of 100 MPa in the fuel-channel tube the minimum critical crack length is found from curve 4 in Fig. 3 for irradiated material at 573°K. This length is 43 mm, which substantially exceeds the maximum possible length of a through defect (developing from a local defect), equal to two wall thicknesses (for the given tubes, 8 mm). This means that the development of local defects may result in only a leak but not complete rupture of the fuel channel.

The following formula has been proposed for the calculation of tubes with surface defects [5]:

$$\delta_c = (\sigma^2\pi b/E\sigma_{0,2})(C_tC_c/Q)^2,$$

where $\delta_c$ is the crack opening in radial crack propagation, b is the crack depth, $Q^2 = \Phi^2 - 0.212(\sigma/\sigma_{0,2})^2$, $C_t = [1 + 0.122(1-b/2l)^2]/\{1-(b/t)^4\}^{1/2}$; $C_c = (A_m - 1)\,b/t + 1$; $A_m = 0.481\,\lambda + 0.614 + 0.386\,e^{-1.25\lambda}$; $\lambda = \{12(1-\nu^2)\}^{1/4}\cdot(l/\sqrt{Rt})$; and $\Phi = \int_0^{\pi/2}(1-(l^2-b^2)/l^2\,[\sin^2\theta)^{1/2}d\theta$.

In the calculation of tubes with surface defects we must use values of the critical crack opening found in tests of samples with a crack oriented over the thickness of the tube wall. Such tests were not carried out with irradiated samples. It was established, however, that the ratio between the critical crack openings for longitudinal and annular samples remains unchanged both before and after irradiation. It was accordingly assumed that this invariability of the ratio is also maintained for samples with cracks oriented in the axial and radial directions. This ratio is 3.3 for samples in the initial state [4] and in view of this in calculating tubes with surface defects we used values from Fig. 2, reduced by a factor of 3.3. The results of the calculations, given in Fig. 4, indicate that rupture of a fuel-channel tube with a working stress of 100 MPa can occur only if the depth of the long surface defect exceeds 3 mm at a length of 80 mm. The formation of such defects in tubes during the operation of the fuel channel is not very probable since there are no factors which could cause them to appear and develop.



Declassified and Approved For Release 2013/02/15 : CIA-RDP10-02196R000800020001-4

Declassified and Approved For Release 2013/02/15 : CIA-RDP10-02196R000800020001-4

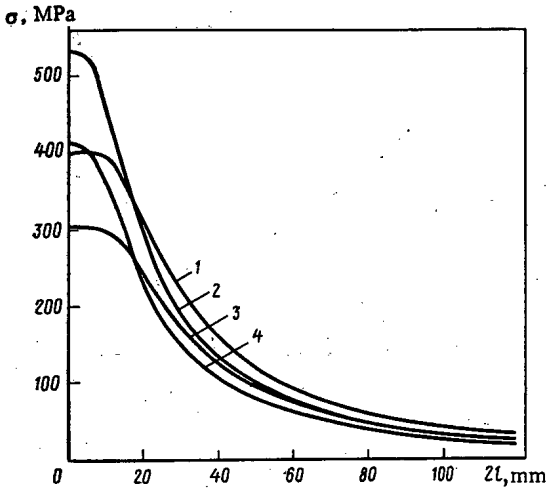


Fig. 3

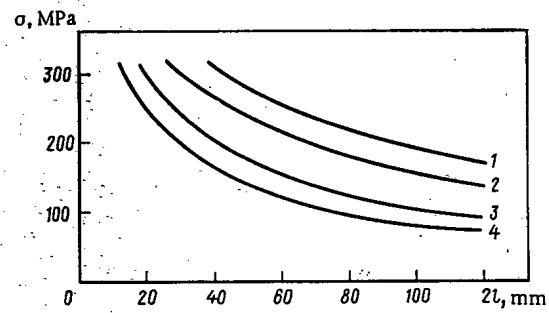


Fig. 4

Fig. 3. Dependence of rupture stress on length of longitudinal through crack (fluence $3.8 \cdot 10^{21}$): 1, 2) without irradiation and after irradiation at 293°K; 3, 4) same, at 573°K.

Fig. 4. Dependence of rupture stress on length of longitudinal surface cracks at 573°K (fluence $3.8 \cdot 10^{21}$): 1, 2) without irradiation and after irradiation at crack depth of 2 mm; 3, 4) same, at crack depth of 3 mm.

The investigations carried out permit the following conclusions to be drawn.

Under irradiation (neutron fluence more than $1.5 \cdot 10^{21}$ neutrons/cm$^2$) the instantaneous strength and the yield point of zirconium fuel-channel tubes increase by 25-40% and the relative elongation decreases by 30-40% while remaining quite high (more than 11%). Irradiation (fluence of up to $3.8 \cdot 10^{21}$ neutrons/cm$^2$) displayed no effect on the toughness of the alloy Zr–2.5% Nb. Irradiation with a fluence of $3.8 \cdot 10^{21}$ neutrons/cm$^2$ reduces the critical crack opening more than twofold for the alloy Zr–2.5% Nb over the entire temperature range investigated, from 293 to 573°K, in comparison with the values measured in the initial state. With a fluence of up to $(1.5\text{-}2) \cdot 10^{21}$ neutrons/cm$^2$ such a reduction is observed only at 293°K whereas at 573°K the critical crack opening decreases by only 30%. The ultimate fracture strength of annealed Zr–2.5% Nb is higher than in a similar alloy subjected to threefold treatment (tempering, cold deformation, and annealing).

Calculations show that with a working stress of about 100 MPa in the fuel-channel tube the critical length of a through notch along the tube axis is 43 mm while the critical dimensions of a surface notch are 3 mm (depth) and 80 mm (length). It is practically impossible for such defects to exist, which warrants the assumption that the necessary resistance of fuel-channel tubes to brittle fracture during operation is ensured.

## LITERATURE CITED

1. E. Yu. Rivkin, B. S. Rodchenkov, and V. M. Filatov, Strength of Zirconium Alloys [in Russian], Atomizdat, Moscow (1974).
2. B. Pickles, Can. Metall. Q., 11, No. 1, 139 (1972).
3. E. Yu. Rivkin, A. M. Vasnin, and V. E. Mozharov, Fiz.-Khim. Mekh. Mater., No. 6, 12 (1976).
4. A. M. Vasnin, V. Yu. Gol'tsev, V. M. Markochev, and E. Yu. Rivkin, Probl. Prochn., No. 12, 111 (1974).
5. F. Erdogan and M. Ratwani, Nucl. Eng. Design, 27, 14 (1974).



Declassified and Approved For Release 2013/02/15 : CIA-RDP10-02196R000800020001-4

Declassified and Approved For Release 2013/02/15 : CIA-RDP10-02196R000800020001-4

# ROLE OF IMPURITIES IN IRRADIATION EMBRITTLEMENT OF LOW-ALLOY STEEL

V. A. Nikolaev, V. V. Rybin, and V. I. Badanin

UDC 621.039.531

As is known, impurity elements (P, Sb, Sn) intensify the irradiation embrittlement of structural steel and binary iron alloys [1-6]. At an irradiation temperature of 300-350°C their influence is related to grain-boundary segregation as a result of radiation-stimulated diffusion. It was of interest to study the irradiation embrittlement of steel, contaminated with impurities, at the lowest possible irradiation temperature when the processes of vacancy migration are retarded substantially. The present paper gives the results of investigations on toughened ferritic–pearlitic steel of the 15Kh2MFA and 15Kh2NMFA types with dosed additions of phosphorus, antimony, and tin. The details of the preparation of the materials and the technique for irradiating and testing them were described earlier [5, 6].

Results of Experiments. Figure 1 shows the mechanical properties of 15Kh2NMFA steel in the initial state after irradiation.

When the phosphorus content is varied within the limits 0.005-0.036% the transitional temperature $T_c$ of brittleness of unirradiated steel changes little, increasing by a mere 30°C (see Fig. 1). The concentration dependence of $T_c$ appears most distinctly after irradiation as a result of intensification of irradiation embrittlement as the phosphorus content rises. A similar result is well known for an irradiation temperature $T_{irr} \approx$ 300°C (see Fig. 1) adjacent to the lower limit of the range of thermal brittleness of the steel. It is more interesting that the effect of the phosphorus manifests itself so clearly at $T_{irr}$ = 80°C as well. At a fluence of $3.5 \cdot 10^{19}$ neutrons/cm$^2$* the increase in $T_c$ is $\Delta T_c$ = 60°C in steel containing 0.005% and 130°C at maximum phosphorus content (0.036%).

The considerable effect of impurity elements at both low and elevated $T_{irr}$ is illustrated graphically in Fig. 2, which shows the dependence of the coefficient of radiation embrittlement $A = \Delta T_c / F^{1/3}$ (F is the neutron fluence, $10^{18}$ neutrons/cm$^2$) on $T_{irr}$ for steels differing as to the P, Sb, and Sn content. Against the background of the monotonic decrease in A with an increase in $T_{irr}$ it is clearly seen that it increases as the impurity content grows.

The experiments showed that embrittling impurities do not increase the irradiation hardening of the steel. †

The change in the average size of the former austenitic grains from 25 to 225 $\mu$m does not cause a displacement of $T_c$, this being characteristic of steel with both a low and an elevated phosphorus content (see Table 1). No contribution from grain-boundary effects is revealed also in fractographic analysis in a scanning electron microscope. The transcrystalline character of brittle fracture (quasicleavage), character typical of the steel studied after irradiation at 80°C, is completely preserved at maximum phosphorus content, as noted earlier [5].

In experiments on annealing the effects of irradiation it was found that embrittlement of 15Kh2NMFA steel at 80°C is eliminated almost completely in the temperature range from 250 to 400°C after annealing for 1 h (Fig. 3). Only in steel with a 0.036% phosphorus content is a residual $\Delta T_c$, equal to roughly 30°C, preserved after annealing at 400°C. The increment $\Delta H_V$ of the hardness of irradiated steel with a various phosphorus content is eliminated in this temperature range (a certain difference in the curves for the restoration of the values of $T_c$ and $H_V$ is due to different annealing times).

* Here and henceforth a fluence of neutrons with an energy of more than 0.5 MeV.

† Since before and after irradiation the yield point of the steel does not depend on the phosphorus concentration (see Fig. 1).

Translated from Atomnaya Énergiya, Vol. 47, No. 1, pp. 21-25, July, 1979. Original article submitted June 2, 1977; revision submitted January 22, 1979.

0038-531X/79/4701-0523$07.50 © 1980 Plenum Publishing Corporation



Declassified and Approved For Release 2013/02/15 : CIA-RDP10-02196R000800020001-4

Declassified and Approved For Release 2013/02/15 : CIA-RDP10-02196R000800020001-4

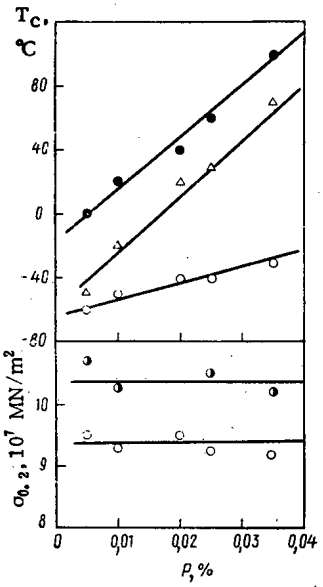


Fig. 1

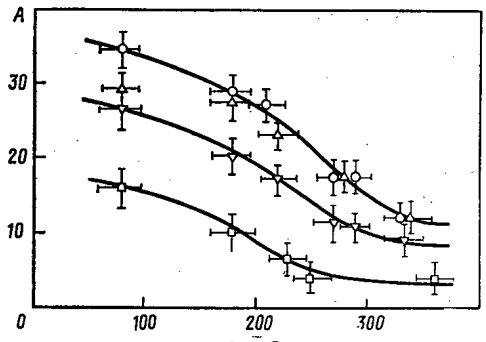


Fig. 2

Fig. 1. Effect of phosphorus content on yield point and $T_c$ of 15Kh2NMFA steel in initial state (○) and after irradiation with fluence of $3.5 \cdot 10^{19}$ neutrons/cm$^2$ (◑, ●) at $T_{irr}$ = 80°C and with fluence of $1.3 \cdot 10^{20}$ neutrons/cm$^2$ (△) at $T_{irr}$ = 300-350°C.

Fig. 2. Effect of irradiation temperature on coefficient of radiation embrittlement of 15Kh2NMFA steel containing 0.005 and 0.026% phosphorus (□, ○), 0.03% tin (▽), and 0.02% antimony (△).

Discussion of Results. The body of experimental data shows clearly that at $T_{irr} \approx 80$°C phosphorus and its analogs considerably intensify the irradiation embrittlement of steel. Moreover, the contribution of these elements to the increase in $T_c$ is not in any way noticeably related to grain-boundary effects. Data on the restoration of $T_c$ testify against the model of segregation weakening of boundaries. Indeed, a temperature of 400°C is too low for dissolving grain-boundary segregations of P, Sb, or Sn in alloys based on $\alpha$-Fe [7]. At the same time, in an experiment on the elimination of irradiation embrittlement, dissolving is observed at 400°C and even at a lower temperature (see Fig. 3). Therefore, the cause of embrittling effect of the impurity should be sought in those structural changes which arise inside grains in the presence of the elements indicated. It is believed that the same radiation-induced defects cause both hardening and embrittlement of steel irradiated at 80°C.

Numerous experimental facts confirm the correlation between some manifestations of irradiation hardening and embrittlement of steel. These include the similar dose dependence of $\Delta\sigma_{0.2}$ and $\Delta T_c$, as well as the coincidence of the temperature ranges of the restoration of the strength and $T_c$.

The embrittling effect of impurities, it would seem, can manifest itself in their effect on the volume density of defects. The addition of copper and nickel to steel and iron, for example, stimulates irradiation embrittlement and hardening in this very way. Thus, it was shown by transmission electron microscopy in [8] that the density of dislocation loops and pores in a Fe + 0.3% Cu alloy after irradiation at 280°C with a fluence of $4.5 \cdot 10^{20}$ neutrons/cm$^2$ ($E > 1$ MeV) is four times that in pure iron. It was also found [9] that $T_c$ and the yield point of irradiated steel grow linearly with the nickel content in the steel. The presence of phosphorus, however, does not significantly alter the volume density of radiation-induced defects in iron [8], and this impurity, stimulating irradiation embrittlement, does not cause any additional increase in $\sigma_{0.2}$.

This paradox can be explained with the assumption that the complex radiation defects (accumulation of point defects, dislocation loops of the vacancy and interstitial types, etc.) as well as extraplanes added on are enriched with atoms of phosphorus and its analogs [4, 10]. The validity of this assumption is confirmed by the experimentally detected [11] segregation of some alloying elements (Si, Ni) on the surface of vacancy pores in austenitic steel irradiated with electrons.

As is known, enrichment of the interface with impurities to a concentration of ~5% embrittles steel [12]. In the case under consideration the role of such a surface can be played by defective regions of crystals



Declassified and Approved For Release 2013/02/15 : CIA-RDP10-02196R000800020001-4

Declassified and Approved For Release 2013/02/15 : CIA-RDP10-02196R000800020001-4

TABLE 1. Effect of Grain Size in Irradiation Embrittlement of 15Kh2NMFA Steel

| Phosphorus content in steel, % | Grain size, μm | $\Delta T_c$ at F = $3.5 \cdot 10^{19}$ neutrons/cm$^2$ and $T_{irr} \approx$ 80°C | Phosphorus content in steel, % | Grain size, μm | $\Delta T_c$ at F = $3.5 \cdot 10^{19}$ neutrons/cm$^2$ and $T_{irr} \approx$ 80°C |
|---|---|---|---|---|---|
| 0,005 | 25 | 60 | 0,025 | 25 | 120 |
| | 80 | 70 | | 75 | 130 |
| | 225 | 70 | | 210 | 120 |

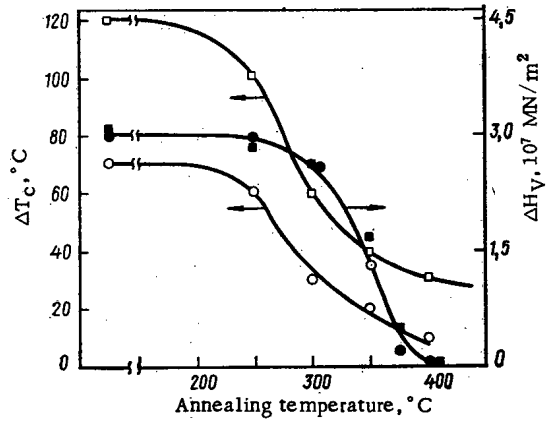


Fig. 3

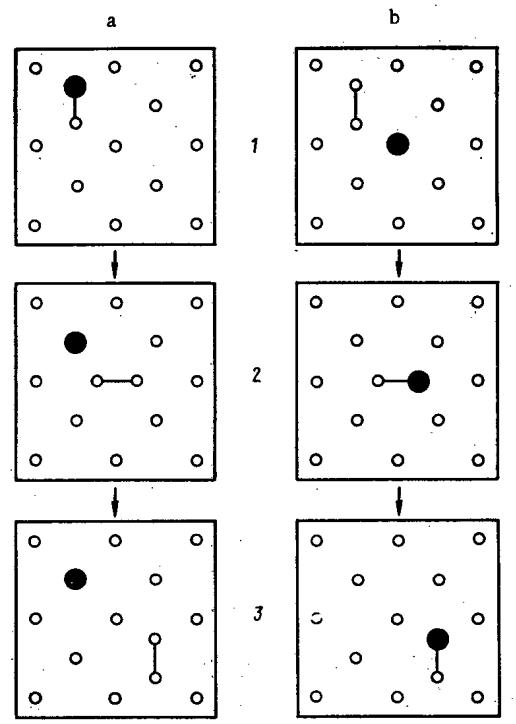


Fig. 4

Fig. 3. Effect of annealing temperature on the restoration of $T_c$ (1, 2) and hardness (3) of 15Kh-2NMFA steel with phosphorus content of 0.005 (○, ●) and 0.036% (□, ■). Irradiation with a fluence of $3.5 \cdot 10^{19}$ neutrons/cm$^2$ at 80°C.

Fig. 4. Variants of atomic rearrangement during migration of interstitial atom in crystal with impurity: 1-3) succession of jumps; ○, ●) matrix and impurity atoms, respectively.

enriched with impurities. If it is borne in mind that the preferential microcrack nucleation occurs on these weakened surfaces, then the increased tendency to brittleness is easily understood within the framework of the model of thermally activated fracture, in which model the formation of primary cracks is considered as a process of thermofluctuational nucleation and formation of many microcracks [13]. At a more phenomenological level a shift of $T_c$ is seen from analysis of the Ioffe scheme: a decrease in the cohesiveness in numerous microsurfaces results in an effective reduction of the rupture strength of the crystal, as a result of which $T_c$ is shifted to the region of higher temperatures. The critical aspect of the hypothesis presented above consists in the necessity to explain why the defective regions are considerably enriched with impurities in comparison with the matrix (by roughly 2-3 orders of magnitude) at an irradiation temperature of 80°C.

Under ordinary conditions P, Sb, and Sn, forming solid substitutional solutions with iron, diffuse into the zone of segregation by a vacancy mechanism. It is not entirely certain that this mechanism can be realized at 80°C but there is evidence [14] of an insignificant vacancy mobility in iron at this temperature. For this reason it is desirable to turn our attention to the possibility of interstitial migration of impurities. Upon entering interstices, P, Sb, and Sn atoms are capable of actively migrating in the crystal even at a negative temperature. However, ease of migration cannot in itself give the required enrichment with impurities, since atoms of the main alloying elements (Fe, Cr, Ni, Mo, etc.), which so easily migrate over the lattice interstices, are knocked out of the lattice sites with practically the same probability as the impurity atoms.



Declassified and Approved For Release 2013/02/15 : CIA-RDP10-02196R000800020001-4

Declassified and Approved For Release 2013/02/15 : CIA-RDP10-02196R000800020001-4

In order to understand the possibility of preferential migration of impurity atoms by an interstitial mechanism, let us consider this process in greater detail. In crystals with a bcc lattice dumbbell configurations are the energetically most convenient state of interstitial atoms. An elementary act of migration of an interstitial atom during the formation of such a configuration takes place by the atom disintegrating and forming a new pair in the neighboring cell with the participation of one atom of the original pair. In pure metals the atoms in the dumbbell configuration are identical and, therefore, it makes no difference which of them makes the jump. The dumbbell configuration into which the impurity atom enters is asymmetric and, therefore, the probability of jumps by matrix and impurity atoms should be different. Precisely which atom predominantly makes the jump is determined by the energy of the final and initial states. Some possible situations are shown in Fig. 4, which gives a systematic representation of the successive displacement of the dumbbell pairs in the crystal of an alloy containing a substitutional impurity. The succession of jumps leads to inversion of the interstitial atoms: In variant *a* an interstitial atom of the matrix is replaced by an impurity atom, and vice versa in variant b. The first situation is of particular interest since it means that in an alloy containing mobile interstitial atoms, under certain conditions the substitutional solid solution is enriched with impurity atoms. There are conditions when, even with a low initial impurity content, the concentration of impurity atoms in the interstices may be equal to, or even exceed, the concentration of interstitial atoms of the matrix element. For this to happen it is necessary that the energetics of the migration process corresponds to variant.

Solving the general problem of the enrichment of a substitutional solid solution with impurity atoms should include analysis of the kinetics of the migration of atoms of both kinds over the lattice sites and interstices and their interaction with each other, with vacancies, and with sinks, which goes beyond the scope of the present article. In the first approximation, however, it is sufficient to consider a two-component system of the matrix (M)-impurity (I) type with a given concentration $C_i$ of interstitial atoms (it consists of the initial concentrations $C_M$ and $C_I$ of the interstitial atoms of the matrix and the impurity, respectively, and the concentration $C_{IM}$ of dumbbell configurations of the matrix-impurity type. For simplicity of consideration we can neglect the existence of vacancies and sinks as well as the interaction of interstitial atoms with each other. While undoubtedly distorting the quantitative estimates, such simplifications are no hindrance to a qualitatively faithful illustration of the principal aspects of the enrichment mechanism.

To this end, let us consider what the equilibrium concentrations $C^0_{IM}$ of the impurity in the interstices should be. Minimization with respect to the specific free energy of the crystal

$$F = E - TS = E_0 + \Delta E C_{IM} - T_{irr} S_c(C_I, C_i, C_{IM}), \tag{1}$$

where $\Delta E$ is the energy difference of concentrations *a*1 and b1 (see Fig. 4) and $S_c$ is the configurational entropy of a unit volume, allows us to obtain an equation for finding the equilibrium concentration $C^0_{IM}$ at the irradiation temperature:

$$C^0_{IM} = (C_i - C^0_{IM})(C_I - C^0_{IM}) \exp(-\Delta E / kT_{irr}). \tag{2}$$

If $\Delta E > 0$ in accordance with situation b (see Fig. 4), then it is more advantageous for the impurities to be located at the lattice sites, and their equilibrium concentration is low:

$$C^0_{IM} \approx C_i C_I \exp(-|\Delta E|/kT_{irr}). \tag{3}$$

If $\Delta E < 0$, then it is more advantageous for the impurities to be located in the interstices:

$$C^0_{IM} \approx C_i C_I \exp\left(+\frac{|\Delta E|}{kT_{irr}}\right)\left[1 + C_I \exp\left(+\frac{|\Delta E|}{kT_{irr}}\right)\right]^{-1}, C_i \ll C_I; \tag{4}$$

$$C^0_{IM} \approx C_i C_I \exp\left(+\frac{|\Delta E|}{kT_{irr}}\right)\left[1 + C_i \exp\left(+\frac{|\Delta E|}{kT_{irr}}\right)\right]^{-1}, C_I \ll C_i. \tag{5}$$

For $C_i \ll C_I$ in the state of equilibrium practically all of the interstices will be occupied by impurities (4). When the concentration of interstitial atoms in the crystal is higher than the impurity concentration (there is irradiation with high neutron fluence), practically all of the impurity atoms will go into the interstices (5). Enrichment of a solid substitutional solution, as seen from Eqs. (2), (4), and (5), increases as $T_{irr}$ decreases. The value of $\Delta E$ is determined by various effects: Disparity between the ionic radii of the elements of the impurity and the matrix, perturbation of the electronic states, etc. Calculation of this value is a complex, separate problem.



Declassified and Approved For Release 2013/02/15 : CIA-RDP10-02196R000800020001-4

Declassified and Approved For Release 2013/02/15 : CIA-RDP10-02196R000800020001-4

The experimental data given above are explained by the assumption that the atoms of the impurities studied, located as they are in the lattice sites and interstices of the bcc lattice of iron, cause crystal distortions which correspond to the case $\Delta E < 0$. If this assumption is correct, it must be admitted that the main contribution to $\Delta E$ is apparently made by local perturbations of the electronic state since phosphorus and antimony have a similar electronic structure. If the main contribution, as has been assumed [11], were to give a dimensional disparity, then one would have to expect a different embrittlement effect by atoms of phosphorus (smaller ionic radius than that of iron) and antimony (larger ionic radius than that of iron).

Inversion of interstitial atoms of type *a* (Fig. 4) explains how a substitutional solid solution can be enriched with impurities. The real situation differs from that considered by the fact that the crystal contains sinks and vacancies which halt the migration of interstitial atoms, as a result of which enrichment of a substitutional solid solution to a concentration corresponding to Eqs. (6) and (7) cannot, generally speaking, be attained.

In recombining with a vacancy, an interstitial atom returns to its normal position at a lattice site, where it remains until the next encounter with an interstitial atom of the solvent, as a result of which inversion can once again occur. Annihilating in a sink, an interstitial atom is left only with the possibility of moving (except for the case of displacing collision) and, therefore, the sinks will be enriched with impurities to the same concentration as the substitutional solution. Grain boundaries, dislocations, and complex radiation-induced defects serve as sinks for interstitial atoms. The defects are of particular interest because at a volume density of defects of about $10^{22}$ $m^{-3}$ [15], which is characteristic of iron at a fluence $\sim 10^{20}$ neutrons/$cm^2$, the mean diffusion length of an interstitial atom to complex defects is equal to half the distance between them (i.e., $\sim 10^{-8}$ m), appreciably less than the mean diffusion length to dislocations ($\sim 10^{-6}$ m) and to grain boundaries ($10^{-5}$-$10^{-4}$ m). Complex defects, therefore, are the main form of sinks for interstitial atoms in a real irradiated crystal. Enrichment with impurities is incapable of changing the efficiency of these defects as barriers to dislocations but does weaken the cohesive bond at the defect-matrix interface, thus intensifying the embrittlement effect. Since the defects are dispersed in the matrix, the relative fraction of the area they occupy in the cleavage plane when their average size is about 5 nm (50 Å) and their density is $\sim 10^{22}$ $m^{-3}$ [15] cannot exceed $10^{-5}$. Obviously, this explains the failure of attempts to detect segregation in fractures of specimens of irradiated steel by means of Auger spectroscopy [16].

The recovery of strength during annealing indicates that radiation-induced defects vanish as a result of heating. However, the zone of increased impurity concentration can be preserved at the site of annealed defects. This probably explains why steel rich in impurities (see Fig. 3) displays a residual irradiation-brittleness which is stable to higher annealing temperatures.

As is observed in experiments, there is no grain-boundary brittleness at a low irradiation temperature because of the high volume density of radiation-induced defects. With a rise in the irradiation temperature the defect density decreases substantially; therefore, the role of boundaries as sinks should grow and the contribution of grain-boundary effects to irradiation embrittlement increase.

## LITERATURE CITED


1. U. Potapova and J. Hawthorne, Nucl. Appl., 6, No. 1, 27 (1969).
2. L. Steele, Am. Soc. Test. Mater. Spec. Tech. Publ., No. 484, 164 (1971).
3. F. Smidt, Am. Soc. Test. Mater. Spec. Tech. Publ., No. 484, 169 (1971).
4. V. A. Nikolaev and V. I. Badanin, in: Radiation Effects in Changing the Mechanical Properties of Structural Materials and Methods of Studying Those Effects [in Russian], Naukova Dumka, Kiev (1977), p. 75.
5. V. A. Nikolaev and V. I. Badanin, Metally, 2, 126 (1975).
6. V. A. Nikolaev and V. I. Badanin, At. Energ., 37, No. 6, 491 (1974).
7. É. Gudremon, Special Steels [in Russian], Metallurgiya, Moscow (1966).
8. F. Smidt and J. Sprague, Am. Soc. Test. Mater. Spec. Tech. Publ., No. 529, 78 (1973).
9. I. V. Gorynin et al., in: Radiation Effects in Changing the Mechanical Properties of Structural Materials and Methods of Studying Those Effects [in Russian], Naukova Dumka, Kiev (1976), p. 59.
10. V. A. Nikolaev, V. V. Rybin, and V. I. Badanin, in: The Physics of Brittle Fracture, Proceedings of the Third All-Union Conference, II, Izd. Inst. Probl. Materialoved., Akad. Nauk UkrSSR, Kiev (1976), p. 89.
11. P. Okamoto and H. Wiedersich, J. Nucl. Mater., 53, 336 (1974).
12. R. Viswanathan and T. Sherlock, Met. Trans., 3, No. 2, 459 (1972).
13. V. A. Petrov, Fiz. Tverd. Tela, 18, 1290 (1976).
14. W. Glaeser and H. Wever, Phys. Status Solidi, 35, 367 (1969).
15. B. Eyre and A. Bartlett, Phil. Mag., 12, No. 116, 261 (1965).
16. L. Steele, Neutron Irradiation Embrittlement of Reactor Pressure Vessel Steels, IAEA, Vienna (1975).




Declassified and Approved For Release 2013/02/15 : CIA-RDP10-02196R000800020001-4

Declassified and Approved For Release 2013/02/15 : CIA-RDP10-02196R000800020001-4

# YIELDS OF SOME FRAGMENTS FROM FISSION OF $^{235}U$, $^{238}U$, AND $^{239}Pu$ BY NEUTRONS FROM SPECTRUM OF BR-1 FAST REACTOR

L. N. Yurova, A. V. Bushuev,
V. N. Ozerkov, V. V. Chachin,
A. V. Zvonarev, Yu. G. Liforov,
Yu. V. Koleganov, V. V. Miller,
and O. V. Gorbatyuk

UDC 539.173.8

The constants used in nuclear calculations of fast reactors at present are measured in integrated experiments for which the accuracy requirements are growing steadily. The error of determination of any parameter consists of the error of the measured values and the error of the data necessary for relating these values with the parameter being determined. This type of data includes the relative yields of fragments per fission event. Some of them can be used as reference values.

Data on the fission-fragment yield are necessary for determining most reactor parameters. To ensure the required accuracy of determination of these parameters, it is necessary to have fragment-yield data with an error of 1-1.5%. Fission-fragment yields can depend essentially on the energy of the neutrons causing the fission and this dependence must be taken into account both when using available data and when planning new experiments.

Consideration of published data [1, 2] permits the following conclusions: Much more extensive information about fission-fragment yields is available for thermal reactors than for fast reactors; the results are more exact and reliable, and the differences between data obtained by various authors in many cases go beyond the limits of the errors indicated above. This apparently can be attributed either to the fact that no account was taken of the systematic error or to the effect of differences in the neutron spectra in the reactors on which the measurements were performed. The present study was undertaken to obtain new, refined information about the fission-fragment yields.

Description of Technique. The absolute values of the fission-fragment yields for fission caused by fast neutrons can be obtained by measuring the ratio $Y_i^F/Y_i^T$ by using the well known values of the fission-fragment yields for fission by thermal neutrons.

The following formula is used:

$$Y_{ij}^{F} = Y_{ij}^{T} \frac{I_{\gamma ij}^{F}}{I_{\gamma ij}^{T}} \frac{F_j^T}{F_j^F},$$

where $I_{\gamma ij}^F/I_{\gamma ij}^T$ is the ratio of the intensity of the $\gamma$ rays of the i-th fragment formed during the fission of the j-th isotope by fast and thermal neutrons and $F_j^T/F_j^F$ is the ratio of the number of fissions of the isotope.

In this case it is not necessary to determine the efficiency of the recording systems. By a suitable choice of the scheme for the experiment it is possible to reduce to a minimum the inclusion of auxiliary reference nuclear data. The error of determination of $Y_j^F$ will be determined mainly by the error of the thermal yields used.

## Experimental Part

Irradiation Conditions. The core of the BR-1 fast reactor with a volume of about 1 liter is filled with rods of metallic plutonium canned in stainless steel. The maximum density of the neutron flux in the center of the core was $10^{10}$ neutrons/cm$^2$·sec. The reactor was furnished with a graphite thermal column measuring 1000 × 1000 × 1000 mm.

Translated from Atomnaya Énergiya, Vol. 47, No. 1, pp. 26-28, July, 1979. Original article submitted June 26, 1978; revision submitted December 11, 1978.



0038-531X/79/4701-0528$07.50 © 1980 Plenum Publishing Corporation

Declassified and Approved For Release 2013/02/15 : CIA-RDP10-02196R000800020001-4

Declassified and Approved For Release 2013/02/15 : CIA-RDP10-02196R000800020001-4

TABLE 1. Experimental Ratios of Fragment Yields in Fission of $^{235}U$, $^{239}Pu$, and $^{238}U$ by Fast and Thermal Neutrons

| Fission fragment | $Y^F_{235U}/Y^T_{235U}$ | $Y^F_{239Pu}/Y^T_{239Pu}$ | $Y^F_{238U}/Y^T_{235U}$ |
|---|---|---|---|
| $^{91m}Y$ | 1,005±0,015 | 1,081±0,022 | 0,693±0,028 |
| $^{97}Zr$ | 1,054±0,019 | 1,047±0,019 | 0,945±0,027 |
| $^{97}Nb$ | 1,074±0,016 | 1,047±0,019 | 0,990±0,026 |
| $^{99}Mo$ | 1,044±0,016 | 1,031±0,014 | 1,168±0,026 |
| $^{131}I$ | 1,216±0,028 | 1,112±0,023 | 1,008±0,031 |
| $^{132}Te$ | 1,172±0,017 | 1,015±0,017 | 1,203±0,023 |
| $^{133}I$ | 1,053±0,018 | 0,984±0,016 | 1,071±0,023 |
| $^{135}Xe$ | 1,059±0,015 | 0,968±0,020 | 1,156±0,030 |
| $^{140}La$ | 0,980±0,017 | 1,045±0,024 | 0,964±0,019 |
| $^{143}Ce$ | 0,943±0,013 | 0,988±0,017 | 0,808±0,017 |
| $^{103}Ru$ | 1,03±0,03 | 0,97±0,03 | |
| $^{147}Nd$ | 0,96±0,04 | 0,96±0,04 | |
| $^{95}Zr$ | 0,96±0,05 | 0,98±0,03 | |
| $^{95}Nb$ | 0,97±0,04 | 0,95±0,03 | |

Specimens. In the experiments we used foils of plutonium and uranium enriched to 90% $^{235}U$, fabricated from uranium dioxide or plutonium and with ends covered with thin (thickness ~10 μm) aluminum foil. The total quantity of fissionable material in the foils was ~ 1 mg/cm$^2$. Calculated estimates showed that the perturbation of the neutron field by the insertion of such specimens into the thermal column is < 0.5%. The specimens were placed in a cylindrical aluminum capsule (diameter 3 mm, height 15 mm, and thickness of side walls 0.5 mm).

Measurement of Ratio of Number of Fissions by Track Detectors. The track detector used in the experiment consisted of a polished glass disk with a diameter of 7 mm and a thickness of 1 mm. The track detector and the layer-radiator were placed inside the experimental capsule. The irradiation conditions (reactor power and irradiation time) were chosen so that the number of tracks on the glass did not exceed $2 \cdot 10^3$. A smaller number of tracks worsened the statistical accuracy whereas a larger number increased the systematic error. To avoid the latter error, the tracks were counted several times by different operators. To eliminate the errors due to the determination of the number of nuclei in the active layers we employed the following procedure: One capsule was placed in the thermal column, and another, in the center of the reactor core. They changed places in the next irradiation. This made it possible to eliminate errors due to inaccuracies in the determination of the nuclei, power, irradiation time, etc.

γ-Ray Spectroscopy. The γ-ray spectra of the specimens irradiated were measured with a system consisting of a Ge(Li) detector with cooling of the first stage of the preamplifier, the main amplifier, and the 4096-channel pulse-height analyzer. The energy resolution of the measuring system was 1.69 keV at $E_\gamma$ = 1333 eV. Measurement of the γ-ray spectra of the irradiated specimens began 8 h after completion of irradiation and was carried out for 4-6 days.

## Error Estimation

The error of determination of $Y_i^F$ consists of the following components: the error arising during irradiation, the error arising during measurements of the intensity of γ rays and counting of tracks, and the error due to the introduction of various corrections.

Errors Arising during Irradiation. These errors are due to the different positions of the indicators and track detectors (the maximum difference in the positions could reach 2 mm; special experiments showed that the correction does not exceed 1.000 ±0.005) and the local distrubance of the neutron spectrum in the experimental part during irradiation of the indicators and track detectors (it was established experimentally that the correction does not exceed 1%).

Errors in Measurements of γ-Ray Intensity and Track Counting. The γ-ray spectrum of each specimen was measured 10-12 times. The statistical accuracy of determination of the ratio was better than 1%. The conditions of the measurements were chosen so that the integrated load did not exceed 5000 counts/sec. With a resolving time of 25 μsec in the measuring channel this guaranteed there would be no counting errors. In counting the number of fissions we made 18-20 measurements with each pair of indicators. The accuracy of the data over the entire series is 1.3%.



Declassified and Approved For Release 2013/02/15 : CIA-RDP10-02196R000800020001-4

Declassified and Approved For Release 2013/02/15 : CIA-RDP10-02196R000800020001-4

TABLE 2. Absolute Values of Fragment Yields in Fission of $^{235}U$, $^{239}Pu$, and $^{238}U$ by Neutrons of BR-1 Spectrum, %

| Fission fragment | $^{235}U$ | | $^{239}Pu$ | | $^{238}U$ |
|---|---|---|---|---|---|
| | present paper | $Y^T_{235}$ [2] | present paper | $Y^T_{239}$ [2] | present paper |
| $^{91m}Y$ | 5,96±0,14 | 5,93±0,11 | 2,75±0,08 | 2,54±0,05 | 4,11±0,12 |
| $^{97}Zr$ | 6,36±0,16 | 6,03±0,10 | 5,85±0,15 | 5,59±0,10 | 5,70±0,23 |
| $^{97}Nb$ | 6,48±0,15 | 6,03±0,10 | 5,85±0,15 | 5,59±0,10 | 5,97±0,20 |
| $^{99}Mo$ | 6,40±0,12 | 6,13±6,06 | 6,52±0,21 | 6,32±0,20 | 7,17±0,17 |
| $^{131}I$ | 3,43±0,10 | 2,82±0,07 | 4,16±0,13 | 3,74±0,09 | 2,84±0,11 |
| $^{132}Te$ | 4,92±0,13 | 4,20±0,09 | 5,31±0,15 | 5,23±0,12 | 5,05±0,16 |
| $^{133}I$ | 7,11±0,20 | 6,75±0,16 | 6,81±0,22 | 6,92±0,19 | 7,23±0,23 |
| $^{135}Xe$ | 6,99±0,20 | 6,61±0,10 | 7,44±0,29 | 7,69±0,26 | 7,62±0,28 |
| $^{140}La$ | 6,23±0,13 | 6,36±0,06 | 5,84±0,16 | 5,59±0,09 | 6,13±0,13 |
| $^{143}Ce$ | 5,61±0,11 | 5,95±0,08 | 4,46±0,10 | 4,51±0,06 | 4,81±0,12 |
| $^{103}Ru$ | 3,22±0,10 | 3,12±0,04 | 6,65±0,32 | 6,95±0,29 | — |
| $^{147}Nd$ | 2,16±0,10 | 2,25±0,04 | 2,05±0,10 | 2,13±0,07 | — |
| $^{95}Zr$ | 6,24±0,33 | 6,50±0,09 | 4,91±0,17 | 5,01±0,08 | — |
| $^{95}Nb$ | 6,30±0,30 | 6,50±0,03 | 4,75±0,17 | 5,01±0,08 | — |

Errors Due to the Introduction of Corrections. The correction for the contribution of $^{238}U$ and $^{240}Pu$ fission to the activity of uranium and plutonium specimens was calculated. The corrections did not exceed 1.016 and 1.015, respectively.

## Analysis of the Results

Table 1 gives the experimental values of $Y_i^F/Y_i^T$. The absolute values of the yields were obtained on the basis of the data of Table 1 and recommended thermal-yield data taken from [2] (Table 2). Valuable information is given by measurements of the functionals $\bar{\sigma}_c^{238}$, $\bar{\sigma}_f^{238}/\bar{\sigma}_f^{235}$, and $\bar{\sigma}_f^{239}/\bar{\sigma}_f^{235}$, characteristic of the ratio of the rates of the principal processes and the neutron spectrum. Such measurements are most often carried out by calibrating the indicators in a thermal neutron flux. In this case it is necessary to know the value of $Y_i^F/Y_i^T$. Analysis of the conditions of experiments on critical assemblies and nuclear data on fragments shows that the values of the functionals can be estimated most accurately if either $^{99}Mo$, $^{140}La$, or $^{143}Ce$ is chosen as the fragment-monitor of the fission reaction.

Let us take a closer look at the available data on the yield of these fragments in systems with an energetic neutron spectrum.

The published data on the $^{99}Mo$ yield are quite contradictory. As the mean energy of the neutrons causing the fission, this yield is observed to decrease as well as to increase. In this situation, it is not possible to recommend $^{99}Mo$ as an indicator of the reaction rate of fission of $^{235}U$ or $^{239}Pu$. It should be noted that because the spectrum contains a number of background lines that are close in energy, it is a difficult problem to measure intensity of the $\gamma$ rays emitted by $^{99}Mo$ without chemically isolating it. Accurate separation of the effect in this case requires the use of apparatus with maximum resolution and this was done in the present study.

The $^{140}La$ yield found in the present paper for the fission of $^{235}U$ and $^{239}U$ is in good agreement with the data of papers by other authors. The weak dependence of the $^{140}La$ yield on the neutron energy in the fission of $^{235}U$ makes it appropriate to use it as an indicator of the fission rate. In this case, the variation in this yield during the passage from the thermal spectrum to the spectrum of fission neutrons does not exceed 2%.

In the fission of $^{239}Pu$ the $^{140}La$ yield rises with the neutron energy. In the limiting case (spectrum of fission neutrons) the yield increases by 4.5% in comparison with the case of thermal neutrons. When $^{140}La$ is used as an indicator of the $^{239}Pu$ fission rate, therefore, the appropriate ratio $Y^F_{La}/Y^T_{La}$ can be used.

The $^{143}Ce$ yield in the fission of $^{235}U$ diminishes as the neutron energy increases. The ratio of the $^{143}Ce$ yield for the spectrum of fission neutrons to the yield for the thermal spectrum is 0.943 ±0.013. As in the preceding case, $^{143}Ce$ can be used as an indicator of the $^{235}U$ fission rate only with the appropriate choice of $Y^F_{Ce}/Y^T_{Ce}$. In the fission of $^{239}Pu$ the $^{143}Ce$ yield remains practically constant when the neutron spectrum is changed from thermal to the fission spectrum, i.e., within the limits of the error of measurement it may be assumed that $Y^F_{Ce}/Y^T_{Ce} = 1$.

## LITERATURE CITED

1. W. Walker, in: Proceedings of the Second International Conference on Nuclear Data for Reactors, Helsinki, June 15-19 (1970), IAEA-CN-26/3.
2. W. Walker, in: Proceedings of the Panel on Fission Product Nuclear Data, Bologna, Nov. 26-30 (1973), Rev. paper No. 11a.



Declassified and Approved For Release 2013/02/15 : CIA-RDP10-02196R000800020001-4

Declassified and Approved For Release 2013/02/15 : CIA-RDP10-02196R000800020001-4

# NEUTRON YIELD OF ($\alpha$, n) REACTION ON OXYGEN

V. I. Bulanenko

UDC 550.35:537.591

The particular interest taken in the ($\alpha$, n) reaction on oxygen is related to the fact that the main nuclear fuel in present-day atomic power plants with Soviet VVÉR, RBMK, and BN reactors and similar foreign reactors is uranium oxide. Spent fuel from these power reactors is characterized by quite intense neutron radiation of $\sim(10^5$–$10^6)$ neutrons/sec·kg $UO_2$ [1, 2], which is caused by the ($\alpha$, n) reaction on oxygen and the spontaneous fission of heavy nuclei. Whereas for reactors of the VVÉR (water-moderated–water-cooled power reactor) type the contribution of neutrons from the ($\alpha$, n) reaction to the total yield is relatively low (~10-20%), in the case of BN (fast-neutron) reactors this component makes the predominant contribution of up to 85-95%. Hence the natural interest in this reaction when developing analytic means for monitoring fissionable materials and ensuring radiation shielding of oxide fuel.

Notwithstanding quite long research, the data available at this time are very incomplete and two basic aspects of the ($\alpha$, n) reaction on oxygen remain not very well investigated:

1) the dependence of the cross section $\sigma(E)$ of the reaction in the energy range from 5.25 to 10 MeV;

2) the relative contribution of neutrons from the $^{17}O(\alpha, n)^{20}Ne$ reaction to the total neutron yield and reliable reference values of the neutron yield q from a thick target at various $\alpha$-particle energies.

Experimental reference values of the neutron yield q from a thick target of natural oxygen were obtained in [3-8], mainly at two energies $E_\alpha = 5.304$ MeV ($^{210}Po$) and $E_\alpha = 7.687$ MeV ($^{214}Po$) [9], these values being q = 0.07 ±0.01 and q = 0.56 ±0.03, respectively, per $10^6$ $\alpha$ particles. In this case only the statistical error is shown whereas the possible systematic error is 10-15% [4]. The foregoing values were obtained with a large error. Nevertheless, they were the basis for obtaining a power law, with certain assumptions, for the dependence of q (neutrons/$10^6$ $\alpha$ particles) on the energy $E_\alpha$ (MeV) for oxygen in the form [4]

$$q(E_\alpha) = 6.36 \cdot 10^{-6} \cdot E_\alpha^{5,58}. \quad (1)$$

The relation obtained is of a qualitative nature and, as shown in [10], the true values may differ by 20% or more in one direction or the other. Nor does the semiempirical formula proposed in [11] accord with the real picture. Therefore, for several years the efforts of many experimenters have been aimed at obtaining an exact value of the neutron yield from the ($\alpha$, n) reaction for $^{238}PuO_2$ [12-19], which is used very extensively to solve various practical problems. According to these papers, the total neutron yield lies within the limits $(1.5\text{-}2.2) \cdot 10^4$ neutrons/sec·g $^{238}Pu$. The most exact measurements, with an error of 1%, were made by Bair and Butler [12], who measured the total neutron yield for high-purity $^{238}PuO_2$ of low mass and, in addition to the ordinary systematic corrections, introduced a correction for the effects of multiplication and absorption by the container as well as differences in the energy spectra of the standard and the source under study. In agreement with the value obtained in [12] are the results of [13] and the special communication of Anderson [14], which determined the neutron yield to within better than 5%. The weight mean value of the neutron yield from these measurement is $(1.706 \pm 0.019) \cdot 10^4$ neutrons/sec·g $^{238}Pu$.

Basing ourselves on this value, we get one more reference q. A constituent component of the neutron yield is the spontaneous fission of $^{238}Pu$, whose calculated value is $(2.62 \pm 0.10) \cdot 10^3$ neutrons/sec·g $^{238}Pu$. This is in accord with the experimental values of [16-19]. The weighted mean half-life of spontaneous fission is calculated from the data of [20-22] and is equal to $T_{1/2}^{SF} = (4.68 \pm 0.10) \cdot 10^{10}$ yr. A value of $\bar{\nu}_{SF} = 2.21 \pm 0.07$ [23] was also used for the mean number of neutrons per fission event. Thus, the neutron yield of the ($\alpha$, n) reaction for $^{238}PuO_2$ was taken to be equal to $(1.444 \pm 0.022) \cdot 10^4$ neutrons/sec·g $^{238}Pu$. If a correction is introduced for the mass and chemical composition [5] with account for the ionization losses of $\alpha$ particles in oxygen [24] and $PuO_2$ [25] and if a recalculation is made with the activity according to the half-life [26], then we have q = 0.078 ±0.002. Here we have taken account of all the components of error, the largest contribution coming from

Translated from Atomnaya Énergiya, Vol. 47, No. 1, pp. 28-31, July, 1979. Original article submitted July 17, 1978.

0038-531X/79/4701-0531 $07.50 © 1980 Plenum Publishing Corporation



Declassified and Approved For Release 2013/02/15 : CIA-RDP10-02196R000800020001-4

Declassified and Approved For Release 2013/02/15 : CIA-RDP10-02196R000800020001-4

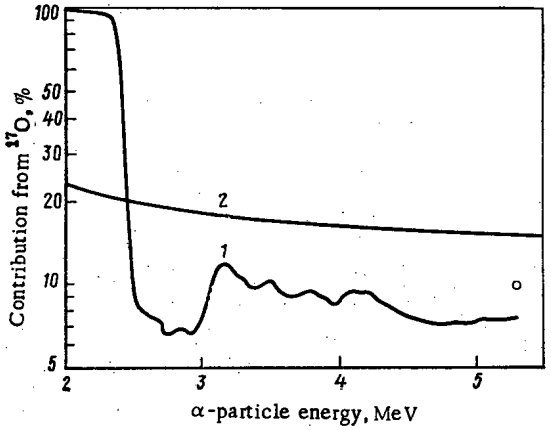


Fig. 1

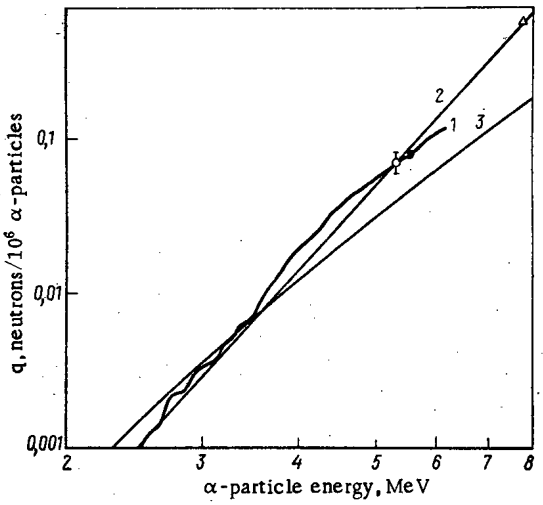


Fig. 2

Fig. 1. Relative contribution of reaction ($\alpha$, n) on $^{17}O$, 0.0307 $q_{17}$ (0.0307 $q_{17}$ + 0.2039 $q_{18}$), to total neutron yield vs $\alpha$-particle energy: 1) calculations of this paper; 2) calculations according to data of [11]; ○) experimental value taken from [6].

Fig. 2. Neutron yield for thick oxygen target vs $\alpha$-particle energy, q = (0.2039$q_{18}$ + 0.0307$q_{17}$): 1) calculations of present paper; 2) calculations from formula (1); 3) calculations from formula of [11]. Experimental values: ●) present paper; ○, △) data of [3] and [4], respectively.

the indeterminacy of the ionization losses. The value obtained for q corresponds to $^{238}Pu$ $\alpha$-particle spectrum, which consists of two lines: 5.499 MeV (72.13%) and 5.456 MeV (27.87%) [9, 26]. Since these energies differ by 43 keV, we can use the mean value of the energy, 5.487 MeV. Such a substitution gives an additional error, not exceeding 0.5% in the worst case.

The weighted mean value of q is the most exact of those obtained earlier and, therefore, it can serve as the most reliable base for normalization of the calculated neutron yields.

Taking the contribution of the reaction $^{17}O(\alpha, n)^{20}Ne$ to the total neutron yield into account, we note that natural oxygen consists of a mixture of three isotopes. The results of many measurements made with oxygen both enriched and impoverished in $^{17}O$ and $^{18}O$ [6, 13, 18] indicate that the ($\alpha$, n) reaction occurs primarily on $^{18}O$ (reaction threshold 0.8536 MeV), although the ($\alpha$, n) reaction on $^{17}O$ is exoergic. The contribution of the reaction $^{17}O(\alpha, n)^{20}Ne$ to the total yield was determined experimentally (~10%) at $E_\alpha$ = 5.304 MeV [6] but not at other energies.

Curves of the energy dependence of the ($\alpha$, n) reaction cross section for $^{17}O$ [27] and $^{18}O$ [27-30] were obtained experimentally. In the case of both isotopes the $\sigma(E)$ curve displays a complex resonance structure which has been studied only at low energies $1.0 \leq E_\alpha < 5.25$ MeV. These cross sections are used to calculate the neutron yield from a thick target as a function of the $\alpha$-particle energy from

$$q(E_\alpha) = N \int_{B_{thr}}^{E_\alpha} \frac{\sigma(E)}{\left(-\frac{dE}{dx}\right)} dE, \qquad (2)$$

where $-dE/dx$ is the ionization loss of $\alpha$-particles in oxygen (MeV/cm), N is the number of atoms per unit volume of the target (atom/$cm^3$), and $B_{thr}$ is the threshold of the ($\alpha$, n) reaction (MeV). The most exact values of $-dE/dx$ were taken for the calculation of $q(E_\alpha)$ [24]. The results of calculation of the relative contribution of neutrons from the reaction $^{17}O(\alpha, n)^{20}Ne$ to the total neutron yield are given in Fig. 1. These calculations show that $^{17}O$ makes a relative contribution which changes little with the energy, except for the region below 2.5 MeV, where the $^{17}O$ contribution predominates; this is attributed to the threshold character of the $^{18}O(\alpha, n)^{21}Ne$ reaction. The calculated contribution at $E_\alpha$ = 5.304 MeV is 7.6 ± 2.7% which is in agreement with the data of [6] within the limits of error. It must be said that calculation from the data of [11] does not convey the detailed behavior of the contribution with an energy resulting from resonances of the cross section $\sigma(E)$. Moreover, the formula in [11] gives a clearly overestimated yield ratio for the two oxygen isotopes, $q_{17} = (1.2\text{-}1.5)q_{18}$, which is at variance with the values of the cross section for the ($\alpha$, n) reaction [27-30] and our calculations, which give $q_{17} = (0.4\text{-}0.5)q_{18}$.



Declassified and Approved For Release 2013/02/15 : CIA-RDP10-02196R000800020001-4

Declassified and Approved For Release 2013/02/15 : CIA-RDP10-02196R000800020001-4

Figure 2 gives the calculated $q(E_\alpha)$ curve for a natural mixture of oxygen isotopes. Since the cross section $\sigma(E)$ for both isotopes was measured to within no better than 25%, the calculated values of q were normalized to the value obtained experimentally with a lower error. Unlike [10], in the present paper the neutron yields were normalized to the value q = 0.078 at $F_\alpha$ = 5.487 MeV. In doing so, we took account of the behavior of $q(E_\alpha)$ in the energy range 4.5-5.3 MeV. Needless to say, any extrapolation is arbitrary to a considerable degree but in the given case is justified. It follows from Fig. 2 that normalization to q = 0.070 [3] and to the calculated q = 0.078 gives practically the same result, notwithstanding the fact that the two normalizations correspond to different $\alpha$-particle energies. As is seen from Fig. 2, calculations by Eq. (1) and the data of [11] do not convey the true behavior of $q(E_\alpha)$.

Analysis of the $q(E_\alpha)$ obtained shows that the energy dependence of the neutron yield q can be represented by a power law only within narrow, definite ranges:

$$q(E_\alpha) = \begin{cases} 1.26 \cdot 10^{-4} \cdot E_\alpha^{3,77} & \text{for} \quad 4.4 \leqslant E_\alpha < 6.1; \\ 8.46 \cdot 10^{-6} E_\alpha^{5,58} & \text{for} \quad 3.6 \leqslant E_\alpha < 4.4; \\ 3.71 \cdot 10^{-6} E_\alpha^{6,16} & \text{for} \quad 2.0 \leqslant E_\alpha < 3.6. \end{cases} \tag{3}$$

Equation (3) allows the neutron yield to be determined to within ~3% for $E_\alpha \geq 3.6$ MeV and to within less than 10% for $E_\alpha < 3.6$ MeV.

The aspects pointed out above require further careful experimental investigations. In particular, it is necessary to measure the neutron yield at higher $\alpha$-particle energies, e.g., as from $^{242}CmO_2$. A decisive role will undoubtedly be played by further measurements of the cross section for the $(\alpha, n)$ reaction for $E_\alpha >$ 5.25 MeV for both oxygen isotopes.

In conclusion, the author wishes to express his gratitude to É. M. Tsenter whose discussion stimulated the appearance of the present paper and to V. V. Frolov for fruitful discussion of the results.

## LITERATURE CITED

1. H. Balley et al., Nucl. Technol., 17, 193 (1973).
2. O. D. Bakumenko et al., At. Energ., 44, No. 2, 140 (1978).
3. G. V. Gorshkov et al., 13, No. 1, 65 (1962).
4. G. V. Gorshkov, V. A. Zyabkin, and O. S. Tsvetkov, At. Energ., 13, No. 5, 475 (1962).
5. G. V. Gorshkov et al., Natural Neutron Background of Atmosphere and Earth's Crust [in Russian], Atomizdat, Moscow (1966).
6. I. A. Serdyukova, A. G. Khabakhpashev, and É. M. Tsenter, Izv. Akad. Nauk SSSR, Ser. Fiz., 21, 1017 (1957).
7. A. G. Khabakhpashev, At. Energ., 7, No. 1, 71 (1959).
8. G. Ben-David, Neutron Dosimetry, 2, 407, IAEA, Vienna (1963).
9. A. Rytz, Atomic Data and Nuclear Data Tables, Vol. 12, Academic Press, New York (1973), p. 479.
10. É. M. Tsenter and A. B. Silin, At. Energ., 19, No. 1, 48 (1965).
11. L. N. Korzhnov, in: Problems of Dosimetry and Radiation Protection [in Russian], Atomizdat, Moscow, No. 9 (1969), p. 44.
12. J. Bair and H. Butler, Nucl. Technol., 19, 202 (1973).
13. V. A. Arkhipov et al., At. Energ., 32, No. 4, 310 (1972).
14. M. Anderson and R. Neff, Nucl. Appl., 7, 62 (1969).
15. T. R. Herold, Nucl. Appl., 4, 19 (1968).
16. W. Rutherford, C. Huffman, and D. Coffey, Nucl. Appl., 3, 366 (1967).
17. L. Millins and J. Leary, Nucl. Appl., 6, 287 (1969).
18. L. Porter and M. Thomson, Inorg. Nucl. Chem. Lett., 5, 129 (1969).
19. J. Burnback, G. Matlack, and G. Metz, Trans. Am. Nucl. Soc., 11, 457 (1968).
20. V. M. Gorbachev, Yu. S. Zamyatnin, and A. A. Lbov, Principal Characteristics of Heavy Elements. Handbook [in Russian], Atomizdat, Moscow (1975).
21. J. Hastings and W. Strohm, J. Inorg. Nucl. Chem., 34, 25 (1972).
22. R. Gay and R. Sher, in: Proceedings of the Conference on Nuclear Cross Sections and Technology, Washington, D. C., Vol. 11 (1975), p. 587.
23. V. M. Gorbachev, Yu. S. Zamyatnin, and A. A. Lbov, Interaction of Radiation with Heavy-Element Nuclei and Nuclear Fission (Handbook) [in Russian], Atomizdat, Moscow (1976).



Declassified and Approved For Release 2013/02/15 : CIA-RDP10-02196R000800020001-4

Declassified and Approved For Release 2013/02/15 : CIA-RDP10-02196R000800020001-4

24. L. Northcliffe and R. Schilling, Nucl. Data Tables, Vol. 7, Academic Press, New York, Nos. 3-4 (1970), p. 223.
25. V. Nitzki and H. Matzke, Phys. Rev. B, 8, 1894 (1973).
26. S. A. Baranov, A. G. Zelenkov, and V. M. Kulakov, At. Energ., 41, No. 5, 342 (1976).
27. J. Bair and F. Haas, Phys. Rev. C, 7, 1356 (1973).
28. J. Bair and H. Willard, Phys. Rev., 128, 299 (1962).
29. G. Chouraque et al., Le J. Phys., 31, 249 (1970).
30. T. Bonner et al., Phys. Rev., 102, 1348 (1956).

# INSTRUMENTAL NEUTRON-ACTIVATION ANALYSIS OF SUBMILLIGRAM AMOUNTS OF GEOCHEMICAL SAMPLES

V. I. Drynkin, E. V. Karus,
V. D. Nartikoev, B. V. Belen'kii,
and A. L. Kerzin

UDC 543.53

Multielement analysis of small amounts of substances (1-5 mg) is becoming an increasingly acute problem in geochemical investigations. This is related to the necessity of analyzing monomineral fractions right down to individual grains, inclusions in crystals, etc. Moreover, frequently analyses are made of unique samples, large quantities of which cannot be obtained from the material under study (lunar soil samples, core samples from very deep boreholes, etc.), and it is desirable to preserve them for other analyses.

In the course of analysis of submilligram samples there arise problems which are usually not considered in instrumental neutron-activation analysis (INAA).

1. Choice of method of packaging ensuring that there will be no introduction of elements from the packaging material to the sample and that the samples will be protected even during long irradiation in a nuclear reactor (100-200 h).

2. Choice of calibration system guaranteeing that reliable results are obtained with least possible error.

Many methods of packaging samples for irradiation in a nuclear reactor (polythylene film, quartz ampuls; phenol-formaldehyde resin) when analyzing submilligram amounts are of little use [1]. The point is that a small sample requires subsequent repackaging in an inactive material since the activity of an impurity in the packaging material is comparable with the activity of the sample. Moreover, under irradiation for longer than 60 h polyethylene film decomposes (because of the simultaneous action of thermal and radiation heating up) and forms a single mass with the material of the sample, a mass which cannot then be separated. Packaging samples in quartz ampuls also makes repackaging practically impossible since, because of the extremely small size of the individual grains of the minerals, packaging and repackaging of samples must be carried out with a binocular instrument.

Aluminum foil is a packaging material which satisfies practically all the requirements. It does not break down even under long irradiation. It is a simple matter to package samples in it and then to extract them, and no special procedures are required.

A question arises, however, as to the possible contamination of the substance of the sample during irradiation by the introduction of some elements from the packaging material. In view of this we performed a special experiment, the material for which should satisfy the following requirements:

– have a weakly activated matrix;

– have the lowest possible level of impurity-element content ($10^{-7}$-$10^{-9}$ wt.%) so that the activity from elements from the packaging material and residual reagents introduced into the sample during irradiation could be detected and estimated quantitatively against their background;

– have a large absorption surface (1-2 $cm^2$) for accumulating a sufficient amount of the extraneous material for estimation;

Translated from Atomnaya Énergiya, Vol. 47, No. 1, pp. 31-34, July, 1979. Original article submitted September 11, 1978.

 0038-531X/79/4701-0534$07.50 © 1980 Plenum Publishing Corporation

Declassified and Approved For Release 2013/02/15 : CIA-RDP10-02196R000800020001-4

Declassified and Approved For Release 2013/02/15 : CIA-RDP10-02196R000800020001-4

TABLE 1. Results of Estimation of Level of Possible Contamination from Packaging Material

| Material | Na × 10⁻⁴, % | | | Fe × 10⁻⁶, % | | | Cr × 10⁻⁶, % | | | Au × 10⁻⁸, % | | | Sb × 10⁻⁸, % | | |
|---|---|---|---|---|---|---|---|---|---|---|---|---|---|---|---|
| | 1 | 2 | 3 | 1 | 2 | 3 | 1 | 2 | 3 | 1 | 2 | 3 | 1 | 2 | 3 |
| Synthetic quartz | 1,9 | 1,9 | — | 0,43 | 0,27 | 0,16 | 15,7 | 11,3 | 4,4 | 0,75 | 0,05 | 0,70 | 12,0 | 5,5 | 6,5 |
| Aluminum foil | — | — | — | 1100 | — | — | 2500 | — | — | 8,6 | — | — | 390 | — | — |
| Material | Sc × 10⁻⁸, % | | | Co × 10⁻⁸, % | | | Zn × 10⁻⁸, % | | | Hf × 10⁻⁸, % | | | La × 10⁻⁶, % | | |
| | 1 | 2 | 3 | 1 | 2 | 3 | 1 | 2 | 3 | 1 | 2 | 3 | 1 | 2 | 3 |
| Synthetic quartz | 0,6 | 0,5 | 0,1 | 4,9 | 4,4 | 0,5 | 10,4 | 6,2 | 4,2 | 0,9 | 0,84 | 0,06 | 0,4 | 0,4 | — |
| Aluminum foil | 575 | — | — | 1950 | — | — | 13000 | — | — | 72,5 | — | — | 31,5 | — | — |

1) Mean content of element in quartzes before etching in $HNO_3$.
2) Same, after etching in $HNO_3$.
3) Difference between 1 and 2, abs. %.

– have a surface which can be easily treated to remove contamination.

Preliminary studies on various materials showed that the material which best satisfies the above requirements is synthetic quartz in which the amount of various impurities is at a level of $10^{-7}$-$10^{-9}$ wt.% ($n \cdot 10^{-4}$% Na and $n \cdot 10^{-5}$% Cr).

Before irradiation, ten wafers of synthetic quartz weighing 0.5-1.2 g and with a surface of ~1-2 $cm^2$ were etched for an hour in a $HNO_3$ (1:1) solution and then washed in twice-distilled water and dehydrated alcohol, after which they were packaged in aluminum foil, also pretreated with alcohol and twice-distilled water, and irradiated for 100 h in a flux of $1.2 \cdot 10^{13}$ neutrons/$cm^2 \cdot$sec in a TVR reactor.

Small tablets of phenol-formaldehyde resin (PFR) weighing 1-2 mg with various contents of trace elements were used as a standard [2]. The absolute content of elements in the references made it possible to calculate a very low concentration of these elements in irradiated synthetic quartz. At the same time, the small size of the standards and the relatively high concentration of trace elements in them allowed the possible contamination from the foil to be neglected.

The irradiated samples were divided into two batches of five samples each. The induced activity was measured in two cycles, cooling for 3 and 10 days, according to the following scheme:

– the induced activity of the quartz freed from the foil was measured;

– the measured samples were etched in diluted $HNO_3$ and then washed in water;

– the induced activity of the same samples was remeasured.

In the second cycle we also measured the induced activity of the aluminum foil. In the first cycle we determined the concentration of Na, Cr, and Au; in the second cycle we determined the concentration of Fe, Cr, Au, Sb, Sc, Co, Zn, Hf, and La. The results of the measurements are given in Table 1. Upon considering the data we can come to the following conclusions:

– the level of contamination is insignificant for Sc, Co, Hf, and La with a content of $n \cdot 10^{-7}$%, Na with a content of $n \cdot 10^{-4}$%, and Fe and Cr with a content of $n \cdot 10^{-5}$%.

– for Au the content decreases by a factor of tens at a level of $n \cdot 10^{-9}$%, which is explained by the presence of contamination, including some from the reagents;

– the level of the Au and Sb content at which the effect of the contamination is insignificant is estimated at $n \cdot 10^{-7}$ wt.%, where $n \geq 4$;

– the impurity content in the foil is 2-4 orders of magnitude higher than the content of the same elements in the synthetic quartz prior to etching.

The second group of problems which arise in the analysis is related to the creation of a system of standards. The point is that the nominal data of available standard composition samples (SCS) of both domestic



Declassified and Approved For Release 2013/02/15 : CIA-RDP10-02196R000800020001-4

Declassified and Approved For Release 2013/02/15 : CIA-RDP10-02196R000800020001-4

TABLE 2. Results of Estimation of Nonuniformities of Distribution of Elements in Standard Samples of Rocks (weighed amounts of 1-3 mg)

| Standard | Na | | | K | | | Mn | | | Fe | | | Cr | | | Sc | | |
|---|---|---|---|---|---|---|---|---|---|---|---|---|---|---|---|---|---|---|
| | Cc, % | $\Delta_n$ | σ | Cc, % | $\Delta_n$ | σ | Cc, % | $\Delta_n$ | σ | Cc, % | $\Delta_n$ | σ | Cc, $10^{-4}$ % | $\Delta_n$ | σ | Cc, $10^{-4}$ % | $\Delta_n$ | σ |
| SGD-1A | 2,09 | 1,9 | 3,3 | 2,46 | 1,6 | 10,9 | 0,13 | 7,7 | 7,6 | 8,03 | 1,4 | 4,3 | 56 | 11,5 | 6,9 | 27 | 11,1 | 3,6 |
| SG-1A | 4,05 | 1,0 | 8,3 | 3,44 | 1,5 | — | 0,15 | 2,6 | — | 1,58 | 3,5 | 17,3 | 12 | 25,0 | 34,3 | 5 | 20,0 | 10,3 |
| ST-1A | 1,58 | 1,0 | 4,7 | 0,58 | 2,1 | 3,1 | 0,17 | 3,0 | 9,3 | 10,7 | 1,5 | 8,7 | 140 | 7,1 | 12,5 | 43 | 11,6 | 15,0 |
| BCR-1 * | 2,42 | — | 4,4 | 1,37 | — | 2,6 | 0,14 | — | 16,3 | 9,37 | — | 12,2 | 17,6 | — | 13,7 | 33 | — | 9,1 |

| Standard | Co | | | Hf | | | Ce | | | Eu | | | Th | | |
|---|---|---|---|---|---|---|---|---|---|---|---|---|---|---|---|
| | Cc, $10^{-4}$ % | $\Delta_n$ | σ | Cc, $10^{-4}$% | $\Delta_n$ | σ | Cc, $10^{-4}$% | $\Delta_n$ | σ | Cc, $10^{-4}$ % | $\Delta_n$ | σ | Cc, $10^{-4}$% | $\Delta_n$ | σ |
| SGD-1A | 40 | 12,5 | 4,0 | 20 | — | 3,7 | 150 | 6,7 | 13,6 | 6,0 | 16,7 | 6,7 | 9 | 11,1 | 11,7 |
| SG-1A | 1,4 | 21,4 | 15,7 | 90 | — | 13,6 | 67 | — | 20,9 | 0,5 | — | — | 120 | 10,8 | 14,2 |
| ST-1A | 46 | 10,9 | 8,9 | 10 | — | 18,2 | 22 | — | 20,3 | 3,0 | 33,3 | 8,3 | 3 | — | 20,2 |
| BCR-1 * | 38 | — | 10,2 | 4,7 | — | 17,0 | 53,9 | — | 13,3 | 1,9 | — | 7,7 | 6 | — | 18,3 |

Cc is the certified content of the element in the standard sample; $\Delta_n$ is the confidence interval, rel. %, for $\alpha = 0.95$ (certified value); σ is the rms error of INAA of parallel tests of standard rock samples, rel. %, for $\alpha = 0.95$.

*Content of element given after [3].

and foreign rocks envisage a minimum representative sample of 50-100 mg, which is two orders of magnitude greater than the weighed amount of the samples analyzed. The use of the minimum representative sample recommended by the certificate as a standard hinders analysis because of differences in the load on the spectrometric channel in measurements in the same geometry. In using SCS, therefore, it is desirable to use weighed amounts comparable with the weighed amounts of the analyzed samples as the standard. With this method, however, it is necessary to know the error due to the standardization.

With a view to resolving this problem we took weighed samples of 1-2 mg of the SCS: SGD-1A, ST-1A, and SG-1A (USSR), and BCR-1 (USA). The selected weighed samples were packaged in aluminum foil and irradiated for 200 h in a TVR reactor with a flux of $1.2 \cdot 10^{13}$ neutrons/cm$^2$·sec. After irradiation, the weighed samples were repackaged in an inactive material. The induced activity was measured in two stages: 1) in the first two days after irradiation we measured the activity of Na, K, and Mn; 2) 30 days after the irradiation we measured the activity of Fe, Co, Sc, Hf, Ce, Eu, and Th.

Table 2 gives the results of estimation of the total error with respect to the elements in the standards indicated. Analysis of the data shows that the rms errors may differ severalfold for the same elements in different standards. However, taking account of the extremely small amounts of the elements determined (for some, $n \cdot 10^{-12}$ g), the agreement of the data can be considered satisfactory. Table 2 also presents a comparison of the errors with the certified values of the confidence intervals with $\alpha = 0.95$. This comparison also shows σ to be close to the certified values for all elements apart from Na, K, Mn, and Fe. Upon considering the data of Table 2 we can reach the conclusion that with combined use of standards for our comparison standards we can choose a standard with which the error due to standardizing will be a minimum, e.g., SGD-1A for the analysis of Cr, BCR-1 for the analysis of K, etc. It must be borne in mind, however, that for many elements analyzed by INAA, the standards are certified only qualitatively and, therefore, it is necessary to have artificial composite standards, e.g., based on PFR, which eliminates this deficiency.

Using the results obtained, we carried out INAA of nine samples of monomineral fractions of lunar soil and two samples of monofractions of terrestrial rock. The weighed amount of the samples was 1-3 mg. The samples were packaged under a binocular instrument in a double layer of aluminum foil and the standards were packaged in a single layer; Soviet (SG-1A, ST-1A, and SGD-1A) as well as foreign (BCR-1) standard samples of rocks were used as the standards. We also used standard-analogs of standard rock samples prepared on the basis of PFR. The weighed amounts of the standards were chosen close to that of the samples, 1-3 mg. The samples were irradiated in a TVR reactor with a flux of $1.2 \cdot 10^{13}$ neutrons/cm$^2$·sec for 200 h.

After irradiation, the samples and standards (the samples under a binocular) were repackaged from aluminum foil into inactive polyethylene packets.

The induced activity was measured in several stages over 3 months. In this case the contents of 18 elements present in macro- and microquantities were determined. The results of the analyses are given in Table 3.



Declassified and Approved For Release 2013/02/15 : CIA-RDP10-02196R000800020001-4

Declassified and Approved For Release 2013/02/15 : CIA-RDP10-02196R000800020001-4

TABLE 3. Results of INAA of Submilligram Weighed Amounts of Rock-Forming Minerals from Lunar Soil

| Sample | Mass, mg | Ca, % | Fe, % | K*, % | Mn, % | Na, % | Co $\times 10^{-4}$, % | Cr $\times 10^{-4}$, % | Sc $\times 10^{-4}$, % | Th $\times 10^{-4}$, % | Ce $\times 10^{-4}$, % | Eu, $\times 10^{-4}$, % | Hf $\times 10^{-4}$, % | La $\times 10^{-4}$, % | Lu $\times 10^{-4}$, % | Sm, $\times 10^{-4}$, % | Yb $\times 10^{-4}$, % | Au* $\times 10^{-4}$, % | Gd* $\times 10^{-4}$, % | Ta* $\times 10^{-4}$, % |
|---|---|---|---|---|---|---|---|---|---|---|---|---|---|---|---|---|---|---|---|---|
| Plagioclases | | | | | | | | | | | | | | | | | | | | |
| 24.1.6 | 0,9 | 0,2 | 0,2 | — | 0,04 | 0,10 | 1,4 | 2,7 | 0,3 | 1,1 | 1,0 | 0,1 | 0,3 | 0,3 | 0,01 | 0,01 | 0,1 | — | 1,3 | 0,01 |
| 24.2.8 | 0,4 | 11,8 | 0,5 | 1,3 | 0,05 | 0,93 | 2,4 | 22,8 | 1,2 | 1,5 | 2,7 | 1,0 | 1,8 | 3,5 | 0,08 | 0,12 | 0,1 | 0,06 | 0,6 | 0,001 |
| 20.1.9 | 3,0 | 14,5 | 0,2 | — | 0,02 | 0,37 | 1,2 | 17,2 | 0,5 | 0,2 | 3,1 | 1,4 | 0,2 | 1,8 | 0,02 | 0,46 | 0,2 | 0,11 | 1,3 | 0,001 |
| 5SP* | 1,7 | 6,8 | 0,3 | — | — | 3,46 | 0,7 | 2,2 | 0,4 | 0,4 | 6,1 | 2,3 | 0,8 | 4,6 | 0,03 | 0,26 | 0,1 | 0,08 | 0,8 | 0,03 |
| Pyroxenes | | | | | | | | | | | | | | | | | | | | |
| 24.1.2 | 1,6 | 8,4 | 18,9 | — | 0,28 | 0,07 | 59,0 | 2330 | 96,1 | — | 12,0 | 0,2 | 6,4 | 3,4 | 0,29 | 0,67 | 2,8 | 0,01 | 1,5 | 0,06 |
| 24.1.3 | 1,2 | 5,8 | 15,2 | — | 0,22 | 0,08 | 63,5 | 3160 | 62,6 | — | 17,0 | 0,4 | 2,2 | 4,1 | 0,17 | 0,29 | 3,2 | 0,07 | 4,8 | 0,08 |
| 24.2.2 | 2,0 | 6,3 | 16,7 | 0,8 | 0,23 | 0,52 | 46,0 | 1710 | 71,4 | — | 16,9 | 0,3 | 6,7 | 8,9 | 0,19 | 0,62 | 2,0 | 0,05 | 5,1 | 0,06 |
| 24.2.5 | 1,3 | 7,6 | 20,8 | 0,1 | 0,28 | 0,04 | 81,9 | 3340 | 74,8 | — | 22,2 | 0,2 | 0,8 | 2,4 | 0,22 | 0,44 | 1,2 | 0,05 | 6,2 | 0,11 |
| 20.1.4 | 0,9 | 3,2 | 13,9 | — | 0,21 | 0,08 | 37,1 | 4510 | 47,6 | 1,0 | 17,3 | 0,2 | 2,7 | 2,3 | 0,99 | 1,08 | 5,3 | — | 2,3 | 0,03 |
| 1.15† | 0,8 | 13,9 | 11,7 | — | 0,26 | 0,18 | 75,3 | 161,5 | 140,7 | 20,6 | 13,5 | 2,0 | 6,9 | 6,9 | 0,65 | 6,30 | 3,9 | 0,07 | 13,1 | 0,08 |
| Olivines | | | | | | | | | | | | | | | | | | | | |
| 24.1.9 | 0,8 | 1,2 | 31,0 | — | 0,32 | 0,22 | 68,4 | 411,3 | 11,2 | 1,5 | 33,6 | 0,6 | 1,8 | 4,0 | 0,42 | 2,82 | 2,5 | — | 8,4 | 0,03 |

*Semiquantitative analysis.
†Monofractions of terrestrial rocks.

For a number of elements (K, Au, Gd, and Ta) we carried out semiquantitative analysis because of the small statistics and possible extraneous interference. The error of the analysis as the result of the total error of reproducibility and standardization was 5-25 rel.% for the macroelements (Ca, Fe, Mn, and Na) and 10-30 rel.% for the other elements with a confidence level $\alpha = 0.95$.

Thus, as the result of the study we estimated the level of the content of elements at which contamination of samples with the packaging material (aluminum foil) is insignificant. We also determined the total errors in using standard rock samples as the comparison standards with weighed amounts of 1-3 mg. It was shown that with the combined use of SCS of rocks and composite standards based on PFR it is possible to obtain data with sufficient accuracy and reliability for most macro- and microelements.

The results obtained served as a basis for the analysis of submilligram weighed amounts of rock-forming minerals of lunar and terrestrial rocks for their content of 18 elements.

In conclusion, the authors express their gratitude for assistance given them in the investigations and measurements by T. S. Magidovich of the Institute of Geology of Ore Deposits, Petrography, Mineralogy, and Geochemistry of the Academy of Sciences of the USSR (IGEM AN SSSR) and by O. V. Gorbatyuk of Laboratory 2 and T. I. Voronina and T. V. Nedostup of Laboratory 11 of VNIIYaGG.

## LITERATURE CITED

1. D. I. Leipunskaya et al., At. Energ., 37, No. 5, 431 (1974).
2. D. I. Leipunskaya et al., J. Radioanal. Chem., 26, 293 (1975).
3. F. Flanagan, Geochim. Cosmochim. Acta, 37, No. 5, 1189 (1973).



Declassified and Approved For Release 2013/02/15 : CIA-RDP10-02196R000800020001-4

Declassified and Approved For Release 2013/02/15 : CIA-RDP10-02196R000800020001-4

# CALCULATION OF PHOTONEUTRON YIELDS FROM THICK TARGETS IN GIANT-RESONANCE REGION

V. I. Isaev and V. P. Kovalev

UDC 539.163:539.124

As is known [1], the photoneutron yield from electron-irradiated targets can be written as

$$B(E_0,\ Z,\ T)=\frac{N_0}{A}\int_0^{E_0} l(E_0,\ Z,\ T,\ k)\,\sigma_{\gamma n}(Z,\ k)\,dk, \tag{1}$$

where $B(E_0, Z, T)$ is the neutron yield per electron; T, target thickness, g/cm$^2$; $N_0$, Avogadro's number; A and Z, mass number and atomic number of the target; $E_0$ and k, energies of the incident electron and the emitted photon, respectively; $\sigma_{\gamma n} = \sigma_{\gamma,1n} + 2\sigma_{\gamma,2n} + 3\sigma_{\gamma,3n} + \sigma_{\gamma,pn} + \bar{\nu}(k)\,\sigma_{\gamma,f} + \ldots$, total cross section for the creation of a neutron by a photon of energy k as a result of the reactions $(\gamma, 1n)$, $(\gamma, 2n)$, $(\gamma, 3n)$, $(\gamma, pn)$, $(\gamma, f)$, etc.; $\bar{\nu}(k)$, mean number of neutrons per photofission; and $l(E_0, Z, T, k)$, photon track length, g·cm$^{-2}$·MeV$^{-1}$.

The principal difficulty in the calculation of photoneutron yields is that of finding the photon track lengths. Calculation of the track lengths on the basis of shower theory does not ensure the required accuracy [1] whereas calculation by the Monte Carlo method is laborious [2, 3]. It is of particular interest, therefore, to obtain a simple expression for crack lengths, making it possible to calculate the photoneutron yield rapidly with sufficient accuracy.

In the present paper, on the basis of a number of simplifying assumptions about the mechanism of the $\bar{e} \rightarrow \gamma$ process we obtained a comparatively simple analytic formula for the photon track length and as a result we could reduce the expression for the photoneutron yield to a simple integral.

Let us write a general expression for the photoneutron yield in the form

$$B(E_0,\ Z,\ T)=\frac{N_0}{A}\int_0^{E_0}\int_0^{t}\frac{N_0}{A}\,n(t)\int_t^{T}\sigma_{br}(Z,\ E,\ k)\,\exp[-\mu(x-t)]\,\sigma_{\gamma n}(Z,\ k)\,dx\,dt\,dk, \tag{2}$$

where t is the thickness of the target in which photons of energy k can be created under the conditions of continuous slowing-down of electrons; x, distance traveled by a photon in the target to absorption ($t \le x \le T$); $\sigma_{br}$, cross section for generation of bremsstrahlung; $\mu(k)$, photon absorption coefficient for a narrow beam; and n(t), electron transmission coefficient.

From Eqs. (1) and (2) we have

$$l(E_0,\ Z,\ T,\ k)=\frac{N_0}{A}\int_0^{t} n(t)\int_t^{T}\sigma_{br}(Z,\ E,\ k)\,\exp[-\mu(x-t)]\,dx\,dt\sigma_{br}(Z,\ E,\ k). \tag{3}$$

The data of [4] indicate that the spectrum of bremsstrahlung from thick targets depends little on the form of the dependence of the cross section $\sigma_{br}$ on the energy of the photon radiated. Let us assume that $\sigma_{br} \sim 1/k$. The proportionality factor is determined from the approximate equation

$$(dE/dx)_{rad}=\frac{N}{A}\int_0^{E}\sigma_{br}k\,dk\approx cE. \tag{4}$$

Hence,

$$\sigma_{br}(Z, E, k)=cA/N_0k. \tag{5}$$

Translated from Atomnaya Énergiya, Vol. 47, No. 1, pp. 34-37, July, 1979. Original article submitted April 24, 1978.



0038-531X/79/4701-0538 $07.50 © 1980 Plenum Publishing Corporation

Declassified and Approved For Release 2013/02/15 : CIA-RDP10-02196R000800020001-4

Declassified and Approved For Release 2013/02/15 : CIA-RDP10-02196R000800020001-4

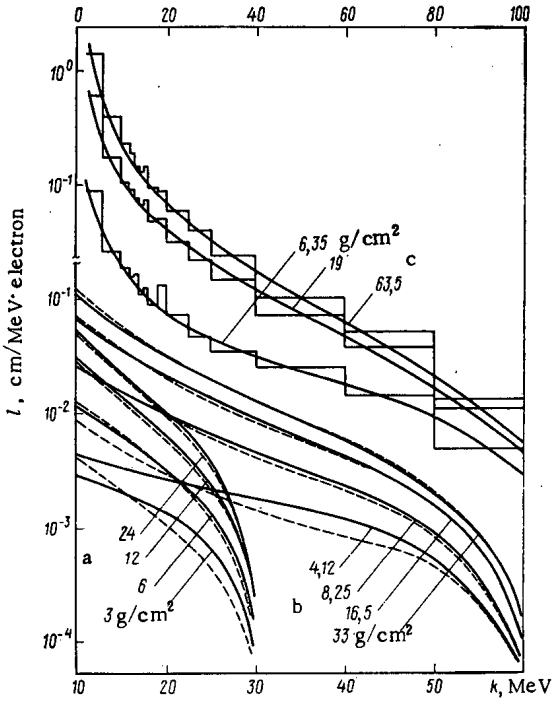


Fig. 1

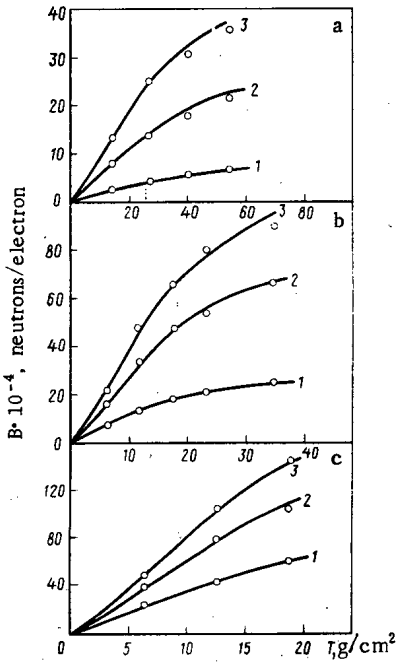


Fig. 2

Fig. 1. Track length of bremsstrahlung of tungsten targets at $E_0 = 30$ MeV (a) and $E_0 = 60$ MeV (b) and tantalum targets at $E_0 = 100$ MeV (c) (the abscissa scale is at the top for c) for various target thicknesses (numbers next to curves): ———, ------, histogram) calculation by Eq. (13), the Berger–Seltzer formula [3], and the Alsmiller–Moran formula [2], respectively.

Fig. 2. Dependence of photoneutron yield of copper (a), lead (b), and uranium (c) on target thickness and electron energy of 1) 19; 2) 28; and 3) 35 MeV: ○) experiment [1]; ———) calculation from Eq. (17).

Integrating Eq. (3) with respect to x, we get

$$l(E_0, Z, T, k) = \frac{c}{\mu k}\int_0^t n(t)\left[1 - e^{-\mu(T-t)}\right] dt. \tag{6}$$

In the range of electron energies from several megaelectron volts to tens of megaelectron volts the expression for the transmission coefficient n(t) can be written approximately as

$$n(t) = 1 - (t/R_e)^{3/2} \tag{7}$$

where $R_e$ is the extrapolated path length, g/cm²:

$$R_e = 0.565\,[125/(Z+112)]\,E^{0.935}. \tag{8}$$

Substituting Eq. (7) in Eq. (6) and performing the integration, we get

$$l(E_0,\ Z,\ T,\ k) = \frac{c}{\mu k}\left\{t - \frac{1}{\mu}(e^{\mu t} - 1) - \frac{2R_e}{5}\left(\frac{t}{R_e}\right)^{5/2}\left[1 - e^{-\mu(T-t/2)}\right]\right\}. \tag{9}$$

The variable t can be written in terms of k by means of the relation between the electron energy and the target thickness [5]:

$$E(t) = E_0 \exp(-\xi t), \tag{10}$$

where $\xi = (dE_0/dx)/E_0 \approx (\alpha + \beta E_0)/E_0$; and $\alpha$ and $\beta$ are the constants of the total energy losses by the electron.

Setting $E(t) = k = \varphi$, we get



Declassified and Approved For Release 2013/02/15 : CIA-RDP10-02196R000800020001-4

Declassified and Approved For Release 2013/02/15 : CIA-RDP10-02196R000800020001-4

TABLE 1. Photoneutron Yield, neutrons/electron

| | Tantalum | | | | | | Copper | |
|---|---|---|---|---|---|---|---|---|
| | 10 MeV | | 15 MeV | | 20 MeV | | 15 MeV | 28 MeV |
| | 0,1 $X_0$ * | 1 $X_0$ | 0,1 $X_0$ | 1 $X_0$ | 0,1 $X_0$ | 1 $X_0$ | 0,1 $X_0$ | 0,1 $X_0$ |
| Calc. by Eq. (17) [present paper] | $5{,}05\cdot10^{-7}$ | $6{,}24\cdot10^{-6}$ | $9{,}7\cdot10^{-6}$ | $2{,}44\cdot10^{-4}$ | $1{,}61\cdot10^{-5}$ | $8{,}46\cdot10^{-4}$ | $2{,}76\cdot10^{-6}$ | $2{,}8\cdot10^{-5}$ |
| Calc. by Monte Carlo method [11] | $3{,}0\cdot10^{-7}$ | $6{,}0\cdot10^{-6}$ | $6{,}0\cdot10^{-6}$ | $2{,}2\cdot10^{-4}$ | $1{,}45\cdot10^{-5}$ | $7{,}5\cdot10^{-4}$ | — | — |
| Experiment [1] | — | — | — | — | — | — | $2{,}0\cdot10^{-6}$ | $3{,}0\cdot10^{-5}$ |

*X is the thickness in radiation lengths.

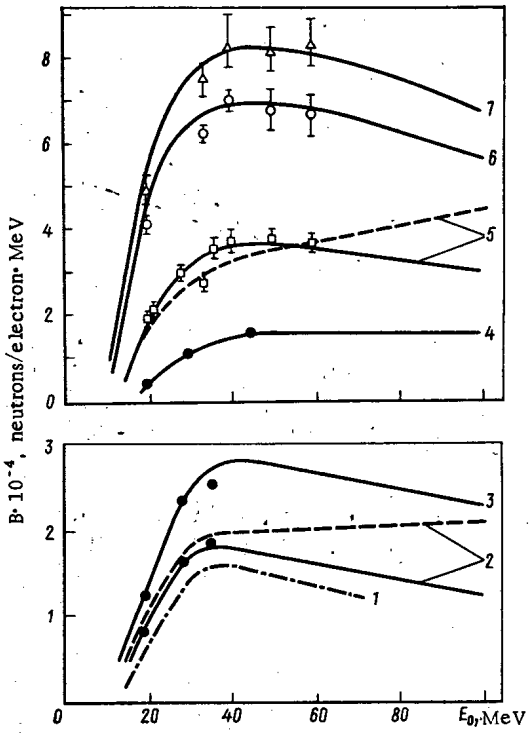


Fig. 3. Dependence of photoneutron yield on electron energy and target thickness: 1) tungsten target with thickness of 16.3 g/cm$^2$; 2, 3, 5) lead targets with thickness of 17.30, 34.45, and 58.2 g/cm$^2$; 4) copper target of infinite thickness; 6, 7) targets of $^{238}$U and $^{235}$U with thickness of 48.6 and 48.4 g/cm$^2$; ●) experiment [1]; △, ○, □) experiment [7]; ———, -·-·-, ----) calculation from Eq. (17) and Berger–Seltzer [3] and Alsmiller–Moran [2] formulas, respectively.

$$t = (1/\xi)\ln(E_0/\varphi). \tag{11}$$

The notation $k = \varphi$ was introduced for convenience. In the range of photon energies from 0 to $E_0$ the quantity $\varphi$ takes on the following values:

$$\begin{aligned} \varphi &= k_T, \text{ if } 0 \leqslant k \leqslant k_T \\ \varphi &= k, \text{ if } k_T \leqslant k \leqslant E_0, \end{aligned} \tag{12}$$

where $k_T = E_0 \exp(-\xi T)$.

On substituting Eq. (11) in Eq. (9), we get the following expression for the photon track length:

$$l(E_0, Z, T, k) = \frac{c}{\mu k \xi}\left\{\ln\frac{E_0}{\varphi} - \frac{\xi}{\mu}\left[\left(\frac{E_0}{\varphi}\right)^{\mu/\xi} - 1\right]e^{-\mu T} - \frac{2\xi R_e}{5}\left(\frac{1}{\xi R_e}\ln\frac{E_0}{\varphi}\right)^{5/2}\left[1 - \left(\frac{E_0}{\varphi}\right)^{\mu/2\xi}e^{-\mu T}\right]\right\}. \tag{13}$$

The results of calculations of the track lengths for tantalum and tungsten from Eq. (13) and by the Monte Carlo method [2, 3] are given in Fig. 1. The results are observed to be in good agreement for thicknesses greater than $0.5R_0$ ($R_0$ is the mean electron path length).

The last term in Eq. (13) is due to the incorporation of the electron transmission coefficient n(t). Near the maximum of the giant resonance its contribution does not exceed several per cent and, therefore, this term can be neglected in calculations of the photoneutron yield. Then the expression for the track length is of the form



Declassified and Approved For Release 2013/02/15 : CIA-RDP10-02196R000800020001-4

Declassified and Approved For Release 2013/02/15 : CIA-RDP10-02196R000800020001-4

$$l(E_0,\ Z,\ T,\ k)=\frac{c}{\mu\xi k}\left\{\ln\frac{E_0}{\varphi}-\frac{\xi}{\mu}\left[\left(\frac{E_0}{\varphi}\right)^{\mu/\xi}-1\right]e^{-\mu T}\right\}. \tag{14}$$

Next, using the approximate equation

$$\left(\frac{E_0}{\varphi}\right)^{\mu/\xi}-1\approx\frac{\mu}{\xi}\left(\frac{E_0}{\varphi}\right)^{\mu/\xi}\ln\frac{E_0}{\varphi}, \tag{15}$$

we write

$$l(E_0,\ Z,\ T,\ k)=L\left[1-\left(\frac{E_0}{\varphi}\right)^{\mu/\xi}e^{-\mu T}\right], \tag{16}$$

where $L = (c/\mu\xi k)\ln(E_0/\varphi)$ is the maximum track length. Substitution of Eq. (16) in Eq. (1) gives us the following expression for the photoneutron yield:

$$B(E_0,\ Z,\ T)=\frac{N_0}{A}\int_0^{E_0}L\left[1-\left(\frac{E_0}{\varphi}\right)^{\mu/\xi}e^{-\mu T}\right]\sigma_{\gamma,n}(Z,\ k)\,dk \tag{17}$$

In Figs. 2 and 3 we give the results obtained by using Eq. (17) to calculate the photoneutron yields from copper, lead, and uranium along with experimental data taken from [1, 6]. There is good agreement between calculation and experiment. In the calculations the values of $\sigma_{\gamma,n}$ were taken from [7, 8], the values of $\mu(k)$ were taken from [9], and in accordance with [10] the quantity $\bar{\nu}(k)$ was written as

$$\begin{aligned}\bar{\nu}(k)&=0.158\,k+1.5 \quad \text{for } {}^{238}\text{U};\\ \bar{\nu}(k)&=0{,}158\,(k-6{,}5)+2{,}43 \quad \text{for } {}^{235}\text{U}.\end{aligned} \tag{18}$$

Analysis of the results of calculation and comparison with the experimental data permit the assumption that the dependence of the electron-neutron conversion factor on the electron energy has a maximum at an energy of $3k_{res}$ for a target of infinite thickness. The maximum is more pronounced for heavy elements. The position of the maximum shifts to lower energies as the target thickness diminishes. The character of the dependence of the electron-neutron conversion factor on the energy, as obtained in the present paper, is in accord with calculations by the Monte Carlo method performed Berger and Seltzer [3] but differs from the calculations of Alsmiller and Moran [2]. The final conclusion about the character of the energy dependence of the conversion factor can be made after reliable data are obtained on the cross sections $\sigma_{\gamma,n}$ in the range of energies above the "tail" of the giant resonance.

Comparison of the normalized spectra of the form 1/k and Schiff spectra shows that they are closest in the energy range above the maximum of the giant resonance, with the 1/k spectrum lying somewhat above the Schiff spectrum. In this energy range and for target thicknesses $\geqslant 0.5\ R_0$ Eqs. (13) and (17) give the best agreement with experiment and with calculations by the Monte Carlo method. With a decrease in the target thickness and the electron energy [region between threshold of ($\gamma$, n) reaction and the maximum of the giant resonance] the agreement deteriorates but the divergence does not exceed 40%. The degree of agreement can be judged from the data of Table 1.

The upper limit of the target thickness is limited by the neutron self-absorption, which becomes significant at a thickness greater than the saturation thickness (5–7 radiation lengths) for the photoneutron yield.

For electron energies above the region of the giant resonance, neglecting $\alpha$ in the expression for $\xi$ and taking account of the fact that $C \approx \beta$, we can write

$$B(E_0,\ Z,\ T)=\frac{N_0}{A}\frac{\sigma_{\gamma n}^{\text{int}}}{\mu_{\text{res}}k_{\text{res}}}\ln\frac{E_0}{k_{\text{res}}}\left[1-\left(\frac{E_0}{k_{\text{res}}}\right)^{\mu_{\text{res}}/\beta}e^{-\mu_{\text{res}}T}\right], \tag{19}$$

where $\sigma_{\gamma n}^{\text{int}}$ is the integrated cross section for creation of photoneutrons. It follows from Eq. (19) that in the region above the giant resonance the photoneutron yield is a logarithmic function of the electron energy. The experimental data do not contradict this conclusion. In view of this it is of interest to measure the photoneutron yield in the range of electron energies ~100 MeV right up to the meson-creation threshold.

## LITERATURE CITED

1. W. Barber and W. George, Phys. Rev., 116, 1551 (1959).
2. R. A. Alsmiller and H. Moran, Nucl. Inst. Methods, 48, 109 (1967).



Declassified and Approved For Release 2013/02/15 : CIA-RDP10-02196R000800020001-4

Declassified and Approved For Release 2013/02/15 : CIA-RDP10-02196R000800020001-4

3. M. Berger and S. Seltzer, Phys. Rev., 2C,(2), 621 (1970).
4. V. E. Zhuchko and Yu. M. Tsipenyuk, At. Energ., 39, No. 6, 66 (1975).
5. C. Emigh, Thick Target Bremsstrahlung Theory, LA-4097-MS (1970).
6. R. I. Sinclair and D. G. Day, in: Problems of Elementary-Particle and Nuclear Physics [Russian translation], Vol. 2, No. 4, Atomizdat, Moscow (1972), p. 981.
7. Y. Miller et al., Nucl. Phys., 32, 236 (1962).
8. B. Berman and S. Fultz, Rev. Mod. Phys., 47, No. 3, 713 (1975).
9. Y. Hubbell, Photon Cross Sections, Attenuation Coefficients, NSRDS-NBS-29 (1969).
10. O. Veyssiere et al., Nucl. Phys., A 199, 45 (1973).
11. S. Seltzer and M. Berger, Phys. Rev., C(7), 858, 1973 (1973).



Declassified and Approved For Release 2013/02/15 : CIA-RDP10-02196R000800020001-4

Declassified and Approved For Release 2013/02/15 : CIA-RDP10-02196R000800020001-4



# AN ACCELERATING SECTION FOR REDUCING THE RADIATION LEVEL IN THE ABSORBER SECTION OF A LINAC

V. S. Balagura, V. M. Grizhko, I. A. Grishaev, L. K. Yakushko, B. G. Safronov, and L. C. Fursov

UDC 621.384.644.3

There is a tendency for the beam intensities in linacs to be raised steadily, and therefore existing biological shields tend to become inadequate. The shielding can be upgraded either by thickening or by installing a local absorber in the beam-exit region, the function of this being to reduce the mean energy of the ionizing radiation incident on the shield, which thereby improves the performance of the latter.

For various reasons, it is not always possible to upgrade a shield by adding to the thickness. This was the case when an injector accelerator [1] was converted to work in 1-mA mean-current mode. Therefore, it was decided to install a local absorber, for which purpose the accelerating section of the linac was employed.

The electron beam loses energy by excitation of hf oscillations [2] when it passes through a diaphragm structure, and this power is absorbed in a load. The energy loss $\Delta E_0$ in a section is proportional to the pulse current:

$$\Delta E_0 = KI, \tag{1}$$

where K is a coefficient of proportionality, which is dependent on the electrodynamic structure of the section. The energy loss becomes substantial if the pulse current is high. It is therefore of interest to examine the result from using an accelerating section not supplied with UHF power as a beam-energy absorber in order to reduce the radiation level.

If the electron energy is completely absorbed in the material, the energy yield of the radiation $(\Delta E_0)_{rad}$ is given by

$$(\Delta E_0)_{rad} = \int_0^{E_0} \left(-\frac{dE_0}{dx}\right)_{rad} \frac{dE_0}{\left(-\frac{dE_0}{dx}\right)_t}, \tag{2}$$

as given in [3], where $(-dE_0/dx)_{rad}$ and $(-dE_0/dx)_t$ are the radiation and total energy losses per cm thickness of the material and $E_0$ is the initial electron energy.

We envisage the case where the electron energy is less than 20 MeV; in that case, the ionization loss in the shielding material (concrete) is very much larger than the radiative loss and can be taken as approximately constant over a wide energy range. Then (2) gives

$$(\Delta E_0)_{rad} \simeq \frac{R(E_0)}{E_0} \int_0^{E_0} \left(-\frac{dE_0}{dx}\right)_{rad} dE_0, \tag{3}$$

where $R(E_0)$ is the mean range for an electron of initial energy $E_0$. For the purpose of shielding calculations, the mean radiation energy $E_\gamma$ is taken as half the initial electron energy, i.e.,

$$\bar{E}_\gamma = \frac{1}{2} E_0. \tag{4}$$

When the electron energy falls by $\Delta E_0$, the mean energy of the x rays falls to

$$\bar{E}_\gamma = \frac{1}{2}(E_0 - \Delta E_0). \tag{5}$$

Translated from Atomnaya Énergiya, Vol. 47, No. 1, pp. 39-40, July, 1979. Original article submitted August 29, 1977.

0038-531X/79/4701-0543$07.50 © 1980 Plenum Publishing Corporation



Declassified and Approved For Release 2013/02/15 : CIA-RDP10-02196R000800020001-4

Declassified and Approved For Release 2013/02/15 : CIA-RDP10-02196R000800020001-4

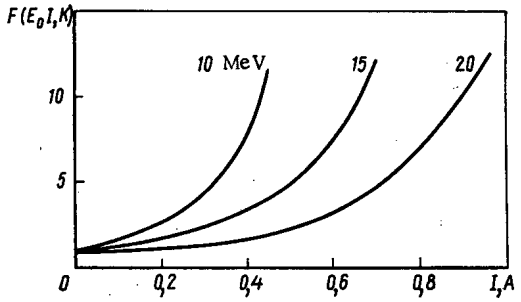


Fig. 1

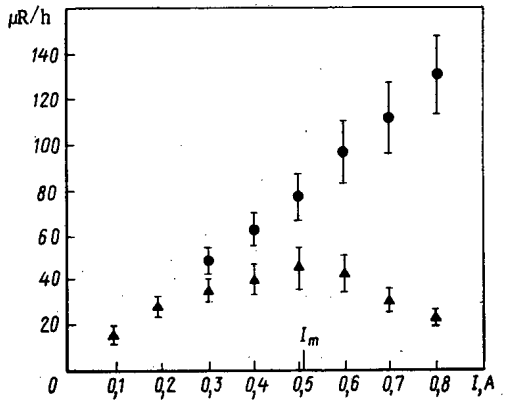


Fig. 2

Fig. 1. Dependence of $F(E_0, I, K)$ on current for three energies.

Fig. 2. Dose rate as a function of pulse current at one of the points in the monitored zone of the accelerator; filled circle) beam energy completely consumed by ionization and $\gamma$-ray emission in the biological shield; filled triangle) part of the beam energy absorbed in an output section not supplied with uhf power.

Absorption of $\Delta E_0$ in the accelerating section is equivalent to increasing the thickness of the biological shield by $h_{eq}$, where the value satisfies

$$\bar{E}_\gamma \exp[-\mu(\bar{E}_\gamma)\rho h_{eq}] = \bar{E}'_\gamma, \tag{6}$$

where $\mu(\bar{E}_\gamma)\rho$ is the product of the mass absorption coefficient for $\gamma$ rays of energy $\bar{E}_\gamma$ and the density of the shielding material; then (6) with (4) and (5) gives

$$h_{eq} = \frac{1}{\mu(\bar{E}_\gamma)\rho} \ln \frac{E_0}{E_0 - \Delta E_c}. \tag{7}$$

The reduction in electron energy in the absorbing section also reduces the total number of mean-energy $\gamma$ rays $M(E_0, \Delta E_0)$ formed in the shield:

$$M(E_0, \Delta E_0) = \left[\frac{(\Delta E_0)_{rad}}{\bar{E}_\gamma}\right] \Big/ [\Delta(E_0 - \Delta E_0)_{rad}/\bar{E}'_\gamma], \tag{8}$$

where $\Delta(E_0 - \Delta E_0)_{rad}$ is the energy yield of $\gamma$ rays for an electron of initial energy $E_0 - \Delta E_0$; if we neglect the screening by the nuclei in the shield, which results in a slight overestimate (not more than 4%) of the x-ray production cross section, we get from (8) and (3) that

$$M(E_0, \Delta E_0) \simeq \frac{E_0}{E_0 - \Delta E_0} f(E_0, \Delta E_0), \tag{9}$$

where

$$f(E_0, \Delta E_0) = \frac{\ln \frac{2E_0}{mc^2} - \frac{7}{12}}{\ln \frac{2(E_0 - \Delta E_0)}{mc^2} - \frac{7}{12}}. \tag{10}$$

The performance factor for the section in reducing the radiation level $F(E_0, I, K)$ is defined as

$$F(E_0, I, K) = M(E_0, \Delta E_0) \exp[\mu(\bar{E}_\gamma)\rho h_{eq}],$$

or from (1), (7), and (9)

$$F(E_0, I, K) = \left(\frac{E_0}{E_0 - IK}\right)^2 f(E_0, \Delta E_0). \tag{11}$$

Figure 1 shows the $F(E_0, I, K)$ relation in terms of the pulse current given by (11) for three different energies and K = 13 MeV/A; this value of the electrodynamic impedance applies for an absorbing section in which the critical current is 1.6 A for a pulse length of 10 $\mu$sec and a section length of 318 cm. Figure 1



Declassified and Approved For Release 2013/02/15 : CIA-RDP10-02196R000800020001-4

Declassified and Approved For Release 2013/02/15 : CIA-RDP10-02196R000800020001-4

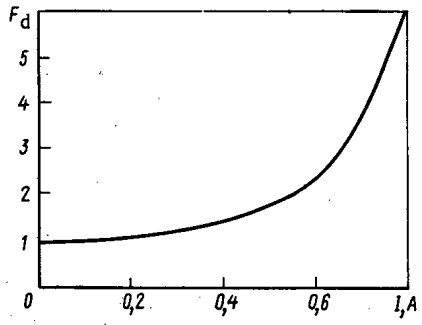


Fig. 3. Dose performance factor as a function of pulse current.

shows that this performance factor should increase at first in proportion to the current itself, but more rapidly at higher currents. An estimate can be made of the pulse current $I_m$ at which the factor begins to increase rapidly. We denote by $U(E_0, I)$ the total leakage of energy as $\gamma$ rays into the monitored zone when a beam of energy $E_0$ falls freely on the shielding. Then we have

$$U(E_0, I) = \frac{I(\Delta E_0)_{\text{rad}}}{S\bar{E}_\gamma} \bar{E}_\gamma \frac{1}{B(\bar{E}_\gamma)}, \tag{12}$$

where S is the space–mark ratio, and $B(\bar{E}_\gamma)$ is a function of the mean $\gamma$-ray energy in the accelerator bay. which is also dependent on the geometry and thickness of the shielding and which defines the total attenuation of the ionizing radiation by the existing shield. If there is an absorbing section at the accelerator output, the total leak $U(E_0, I, K)$ can be put as

$$U(E_0, I, K) = \frac{I\bar{E}_\gamma}{SF(E_0, I, K)B(\bar{E}_\gamma)} = \left[\frac{I(E_0 - IK)^2}{E_0^2}\right] \frac{\bar{E}_\gamma}{SB(E_\gamma) f(E_0, \Delta\bar{E}_0)}. \tag{13}$$

As $f(E_0, \Delta E_0)$ varies with I much more slowly than does the expression in square brackets, as (10) shows, we have

$$\frac{\partial}{\partial I} U(E_0, I, K) \simeq \frac{\bar{E}_\gamma}{SB(\bar{E}_\gamma) f(E_0, \Delta E_0)} \frac{\partial}{\partial I}\left[\frac{I(E_0 - IK)^2}{E_0^2}\right], \tag{14}$$

and therefore $(\partial/\partial I)U(E_0, I, K) = 0$ for $I_{max} = E_0/3K$, which means that the leakage of $\gamma$-ray energy into the monitored zone in the presence of an absorbing section at first increases with the pulse current from zero up to $I_{max}$ but then begins to fall. By definition

$$F(E_0, I, K) = \frac{U(E_0, I)}{U(E_0, I, K)},$$

and therefore the performance factor increases rapidly with current for $I > I_m = I_{max}$.

Figure 2 shows the dose rate as a function of the pulse current as measured for two cases of beam absorption at one of the points in the monitored zone of the accelerator for $E_0 = 15$ MeV, $S = 7200$; it is clear that there is a value $I_m'$ for the case ▲ above which the dose decreases, and this value $I_m'$ agrees qualitatively with the $I_m$ given by (14). We take the ratio of the dose rates for ● and ▲ for identical pulse currents to get the dose-performance factor $F_d$.

Figure 3 shows the dependence of this coefficient on the pulse current for the working point. Qualitatively similar relationships were obtained for other points in the monitored zone. Figures 1 and 3 show that the current dependence of $F(E_0, I, K)$ is closely similar to that of $F_d$. Therefore, an accelerator section working as an absorber provides an efficient means of local absorption of the ionizing radiation for $I > E_0/3K$.

## LITERATURE CITED

1. V. A. Vishnyakov et al., At. Energ., 42, No. 3, 231 (1977).
2. O. A. Val'dner, A. D. Vlasov, and A. V. Shal'nov, Linear Accelerators [in Russian], Atomizdat, Moscow (1969).
3. A. P. Komar, F. P. Kruglov, and I. V. Lopatin, Measurement of Total Beam Energies for X Rays from Electron Accelerators [in Russian], Nauka, Leningrad (1972).



Declassified and Approved For Release 2013/02/15 : CIA-RDP10-02196R000800020001-4

Declassified and Approved For Release 2013/02/15 : CIA-RDP10-02196R000800020001-4

# γ-RAY RECORDING EFFICIENCY OF A SPHERICAL DETECTOR

D. I. Konstantinov

UDC 539.107.43

It is usual to replace a cylindrical detector whose height is equal to the diameter by a spherical device of the same volume in calculating the efficiency and sensitivity of a scintillation detector, working with γ radiation from a large-volume source [1-4]. Various expressions have been given [2, 4] for the recording efficiency of a spherical detector in a isotropic medium containing uniformly distributed activity. In order to obtain a correct formula we determine the efficiency in two stages. We follow [5] and convert from a distributed source to an equivalent surface source and then calculate the efficiency for that source. On the surface of the detector at point A we locate an elementary area dS (Fig. 1) and define the γ-ray direction distribution $N_{A,E}(\Omega)$; the radiation emerging from an element of volume dV at a distance r from A makes a contribution to $dN_{A,E}(\Omega)$ defined by

$$dN_{A,E}(\Omega)\,dS\,d\Omega = a\eta\,dV\,(dS\cos\theta/4\pi r^2)\exp(-\mu r), \tag{1}$$

where $a$ is the activity per unit volume in the source, E is the γ-ray energy, $\eta$ is the number of γ rays emitted per decay (the quantum yield), and $\mu$ is the linear attenuation coefficient for γ rays in the medium.

We integrate (1) with respect to r from 0 to ∞ to get

$$N_{A,E}(\Omega)\,dS\,d\Omega = (a\eta/4\pi\mu)\cos\theta\,dS\,d\Omega.$$

This implies that the specific activity of the equivalent surface source is $a/4\mu$, and the normalized angular distribution of the γ rays $\varphi(\Omega)$ that emerge from dS is of cosine type:

$$\varphi(\Omega)\,d\Omega = (1/\pi)\cos\theta\,d\Omega.$$

The γ rays are emitted from the source into a half space for each point at the surface of the detector, so the total number that will pass through the surface of the detector in unit time is the product of the area of the surface of the detector and the specific activity of the source together with the quantum yield, i.e.,

$$N_{tot} = (1/\mu)\,\pi R^2 a\eta,$$

where R is the radius of the spherical detector.

We now determine the number of γ rays recorded by the detector in unit time. The thickness $m(\theta, R)$ of the detector in the direction of arrival of a γ ray incident on the detector near point A at an angle $\theta$ to the interior normal is $2R\cos\theta$; the probability that the γ ray will interact with the detector material is

$$\varepsilon_{E,R} = 1 - \exp(-2\mu_0 R\cos\theta),$$

where $\mu_0$ is the linear attenuation coefficient for γ rays in the material of the detector. We integrate $\varepsilon_{E,R}$ with respect to Ω to get the number of γ rays recorded by the detector in unit time that enter the detector near A:

$$dN_{rec} = (a\eta\,dS/4\mu) - (a\eta\,dS/2\mu)\left[\frac{1}{(2\mu_0 R)^2} - (1+2\mu_0 R)/(2\mu_0 R)^2\exp(-2\mu_0 R)\right]. \tag{2}$$

We integrate (2) over the surface of the detector and divide the result by $N_{tot}$ to get the efficiency for γ-ray detection for a homogeneous isotropic medium containing uniformly distributed activity:

$$\varepsilon = (N_{rec}/N_{tot}) = 1 - (1/2(\mu_0 R)^2) + [(1+2\mu_0 R)/2\mu_0 R)^2]\exp(-2\mu_0 R). \tag{3}$$

Translated from Atomnaya Énergiya, Vol. 47, No. 1, pp. 41-42, July, 1979. Original article submitted November 2, 1977.



0038-531X/79/4701-0546$07.50 © 1980 Plenum Publishing Corporation

Declassified and Approved For Release 2013/02/15 : CIA-RDP10-02196R000800020001-4

Declassified and Approved For Release 2013/02/15 : CIA-RDP10-02196R000800020001-4

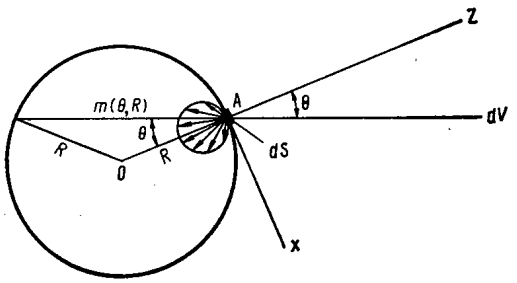


Fig. 1

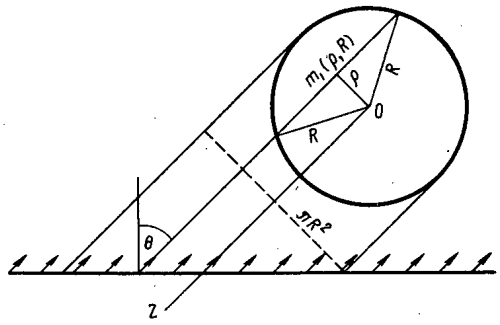


Fig. 2

Fig. 1. A spherical detector recording $\gamma$ rays in a homogeneous isotropic medium containing uniformly distributed activity.

Fig. 2. Recording of $\gamma$ rays from a planar source with a spherical detector.

This expression differs from the corresponding formula of [4], and the difference is due to the inexplicit assumption in the latter study that the angle of distribution of the radiation at the surface of the detector is isotropic, which our argument shows to be incorrect.

We now consider the efficiency of this detector for $\gamma$ rays from a planar source having any angular distribution for the radiation, which is however the same for any point on the source. Clearly, such a source can be represented as the superposition of planar unidirectional sources. In many practical instances one can neglect the attenuation of the radiation in the medium between the source and the detector, and then the spherical form of the detector makes the efficiency the same as that for any of the unidirectional sources constituting the planar source. It is therefore sufficient to consider the radiation from a planar unidirectional source. The efficiency of a $\gamma$-ray detector in an isotropic medium containing uniformly distributed activity can also be derived from the efficiency in the field of a planar unidirectional source [2].

We introduce a cylindrical coordinate system with its origin at the center of the detector and with its z axis parallel to the radiation direction of the unidirectional source (Fig. 2). The total number of $\gamma$ rays passing through the surface of the detector in unit time is

$$N'_{\text{tot}} = \pi R^2 a_1 \eta_1 [\varphi(\theta)/\cos\theta],$$

where $\theta$ is the angle between the z axis and the normal to the plane of the source, $a_1$ is the specific activity, and $\eta_1$ is the quantum yield.

The thickness of the detector $m_1(\rho, R)$ in the direction of arrival of a $\gamma$ ray at a distance $\rho$ from the z axis is $2\sqrt{R^2-\rho^2}$. Then the $\gamma$-ray detection efficiency is

$$\varepsilon = (N_{\text{rec}}/N'_{\text{tot}}) = (1/\pi R^2)\int_0^{2\pi}\int_0^{R}[1-\exp(-2\mu_0\sqrt{R^2-\rho^2})]\,\rho\,d\rho\,d\psi \qquad (4)$$

$$= 1-\frac{1}{2(\mu_0 R)^2}+\frac{1+2\mu_0 R}{2(\mu_0 R)^2}\exp(-2\mu_0 R),$$

which agrees with (3), as would be expected. The error in [2] is due to an error in calculating the integral in (4).

Numerical integration has been used [3] to determine the efficiency for such a detector in the $\gamma$-ray field set up by a planar source with a cosine distribution and arbitrary dimensions. The values for the efficiency given in [3] for an infinite source agree with those from (3) within the error of the numerical integration.

This efficiency formula can be used in sensitivity calculations for radiometers, as well as in determining the photoelectric efficiency and the activity of bulk-distributed sources.

I am indebted to Professor V. V. Matveev for valuable comments.

## LITERATURE CITED

1. C. Sybesma, Measurements of Continuous Energy Distribution $\gamma$ Rays in a Scattering Medium, Amsterdam (1961).
2. Yu. A. Egorov, Scintillation Spectrometry of $\gamma$ Rays and Fast Neutrons [in Russian], Gosatomizdat, Moscow (1963).



Declassified and Approved For Release 2013/02/15 : CIA-RDP10-02196R000800020001-4

Declassified and Approved For Release 2013/02/15 : CIA-RDP10-02196R000800020001-4

3. D. I. Konstantinov et al., in: Dosimetry and Radiation Protection, Issue 6 [in Russian], Atomizdat, Moscow (1967), p. 121.
4. Yu. A. Sapozhnikov, V. A. Lopatin, and V. P. Ovcharenko, At. Energ., 40, No. 3, 246 (1976).
5. H. Hurwicz, G. Reau, and M. Storm, in: Physics of Intermediate Reactors [Russian translation], Gosatomizdat, Moscow (1961), p. 382.

# EXAMINATION OF IRRADIATED METAL DIBORIDES BY X-RAY DIFFRACTION

Kh. É. Maile, I. A. Naskidashvili, and T. Sh. Berdzenishvili

UDC 154-162:539.16.04

It has been shown [1-4] that metal diborides exposed to high thermal-neutron fluences (~ $10^{20}$ neutrons/$cm^2$) undergo considerable changes, even extending to failure. We consider that these changes are due to the production of helium atoms, which escape from the matrix and accumulate in the intergranular pores. However, the neutron fluence required to cause failure in metal diborides is reduced by up to a factor 100 if the material is irradiated at 15°K [5]. This result cannot be explained in terms of the above mechanism, because it is unlikely that the escape of helium from the matrix will be accelerated on reducing the temperature.

For this reason we examined the changes in lattice parameters of titanium and zirconium diborides and the corresponding changes in unit-cell volume produced by low-temperature irradiation in a nuclear reactor.

The specimens of $ZrB_2$ and $TiB_2$ were plates of size 10 × 15 × 1.5 mm, which were examined before and after irradiation by x-ray diffraction with a DRON-1 diffractometer at room temperature. Photographic powder patterns were recorded for the specimens; the diffraction lines were broad rings composed of individual spots. The distortion of the line shape caused by the large grain size was eliminated with the DRON-1 by oscillating the specimen in its own plane.

The specimens were irradiated in low-temperature channels of the reactor at 110 and 300°K, where the temperatures did not fluctuate by more than ±5°K throughout the irradiation.

Figures 1-3 and Table 1 give the results for the $ZrB_2$ and $TiB_2$ specimens, in which the changes in lattice parameters $\Delta a/a_{in}$ and $\Delta c/c_{in}$ are given along with the changes in unit-cell volume $\Delta V/V_{in}$. The reflections from the irradiated specimens are displaced towards smaller angles (the more so the higher the fluence), which indicates an increase in the lattice parameters, which is usually caused by interstitial atoms or groups. As the lattice parameters were measured at room temperature (although the specimens were irradiated at 110°K), only the helium atoms will largely persist as free interstitial atoms out of all those produced by the irradiation (the helium is derived from the $^{10}B$). Therefore, the observed increase in the lattice parameters, particularly in the c parameter, must be due to predominant accumulation of interstitial helium atoms in the lattice.

Table 1 shows that $(\Delta c/c)/(\Delta a/a) < 1$ for $TiB_2$, no matter what the irradiation temperature, whereas $(\Delta c/c)/(\Delta a/a) > 1$ for $ZrB_2$ on low-temperature irradiation, which apparently means that the lattice of $ZrB_2$ retains more helium atoms than does $TiB_2$. This is due on the one hand to the smaller size of the pores in $TiB_2$ (because the lattice parameters are smaller than those of $ZrB_2$) and on the other to the stronger bonds between the atomic layers of metal and boron in $TiB_2$ [1, 3, 6], and therefore the helium atoms are ejected from the $TiB_2$ matrix more readily. If we assume that the change in lattice parameters is due in the main to interstitial helium, we have that the microcracks and failure are due to the internal stresses set up by these interstitial atoms, not to the marked increase in the helium pressure in the pores. If on the other hand the cause of the failure were such pressure rise, then reducing the radiation temperature, which greatly reduces the mobility of the helium, should mean that the failure would occur at higher neutron fluences. However, the failure in $TiB_2$ in fact occurs at a much lower neutron fluence on reducing the irradiation temperature to 110°K [3-5].

Translated from Atomnaya Énergiya, Vol. 47, No. 1, pp. 42-44, July, 1979. Original article submitted December 28, 1977.



0038-531X/79/4701-0548$07.50 © 1980 Plenum Publishing Corporation

Declassified and Approved For Release 2013/02/15 : CIA-RDP10-02196R000800020001-4

Declassified and Approved For Release 2013/02/15 : CIA-RDP10-02196R000800020001-4

TABLE 1

| Specimen | Low-temperature irradiation | | | | | | |
|---|---|---|---|---|---|---|---|
| | $T_{irr} = 110°K$ | | | | $T_{irr} = 300°K$ | | |
| | radiation dose, neutrons/cm² | $\frac{\Delta a}{a_{in}}$ % | $\frac{\Delta c}{c_{in}}$ % | $\frac{\Delta V}{V_{in}}$ % | $\frac{\Delta a}{a_{in}}$ % | $\frac{\Delta c}{c_{in}}$ % | $\frac{\Delta V}{V_{in}}$ % |
| $ZrB_2$ | $5\cdot10^{15}$ | — | 0,04 | 0,04 | 0,01 | 0,01 | 0,03 |
| | $2\cdot10^{16}$ | 0,08 | 0,10 | 0,26 | 0,04 | 0,06 | 0,14 |
| | $1\cdot10^{17}$ | 0,19 | 0,42 | 0,80 | 0,21 | 0,35 | 0,77 |
| $TiB_2$ | $2\cdot10^{16}$ | 0,04 | 0,01 | 0,09 | — | — | — |
| | $1\cdot10^{17}$ | 0,10 | 0,08 | 0,28 | 0,08 | 0,06 | 0,22 |
| | $5\cdot10^{17}$ | 0,46 | 0,25 | 1,17 | 0,34 | 0,22 | 0,90 |
| | High-temperature irradiation [4] | | | | | | |
| | $T_{irr} = 570°K$ | | | | | | |
| $ZrB_2$ | $10^{20}$ | 0,30 | 0,23 | 0,83 | | | |
| $TiB_2$ | $10^{20}$ | 1,50 | 0,13 | 3,13 | | | |

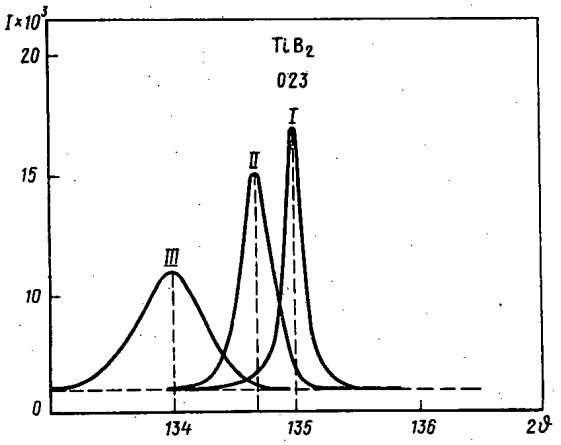


Fig. 1

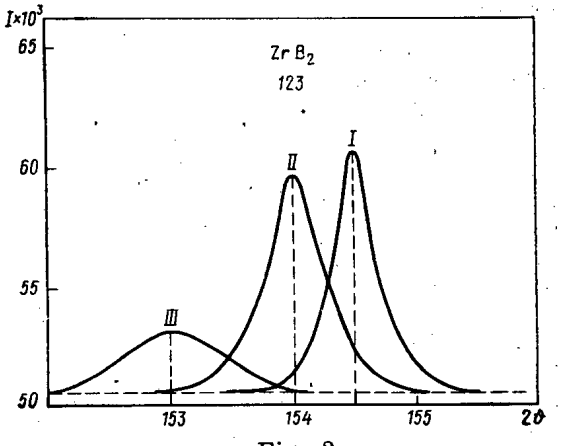


Fig. 2

Fig. 1. The (023) diffraction peaks of $TiB_2$ specimens: I) not irradiated; II) exposed to a neutron fluence of $1\cdot10^{17}$ neutrons/cm² at 110°K; III) the same for $5\cdot10^{17}$ neutrons/cm².

Fig. 2. The (123) diffraction peaks of $ZrB_2$ specimens: I) not irradiated; II) exposed to a neutron fluence of $2\cdot10^{16}$ neutrons/cm² at 110°K; III) the same for $1\cdot10^{17}$ neutrons/cm².

No matter what the irradiation temperature, the maximum increase in unit-cell volume for $ZrB_2$ before the onset of failure is about 0.8%; we therefore conclude that there is a critical concentration of interstitial atoms in $ZrB_2$ above which the expansive force becomes greater than the binding forces between the alternating crystallographic basal planes. This leads to mechanical failure of the crystal. Prolonged irradiation results in reduction in the grain size of the crystal without change in the increment in cell volume, whose value remains around 0.8% for $ZrB_2$.

Figure 3 shows that the increase $\Delta c/c$ produced by the radiation in $ZrB_2$ is almost completely eliminated by annealing the specimen at 670°K, whereas $\Delta a/a$ is then reduced by only 70%. This explains the differences in the data on the lattice-parameter changes obtained on low-temperature and high-temperature forms of irradiation for $ZrB_2$. At high temperatures ($T_{irr} \geq 600°K$), the helium atoms escape into the intergranular pores, and only atoms bound to lattice distortions remain in the diboride lattice, and the concentration of these is much lower. Therefore, the diboride withstands a much higher neutron fluence at high irradiation temperatures because most of the helium remains in the lattice at low temperatures.

When specimens irradiated at 15 or 120°K are heated to room temperature, there is fairly substantial annealing of the radiation-induced defects [5], and it is therefore obvious that the stages of isochronous annealing seen in the radiation-induced increase in the lattice parameters at 300-670°K (Fig. 3) cannot be due to annealing of single defects. These stages in the annealing may be due to the flow of various defect complexes to sinks (helium atoms plus vacancies, pairs formed by interstitial atoms with lithium, etc.), or else the breakup of these into isolated defects, which at these temperatures also migrate to sinks.



Declassified and Approved For Release 2013/02/15 : CIA-RDP10-02196R000800020001-4

Declassified and Approved For Release 2013/02/15 : CIA-RDP10-02196R000800020001-4

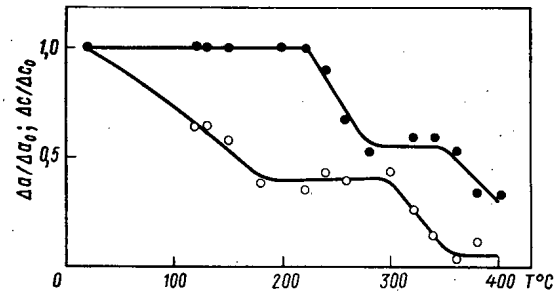


Fig. 3. Isochronous-annealing curves for the radiation-induced increases in lattice parameters for zirconium diboride: ○) $\Delta c/\Delta c_0$; ●) $\Delta a/\Delta a_0$.

Therefore, these results and the available evidence [2-5] indicate that the failure in metal diborides during reactor irradiation is due mainly to internal stresses in the matrix produced by interstitial helium atoms.

Z. A. Titik assisted in the experiments, and we are also indebted to O. I. Yurina for assistance with the calculations and to our colleagues on the nuclear reactor at the Institute of Physics, Academy of Sciences of the Georgian SSR, for general collaboration in performing the low-temperature irradiations.

## LITERATURE CITED

1. G. V. Samsonov, At. Energ., 14, No. 6, 588 (1963).
2. V. V. Ogorodnikov et al., At. Energ., 23, No. 4, 341 (1967).
3. G. V. Samsonov et al., At. Energ., 24, No. 2, 191 (1968).
4. M. S. Koval'chenko and V. V. Ogorodnikov, Fiz. Khim. Obrab. Mat., No. 4, 14 (1971).
5. L. S. Topchyan et al., At. Energ., 42, No. 3, 226 (1977).
6. G. V. Samsonov, Dokl. Akad. Nauk SSSR, No. 83, 689 (1953).

# NEUTRON SPECTRA IN THE MeV RANGE IN FAST CRITICAL ASSEMBLIES

V. M. Lityaev, V. A. Dulin, and Yu. A. Kazanskii

UDC 621.039.51

Neutron spectra are extremely important reactor characteristics, because the quantitative aspect of any process in a reactor may be represented by averaging the neutron interaction cross sections over the neutron spectrum. A spectrum itself is dependent in a complicated fashion on the cross sections for interaction of the neutrons with the materials in the reactor. Further, the theoretical spectrum is also dependent on the approximation used in the treatment. Therefore, neutron-spectrum measurements in reactors are of some interest. Measured and theoretical values provide refinement of the inelastic-scattering matrix for $^{238}U$ and estimation of the error of the group approximation arising near fission thresholds and thresholds for (n, 2n) reactions.

A scintillation spectrometer with $\gamma$-ray discrimination by decay time in a stilbene crystal of diameter 7 mm and thickness 8 mm was used to measure the neutron spectra at the centers of three critical assemblies; this crystal was mounted in a Teflon jacket with a wall thickness of 2 mm. The working principle has been described previously [1]. The energy scale was calibrated from the upper limits of the Compton distributions given by $\gamma$ rays of known energy from $^{137}Cs$, $^{22}Na$, $^{65}Zn$, $^{88}Y$ sources and the 4.42 MeV $\gamma$-ray line from a Po-$\alpha$-Be source. The spectrometer was also calibrated with monoenergetic neutrons from a Van der Graaf accelerator. The reference neutron source was a miniature isotropic $^{252}Cf$ source. The apparatus recoil-proton spectra were converted to neutron energy spectra by differentiation [2] with respect to energy with a variable step ($\sim\sqrt{E}$) (Fig. 1). A correction was made for the edge effect [3], whose values were 1 and 13.5%, respectively, at 0.8-1.4 and 6.5-10.5 MeV. In measurements on the $^{252}Cf$ source, the temperature in the energy range 0.4-10 MeV was 1.41 ±0.03 MeV, which agrees with published values.

Translated from Atomnaya Énergiya, Vol. 47, No. 1, pp.44-45, July, 1979. Original article submitted January 30, 1978.



0038-531X/79/4701-0550$07.50 © 1980 Plenum Publishing Corporation

Declassified and Approved For Release 2013/02/15 : CIA-RDP10-02196R000800020001-4

Declassified and Approved For Release 2013/02/15 : CIA-RDP10-02196R000800020001-4

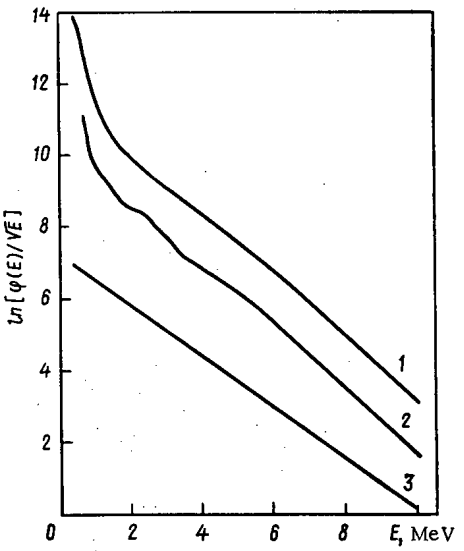


Fig. 1

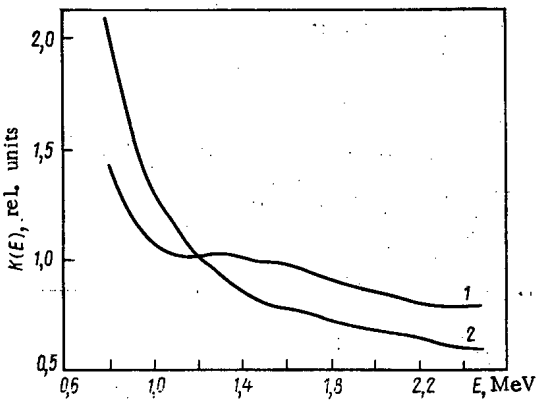


Fig. 2

Fig. 1. Neutron spectra: 1) at the center of the BFS-35-1 assembly; 2) the same for the BFS-33 assembly; 3) for a $^{252}Cf$ source.

Fig. 2. Ratio K(E) of the measured spectra to a 1/E spectrum for the following assemblies: 1) BFS-30; 2) BFS-35-1.

TABLE 1. Measured and Calculated Neutron Fluxes

| Assembly | Energy range, MeV | $\varphi^j_{exp}$ | $\varphi^j_{exp}/\varphi^j_{th}$ with matrices given in | | $(\sigma_f^{238})$ |
|---|---|---|---|---|---|
| | | | [7] | [8] | |
| BFS-30 | 10,5—6,5 | 0,01047 | 0,878 | 0,914 | |
| | 6,5—4,0 | 0,0636 | 0,887 | 0,886 | |
| | 4,0—2,5 | 0,1640 | 0,965 | 0,927 | |
| | 2,5—1,4 | 0,3510 | 1,050 | 1,044 | 0,459 |
| | 1,4—0,8 | 0,4107 | 0,996 | 1,018 | 0,0317 |
| BFS-33 | 10,5—6,5 | 0,0114 | 0,943 | 1,029 | |
| | 6,5—4,0 | 0,0792 | 1,092 | 1,115 | |
| | 4,0—2,5 | 0,1675 | 0,991 | 0,950 | |
| | 2,5—1,4 | 0,3208 | 0,968 | 0,957 | 0,461 |
| | 1,4—0,8 | 0,4212 | 1,015 | 1,037 | 0,0291 |
| BFS-35-1 | 10,5—6,5 | 0,01432 | 1,225 | 0,225 | |
| | 6,5—4,0 | 0,0755 | 1,282 | 1,083 | |
| | 4,0—2,5 | 0,1521 | 1,197 | 1,998 | |
| | 2,5—1,4 | 0,2820 | 1,161 | 1,046 | 0,457 |
| | 1,4—0,8 | 0,4761 | 0,851 | 1,959 | 0,0274 |
| 1/E neutron spectrum | 2,5—1,4 | | | | 0,467 |
| | 1,4—0,8 | | | | 0,0338 |

The main errors in measuring the neutron spectra arise from errors in converting the pulse-height distributions to energy spectra; if one assumes that the Terrell analytical representation applies for a fission-neutron spectrum of $^{252}Cf$, the likely error in determining the neutron flux at 10 MeV relative to 1 MeV is about 15%.

The BFS-30 assembly has a composition close to that in the high-enrichment zone of a fast power reactor with oxide fuel and sodium cooling, while the BFS-33 and -35-1 were constituted by media of uranium oxide and metallic uranium whose enrichment was such as to produce $K_\infty \simeq 1$ [4, 5].

The neutron fluxes were calculated by means of the M-26 program [6] with the BNAB-70 constants [7] (see Table 1). Table 1 also gives the ratios of the measured group neutron fluxes $\varphi^j$ to the theoretical ones for the various inelastic-scattering matrices for $^{238}U$ [7, 8]. The differences between the group fluxes



Declassified and Approved For Release 2013/02/15 : CIA-RDP10-02196R000800020001-4

Declassified and Approved For Release 2013/02/15 : CIA-RDP10-02196R000800020001-4

calculated with the various $\sigma_{in}^{i\to j}$ matrices increase with the ratio of $^{238}U$ to $^{235}U$ (this was 16.8 for the BFS-35-1 assembly) and as the proportions of constructional and moderator materials decrease. The measured group fluxes agreed best with those calculated from the matrix of [8]. Figure 2 shows how the measured neutron spectra differ from a 1/E spectrum. Table 1 also gives the mean group fission cross sections for $^{238}U$ [9] as obtained by averaging for a 1/E spectrum and as derived from the measured spectra. The changes in the mean fission cross section for $^{238}U$ are, respectively, −1.2%, −1.1%, and −2% for the BFS-30, −33, and -35-1 when the measured neutron spectra are used instead of a 1/E spectrum in the averaging.

The value of the theoretical neutron flux above 6 MeV is important in correct allowance for the (n,2n) reactions on $^{239}Pu$ ($^{23}Na$, $^{238}U$); Table 1 shows that the calculations and measurements are in agreement in this region.

## LITERATURE CITED


1. F. Brooks, Nucl. Instrum. Meth., 4, 151 (1959).
2. C. Lanczos, Applied Analysis, Prentice-Hall (1956).
3. Fast-Neutron Physics [in Russian], Vol. 1, Gosatomizdat, Moscow (1963).
4. V. A. Dulin et al., At. Energ., 40, No. 5, 377 (1976).
5. E. N. Kuzin et al., FÉI-698 Preprint, Obninsk (1976).
6. Sh. S. Nikolaishvili et al., in: Proceedings of the Trilateral Soviet–Belgian–Dutch Symposium on Fast-Neutron Physics [in Russian], Vol. 1, Izd. TsNIIatominforma, Moscow (1970), p. 37.
7. L. P. Abagyan et al., Group Constants for Calculations on Nuclear Reactors [in Russian], Atomizdat, Moscow (1964).
8. A. S. Krivtsov and V. I. Popov, in: Neutron Physics [in Russian], Vol. 4, Izd. TsNIIatominforma, Moscow (1977), p. 113.
9. Y. Stehn et al., BNL-325, Supp. No. 2 (1965).


# EFFECTS OF VARIOUS FACTORS ON THE ABSORBED-DOSE DISTRIBUTION IN THIN LAYERS

V. V. Krayushkin

UDC 539.12.08

A specified distribution of absorbed radiation energy within the object must be provided in applied radiation-treatment systems, including industrial ones; we have examined the distribution of the absorbed dose D over the thickness of the material in relation to the angle of incidence of the electron beam, and also the effects of back-scattering metal plates on the distribution of D in thin layers (thickness less than the electron stopping length).

The experiments were performed with electrostatic accelerators at energies of 0.3-1.0 MeV. A thin foil in the exit window resulted in a virtually monoenergetic electron beam. The dosimeters were cellulose triacetate (CTA) films of thicknesses 70 and 140 $\mu$m ($\rho = 1.25$ g/cm$^3$), which simulated thin layers of the target material. The value of D was determined from the difference in the optical densities of the CTA films before and after irradiation as measured with an SFD-2 spectrophotometer by a standard method [1] giving a coefficient of variation of ±8%. Stacks of CTA films were used to adjust the thickness.

The distribution of D in a homogeneous material exposed to a beam incident at right angles containing electrons of energy 0.3-2.0 MeV can be put as

$$D(x) = (D_{max}/2)[1 + \sin(0.2 + \theta_x)], \quad (1)$$

where x is measured in the material in g/cm$^2$, $D_{max}$ is the maximum value of D within the material, and $\theta$ is a parameter dependent on the electron energy [2].

Experiments with these CTA films were performed with the electrons incident at various angles $\alpha$, which led to the empirical formula

$$D_\alpha(x) = [(1 + \cos\alpha)/4]\, D_{max}\{1 + \sin[4.7 + (\theta_x - 4.5)\cos\alpha]\}. \quad (2)$$

Translated from Atomnaya Énergiya, Vol. 47, No. 1, pp. 46-47, July, 1979. Original article submitted February 13, 1979.



0038-531X/79/4701-0552$07.50 © 1980 Plenum Publishing Corporation

Declassified and Approved For Release 2013/02/15 : CIA-RDP10-02196R000800020001-4

Declassified and Approved For Release 2013/02/15 : CIA-RDP10-02196R000800020001-4

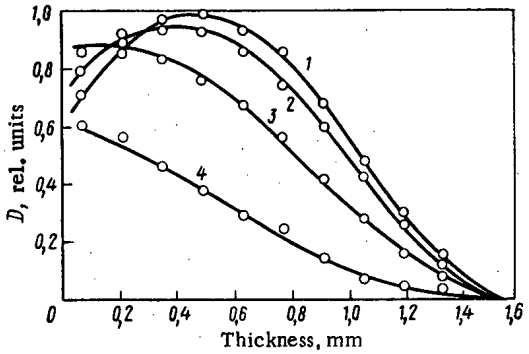


Fig. 1

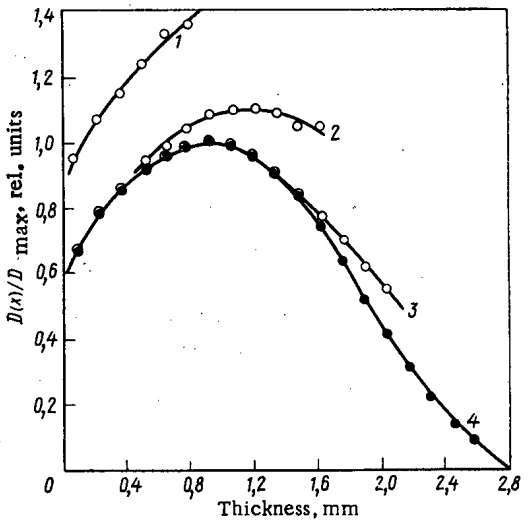


Fig. 2

Fig. 1. Distribution of the absorbed dose over the thickness of CTA films for angles of incidence of the electron beam of 0 (1), 20 (2), 40 (3), and 60° (4) (the points are from experiment).

Fig. 2. Absorbed-dose distributions for specimens of thickness 0.84 (1), 1.68 (2), and 2.1 mm (3); (4) material irradiated without a substrate (semi-infinite geometry).

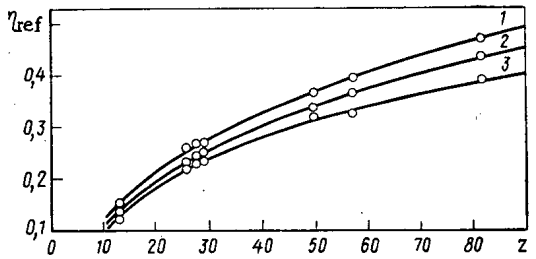


Fig. 3

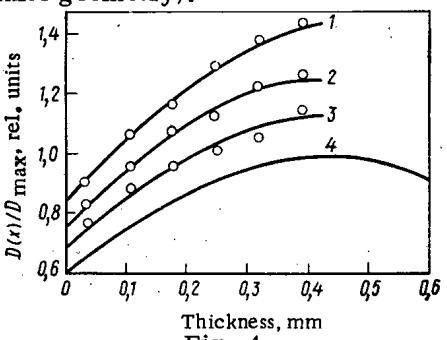


Fig. 4

Fig. 3. Reflected-dose factor in relation to atomic number of metal substrate at energies of 0.4 (1), 0.7 (2), and 1.0 MeV (3).

Fig. 4. Absorbed-dose distribution in CTA films of thickness 0.42 mm exposed to 0.5 MeV electrons on substrates of: 1) lead; 2) nickel; 3) aluminum; 4) no substrate (semi-infinite geometry); the points are from experiment and the lines are from theory.

If the beam is incident normally, i.e., if cos $\alpha = 1$, then (2) becomes (1).

Figure 1 shows the distribution of D over the CTA films for various angles of incidence at 0.5 MeV; there is agreement to within ±7%. It is also of interest to examine the distribution of D in a layer of material irradiated on a metal substrate, since then there is back-scattering from the metal substrate if the thickness of the material is less than electron range, and therefore there is an increase in D near the surface of the substrate.

The metals used in the experiments were aluminum, iron, nickel, copper, tin, brass, and lead. These were used as plates of thickness 1 mm (this thickness was greater than the electron range in the relevant energy), and these were fitted with several CTA films assembled in stacks.

Figure 2 shows the distribution of D in material on a tin substrate exposed to a 0.8-MeV beam. The value of D in the material increases the more substantially the less the thickness for a given electron energy.

The distribution of D over the thickness on irradiation on a metal substrate can be put as the sum of two functions:

$$D_t(x) = \begin{cases} D(x) \text{ for } x \leqslant 2a - 4{,}5/\theta; \\ D(x) + \eta^i_{ref} D(2a - x) \text{ for } x > 2a - 4{,}5/\theta, \end{cases} \quad (3)$$



Declassified and Approved For Release 2013/02/15 : CIA-RDP10-02196R000800020001-4

Declassified and Approved For Release 2013/02/15 : CIA-RDP10-02196R000800020001-4

where D(x) is the distribution of D when the material is irradiated without a substrate by a beam in normal incidence, as (1) shows, and $\eta^{i}_{ref}$ is the dose factor representing backscattering from metal substrate i, and $a$ is the thickness of the irradiated material in g/cm$^2$.

The backscattering correction factors were determined by experiment with the beam incident normally on the target for various electron energies; D increased for CTA films on metal substrates of high atomic number (under otherwise equal conditions). Graphs were drawn up relating the backscattering factor to the atomic number for various electron energies (Fig. 3). The results for the effective reflection factor are in good agreement with the measurements of [3].

Figure 4 shows the distribution of D for material on substrates of various metals for an electron energy of 0.5 MeV; the following formula was devised to calculate D for various angles of incidence in the presence of backscattering substrates:

$$D_{\alpha t}(x)=\begin{cases} D_{\alpha}(x) \text{ for } x\leqslant 2a-4.5/\theta; \\ D_{\alpha}(x)+\eta_{ref}D_{\alpha}(2a-x) \text{ for } x> \\ >2a-4.5/\theta. \end{cases} \quad (4)$$

The observed and calculated values agreed to within ±10%, which indicates that one is justified in using empirical formulas (2)-(4) to calculate the major parameters of radiation-treatment systems.

## LITERATURE CITED

1. A. K. Pikaev, Dosimetry in Radiation Chemistry [in Russian], Nauka, Moscow (1975).
2. V. V. Krayushkin and V. P. Suminova, in: Proceedings of the Second All-Union Conference on Industrial Uses of Charged-Particle Accelerators [in Russian], Vol. 1, Izd. NIIÉFA, Leningrad (1976), p. 347.
3. W. Bothe, Ann. Phys., 6, 44 (1949).

# A CALORIMETER FOR MEASURING LOCAL ELECTRON-BEAM ABSORBED DOSES

V. A. Berlyand, V. V. Generalova, and M. N. Gurskii

UDC 539.12.08

Electron beams of energy between 0.2 and 10 MeV are widely used in radiobiology, industrial applications, and research in many areas; exact measurements on absorbed dose are performed by means of point dosemeters or calorimeters. Many such calorimeters have been described [1] for electrons of energy over 1-2 MeV.

The instrument of [2] allows measurements to be made at electron energies above 150 keV; a single component acts as absorber, temperature transducer, and heater, namely a conducting polyamide film [3], which is made from polyamide lacquer with the addition of carbon black. These films are of high thermal stability and can work at temperatures of 350-400°C for several months or briefly (a few hours) at 450-500°C; the radiation resistance of such a film is also higher by several orders of magnitude than that of the most radiation-resistant polymer, polystyrene. The thickness of the film can be varied over the range 1.5-6 mg/cm$^2$. The carbon content is 20-40 mass%. Measurements show that the thermal defect is not more than 0.3%.

The temperature coefficient of resistance of the material is negative, $\beta = -0.0004$, and this is less by about an order of magnitude than the values for copper and platinum, but the value is still quite sufficient for the measurement of dose rates above $10^3$ rad/sec.

The calorimeter proper is a strip of this film 10 × 20 mm; the inherent resistance is ~200-300 Ω, and this is inserted in one arm of a dc bridge. The bridge is balanced by adjusting the input current at some temperature $T_b$, which is above the environmental temperature. The absorbed dose rate P is defined by

$$P=\frac{(I_1^2-I_0^2)\,R\,(T_b)}{M}, \quad (1)$$

Translated from Atomnaya Énergiya, Vol. 47, No. 1, pp. 47-48, July, 1979. Original article submitted March 23, 1976; revision submitted February 6, 1979.



0038-531X/79/4701-0554$07.50 © 1980 Plenum Publishing Corporation

Declassified and Approved For Release 2013/02/15 : CIA-RDP10-02196R000800020001-4

Declassified and Approved For Release 2013/02/15 : CIA-RDP10-02196R000800020001-4

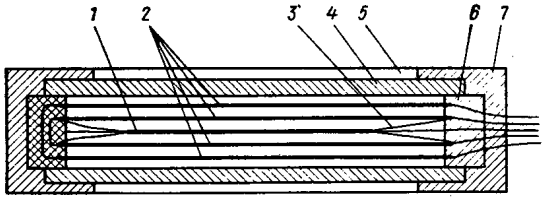


Fig. 1. The dose-rate meter: 1) calorimeter; 2) screen of diameter 40 mm; 3) nylon filaments; 4) radiator; 5) hole of diameter 35 mm; 6) mounting ring; 7) screening body of 60-mm diameter.

where $I_1$ and $I_2$ are the currents in the device for which the bridge is balanced before and during the irradiation respectively, while $R(T_b)$ is the resistance of the device at temperature $T_b$ and M is the mass of the device. Instruments have been devised in uhf engineering [4] for keeping such bridges constantly in balance automatically; these can be used in conjunction with this calorimeter in ionizing-radiation dosimetry.

In our dosemeter (Fig. 1), the calorimeter is surrounded by screens also made of the same material in order to minimize effects from environmental-temperature fluctuations and convection. The distance between the calorimeter and the screen is 1 mm. The design of the mounting ring allows radiators of various materials to be mounted on both sides, and it is therefore possible to make measurements in any material at any depth. The screens and the calorimeter are made of the same material, so the radiation itself sets up quasiadiabatic conditions. If the measurement time is much less than the time constant of the calorimeter, which is about 30 sec, one can assume that

$$P = k\,(dR/dt), \tag{2}$$

where dR/dt is the rate of change of the resistance and k is a coefficient of proportionality. This means that measurements can be made in dynamic mode, which is often preferable, because the electron-beam intensities are high and the time stability is poor.

This instrument in principle provides a means of precision dose-rate measurement; the calorimeter employing this material contains no foreign materials and therefore there are no errors due to energy deposition in foreign inclusions. The material combines the functions of absorber, heater, and transducer, and therefore there is virtually complete identity in the substitution of electrical heating for radiation heating. The systematic error in dose-rate measurement is 0.7% at the 0.95 confidence level, while the random error, expressed as the coefficient of variation, is not more than 2%. The calorimeter provides for dose-rate measurement on electron beams between $10^3$ and $2 \cdot 10^7$ rad/sec for electron energies from 0.15 to 10 MeV or more, while it substantially simplifies the methods used in calibrating film chemical dosimeters in which a total-absorption calorimeter is required [5]. Also, the film calorimeter can be used in the dosimetry of photon radiation, including low-energy x rays, as well as the $\beta$ radiation from large radiation sources.

## LITERATURE CITED

1. S. Gunn, Nucl. Instrum. Meth., 85, No. 2, 285 (1970).
2. V. A. Berlyand, V. V. Generalova, and M. N. Gurskii, Inventor's Certificate No. 593554, Byull. Izobret., No. 39, 212 (1978).
3. V. E. Gul', V. F. Blinov, and M. G. Golubeva, Plastmassy, No. 9, 45 (1976).
4. M. I. Bil'ko et al., UHF Power Measurement [in Russian], Sov. Radio, Moscow (1976).
5. V. A. Berlyand et al., At. Energ., 42, No. 3, 199 (1977).



Declassified and Approved For Release 2013/02/15 : CIA-RDP10-02196R000800020001-4

Declassified and Approved For Release 2013/02/15 : CIA-RDP10-02196R000800020001-4

# DETERMINATION OF NUCLEAR CONSTANTS AS AN INVERSE PROBLEM IN RADIATION TRANSPORT

V. N. Dushin

UDC 539.125.52

The values of nuclear constants obtained by measurement are distorted by various effects arising from the finite dimensions of the systems, including attenuation of radiation fluxes, multiple scattering, etc. The requirements of reactor engineering impose closer tolerances on the determination of constants, and these can no longer be met by correcting for such effects via average factors or terms. Therefore, one has to consider the extraction of nuclear constants from the data of neutron experiments as an inverse problem in the theory of radiation transport [1], for which we give a method applicable to the real geometry, and for which we demonstrate the good performance in recovery of an inelastic-scattering cross section.

We write the transport equation for the system as

$$\Phi(x)=\int K(x'\to x)\,\Phi(x')\,dx'+S(x), \tag{1}$$

where $\Phi(x)$ is the particle-collision density, $x=(\mathbf{r}, \Omega, E)$, $S(x)$ is the collision density for the first collision, and $K(x'\to x)$ is the kernel of the transport equation. The unknown parameters (cross section, scattering indicatrix) appear in $K(x'\to x)$. The collision density $\Phi(x)$ is measured or is calculated from measurements for various values of x and is therefore known approximately. This $\Phi(x)$ may not correspond to any physical kernel $K(x'\to x)$, and therefore one has to avoid solving the inverse problem in the ordinary sense of the word and instead consider the definition of some general solution. Following [2], we take the functions $\sigma(x)$ as the solution ($\sigma(x)$ are the desired nuclear constants), which are such as to provide

$$\Psi_0=\inf_{\sigma(x)\in C}\Psi(\sigma), \tag{2}$$

where

$$\Psi(\sigma)\equiv\int_D[\Phi(x)-\Phi^e(x)]^2\,dx. \tag{3}$$

Here $\Phi^e(x)$ is the experimental collision density, while $\Phi(x)$ is the collision density calculated by means of $\sigma(x)$, and D is the region of definition (measurement) of $\Phi^e(x)$, $\Phi(x)\in L_2$; the condition for physical reality of the target parameters requires that

$$\sigma(x)\geqslant 0. \tag{4}$$

Therefore, the inverse problem in radiation transport amounts to defining the turning point in the function of (3) subject to conditions (4) and (1). The Monte Carlo method is used to solve (1) on account of the complexity of the geometrical conditions in real experiments; this makes the problems stochastic. Stochastic quasigradients [3] are used in solving stochastic turning-point problems, where this gradient is a random quantity whose mathematical expectation is similar to a gradient or generalized gradient in a certain sense. The turning point is defined by a sequence of random vectors

$$\sigma^s,\ s=0, 1, 2, \ldots;\ \sigma^{s+1}=\pi_x(\sigma^s-\rho_s\nu^s);\ s=0, 1, 2, \ldots, \tag{5}$$

where $\pi_X$ is the operator for projection of the acceptable values of the parameters $\sigma$ on the region; $\sigma_0$ is an arbitrary initial point, $\rho_S$ is the step size, and $\nu^S$ is the stochastic quasigradient vector, whose mathematical expectation is

$$M(\nu^s/\sigma^0, \sigma^1, \ldots, \sigma^s)=a_s\hat{\Psi}_\sigma(\sigma^s)+b^s. \tag{6}$$

Here $a_S$ is a nonnegative random quantity, $b^S$ is a random vector, and $\hat{\Psi}_\sigma(\sigma^S)$ is the vector for the generalized gradient, i.e., a vector that for any z satisfies

Translated from Atomnaya Énergiya, Vol. 47, No. 1, pp. 48-50, July, 1979. Original article submitted May 22, 1978.



0038-531X/79/4701-0556$07.50 © 1980 Plenum Publishing Corporation

Declassified and Approved For Release 2013/02/15 : CIA-RDP10-02196R000800020001-4

Declassified and Approved For Release 2013/02/15 : CIA-RDP10-02196R000800020001-4

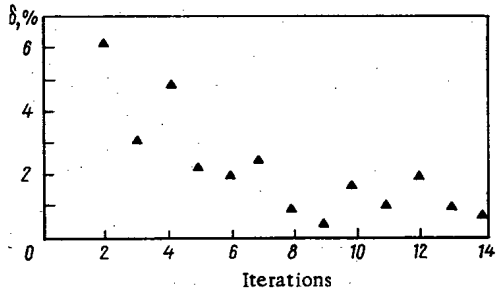


Fig. 1

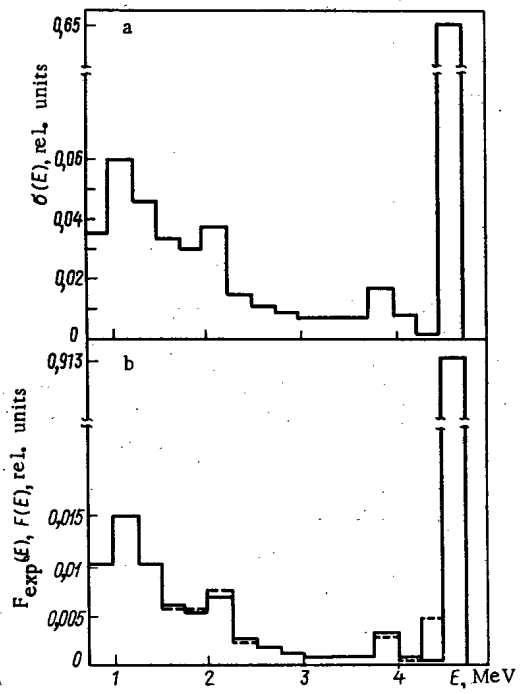


Fig. 2

Fig. 1. Convergence of the minimization in a model experiment; specimen size about 0.5 mean free path.

Fig. 2. Results from processing inelastic-scattering spectra for neutrons in lead: a) recovered cross section; b) solid line – observed spectrum, broken line – spectrum calculated from recovered cross section.

$$\Psi(z)-\Psi(\sigma^s)\geqslant(\hat{\Psi}_\sigma(\sigma^s),\ z-\sigma^s). \tag{7}$$

The process of (5) may not give a monotonic reduction in the target function $\Psi(\sigma)$ at each step, and this is a qualitative difference from the usual gradient method. Some theorems [3, 4] ensure that the process of (5) converges in an infinite number of steps. Only a restricted number of tests can be performed in a practical case, which is equivalent to restricting the processing time, and this requires the introduction of some statistical criterion that will provide some given error level in the functional, Such a criterion can be used with known values for the variances of $\Phi(x)$ and $\Phi^e(x)$ to estimate whether a statistically significant deviation of $\Psi(\sigma)$ from zero occurs, and therefore to determine the points at which the search is stopped. If the target function does not decrease during the minimization and also remains statistically significant, this means either that the gradient describing the radiation transport is inadequate to describe the experimental conditions or that there are systematic errors in the experimental data.

As an example, we give results on the inelastic-scattering cross section for neutrons of energy 4.7 MeV [5]. The experiments were performed at the Khlopin Radium Institute with cylindrical geometry by the time-of-flight method. A program was written for the BÉSM-6, which used a subroutine for solving the transport equation by Monte Carlo methods. Local estimation of the neutron flux is employed [6] together with statistical weights that incorporate the loss of neutrons from the specimen and the absorption. Random termination of the paths was also incorporated. The partial derivatives of the flux required to calculate the stochastic quasigradient were estimated at the same time as the neutron flux itself [7]. The workability of the algorithm was checked out on a model experiment. The spectrum of inelastically scattered neutrons calculated in this way was used to recover the initial model cross section. Figure 1 illustrates the convergence of the minimization, where $\delta$ is defined as

$$\delta=\left\{\int_{\bar{E}}[F_{\exp}(E)-F(E)]^2/F(E)\,dE\right\}^{1/2}. \tag{8}$$

Here $F_{exp}$ (E) and F (E) are the measured and calculated neutron fluxes; as $F_{exp}$ (E) and F (E) are calculated with an error of about 1.6%, we can say that the minimization converges in 5-7 iterations.



Declassified and Approved For Release 2013/02/15 : CIA-RDP10-02196R000800020001-4

Declassified and Approved For Release 2013/02/15 : CIA-RDP10-02196R000800020001-4

This method was used to recover inelastic-scattering cross sections from experiments with specimens of size up to two mean free paths. Figure 2 shows a typical example.

This method can also be used to optimize the shape and size of the specimen, as well as the parameters of the time-of-flight spectrometer.

## LITERATURE CITED

1. A. V. Van'kov, in: Nuclear Science and Technology, Nuclear Constants Series [in Russian], No. 16, Atomizdat, Moscow (1974), p. 11.
2. A. N. Tikhonov and V. Ya. Arsenin, Methods of Solving Incorrectly Formulated Problems [in Russian], Nauka, Moscow (1974).
3. Yu. M. Ermol'ev, Stochastic Programming Methods [in Russian], Nauka, Moscow (1967).
4. Yu. M. Ermol'ev and Z. V. Nekrylova, Kibernetika, 6, 4 (1966).
5. V. N. Dushin et al., [1], No. 24 (1977), p. 27.
6. V. G. Zolotukhin and S. M. Ermakov, in: Physics of Reactor Shielding [in Russian], Gosatomizdat, Moscow (1963), p. 171.
7. E. V. Pletnikov and G. Ya. Trukhanov, [1] (1974), p. 106.

# EFFECTS OF BOMBARDMENT BY $He^+$, $Ni^+$, AND $Cr^+$ ON MICROHARDNESS AND CORROSION CRACKING OF STAINLESS STEELS

B. G. Vladimirov, V. M. Gusev, and V. S. Tsyplenkov

UDC 620.197

One reason for the failure of components made of stainless steels and alloys working at elevated temperatures in water or water–steam mixtures is intercrystallite corrosion followed by cracking under stress [1]. The cracks arise under such conditions at the solid–liquid (or solid–gas) interface, where the state of the metal surface largely determines the rate and type of corrosion failure, particularly in the initial stages. Improved resistance to corrosion cracking is provided by mechanical treatment that produces compressive stresses in the surface layer [2-4].

Also, bombardment with various ions alters the mechanical and physicochemical parameters of the surface layers because the implanted ions produce chemical effects and various defects. In particular, the implantation of $He^+$, $Ni^+$, and $Cr^+$ has been used to improve the corrosion resistance in metals [5, 6]. It is therefore of interest to examine the scope for improving the corrosion resistance of stainless steel by surface treatment with $He^+$, $Ni^+$, and $Cr^+$ ions at energies of rather more than 10 keV.

## Methods

Rectangular plates (size 80 × 5 × 0.6 mm) of stainless steels type 0Kh16N15M3B of the austenite class (after heating to 1050° C) and type 1Kh13S2M2 of the ferrite–martensite class (after annealing at 850°C) were used with grain sizes of 20-30 $\mu$m.

The steels were bombarded with $He^+$, $Ni^+$, and $Cr^+$ ions at 40 keV in an ILU-3 accelerator [7] at a current density of 15-20 $\mu A/cm^2$ to a total dose of $10^{18}$ ions/$cm^2$. The specimens were set up in two different devices. One of these provided for maintenance of a set temperature during irradiation (e.g., 500°C on treatment with $Cr^+$ ions). In the other, the specimens were mounted on a water-cooled table. However, the poor thermal contact meant that the temperature indicated by a Chromel–Alumel thermocouple rose to about 100°C during the bombardment.

The corrosion tests on the original and irradiated specimens were performed in an autoclave made of 0Kh18N10T steel of volume 0.35 liter with an aqueous solution of $FeCl_3$ having a chloride concentration of 100

Translated from Atomnaya Énergiya, Vol. 47, No. 1, pp. 50-51, July, 1979. Original article submitted June 26, 1978.

 0038-531X/79/4701-0558$07.50 © 1980 Plenum Publishing Corporation

Declassified and Approved For Release 2013/02/15 : CIA-RDP10-02196R000800020001-4

Declassified and Approved For Release 2013/02/15 : CIA-RDP10-02196R000800020001-4

TABLE 1. Results of Tests on Corrosion Cracking of Steels in $FeCl_3$ at 360°C and a Pressure of 190 mm Hg (chloride concentration 100 mg/liter)

| Doping element (ion) | Irradiation temperature, °C | Time to failure, h | |
|---|---|---|---|
| | | 0Kh16N15M13B | 1Kh13S2M2 |
| $He^+$ | ~100 | 350 | 90 |
| $Ni^+$ | ~100 | 350 | 30 |
| $Cr^+$ | ~100 | 230 | 60 |
| $Cr^+$ | ~500 | 30 | 70 |
| Original specimen | | 130 | 40 |

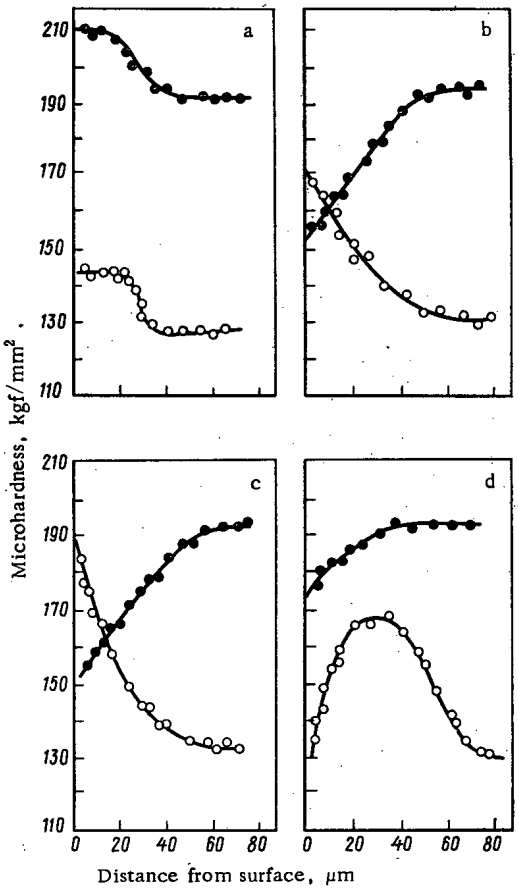


Fig. 1. Change in the microhardness of steels type 0Kh16N15M3B (open circles) and 1Kh13S2N2 (filled circles) over the cross section after surface implantation at 100°C of helium (a), nickel (b), and chromium ions (c), and also chromium at about 500°C (d).

mg/liter at 360°C and 190 mm Hg. The stresses in the specimens were produced by bending in a circular mount [1]. The strain in the stretched outer surface layer after bending was 5%. Constant strain during the test was ensured by contact welding of the ends of the specimen. The onset of failure (occurrence of cracking) was observed by examination with an MBS-2 microscope every 10 h in tests lasting up to 100 h, 20 h for tests lasting up to 200 h, and 90 h for tests lasting up to 500 h. The $FeCl_3$ solution was replaced after each cycle; the tests were continued until the first visible crack appeared. Also, a PMT-3 instrument was used with a load of 100 g to measure the microhardness at various depths by oblique-section methods.

## Experiment Results

The measurements showed that irradiation of 0Kh16N15M3B steel with nickel, helium, or chromium ions at temperatures up to 100°C increased the microhardness down to depths of 40-60 μm; the ranges of $He^+$, $Cr^+$, and $Ni^+$ ions of energy 40 keV in steel are [8] substantially less than 1 μm, and the change in microhardness to much greater depths may be due to radiation-stimulated diffusion of point defects and the formation of dislocation loops, which distort the lattice and harden the material [9].

Figure 1a-c shows that the implantation of the metal ions (nickel and chromium) produces a greater increase in the microhardness at the surface than does implantation of helium; however, helium produces a layer of constant hardness (142 kgf/mm²) throughout a thickness of about 30 μm, whereas the metals produced a rapidly decreasing microhardness. A similar layer of thickness about 20 μm of constant but elevated microhardness (about 210 kgf/mm²) was produced by bombarding 1Kh13S2M2 ferrite-martensite steel with helium (Fig. 1a).



Declassified and Approved For Release 2013/02/15 : CIA-RDP10-02196R000800020001-4

Declassified and Approved For Release 2013/02/15 : CIA-RDP10-02196R000800020001-4

Figure 1d shows that there is a complicated change in the microhardness for 0Kh16N15M3B steel exposed to chromium ions at 500°C; this is clearly the joint effect of several processes, some of which produce hardening and others softening. In particular, lattice distortion due to radiation defects and the formation of finely divided phases tends to harden the implantation layer. However, the radiation may also accelerate the stress relaxation. The peak (Fig. 1d) may reflect the joint effects of these various processes. Type 1Kh13S2M2 steel has a bcc lattice (Fig. 1b-d), and stress relaxation appears to be the dominant effect on bombardment with metal ions.

The corrosion results (Table 1) show that surface treatment with helium, nickel, and chromium ions at about 100°C substantially increases the time to failure for 0Kh16N15M3B steel; by a factor 2.7 for nickel and helium ions or by 1.7 for chromium. Table 1 shows that helium ions (and to a smaller extent chromium ions) also increase the time to failure for ferrite–martensite steel.

Figure 1 and Table 1 show that there is a correlation between the change in microhardness and the corrosion resistance in the implantation layer, apart from the case of 1Kh13S2M2 steel exposed to $Cr^+$ ions. The improved corrosion resistance in the implantation layer may be due to a surface barrier of doping atoms, which prevents the chloride ions from diffusing into the metal and also may prevent the diffusion of oxygen and other corrosion stimulators. There was a certain increase in the corrosion resistance of 1Kh13S2M2 steel after bombardment with $Cr^+$ undoubtedly on account of the surface-barrier effect.

We are indebted to V. P. Voeikov for considerable assistance in performing the corrosion tests.

## LITERATURE CITED

1. V. P. Pogodin, V. L. Bogoyavlenskii, and V. P. Sentyurev, Intercrystallite Corrosion and Corrosion Cracking in Steels in Aqueous Solutions [in Russian], Atomizdat, Moscow (1970).
2. H. Suss, Corrosion, 18, No. 1, 17 (1962); 17, No. 2, 63 (1961).
3. X. Tozano, J. Jpn. Inst. Met., 24, No. 12, 786 (1960).
4. W. Ruttmann and T. Gunther, Werkst. Korros., No. 2, 104 (1965).
5. Yu. M. Khirnyi and A. P. Solodovnikov, Dokl. Akad. Nauk SSSR, 214, No. 1, 82 (1974).
6. A. Autill et al., Corr. Sci., 16, No. 10, 729 (1976).
7. N. P. Busharov et al., Prib. Tekh. Eksp., 4, 19 (1967).
8. J. Lindhard, M. Scharff, and H. Schiott, Kgl. Danske Vid. Selskab, Mat.-Fys. Medd., 33, No. 14 (1963).
9. V. N. Bykov and V. A. Troyan, Phys. Status Solidi, 32, 53 (1975).

# NONSTATIONARY PROMPT-NEUTRON DIFFUSION IN A FAST ASSEMBLY

V. E. Kolesov, O. I. Makarov, and I. P. Matveenko

UDC 621.039.514.4

The characteristic time dependence $\varphi_a(\bar{r}, \bar{v}) \exp(-\alpha_0 t)$ occurs in experiments with pulsed prompt-neutron sources after the transient period, where $\alpha_0$ describes the asymptotic decay of the neutron pulse and is the same no matter what detector is used at any point in the system. If $\alpha_0$ is only slightly dependent on $\bar{r}$ and $\bar{v}$ (which is typical of fast reactors), one says that there is a quasiasymptotic neutron-flux distribution.

One can estimate the limits of an asymptotic or quasiasymptotic distribution by numerical calculation on nonstationary processes; we restrict consideration to the multigroup one-dimensional nonstationary diffusion equation. The numerical method of solving this equation with two or three groups has been described [1]. Here we consider a multigroup treatment with over 20 groups. Consider the equation

$$\hat{v}^{-1} \left.\frac{\partial \bar{\varphi}}{\partial n}\right|_{\nu} - \operatorname{div} \hat{D} \operatorname{grad} \bar{\varphi} + \hat{\Sigma} \bar{\varphi} = \hat{S} \bar{\varphi} + \hat{T} \bar{\varphi} \qquad (1)$$

Translated from Atomnaya Énergiya, Vol. 47, No. 1, pp. 51-52, July, 1979. Original article submitted July 17, 1978.



0038-531X/79/4701-0560$07.50 © 1980 Plenum Publishing Corporation

Declassified and Approved For Release 2013/02/15 : CIA-RDP10-02196R000800020001-4

Declassified and Approved For Release 2013/02/15 : CIA-RDP10-02196R000800020001-4

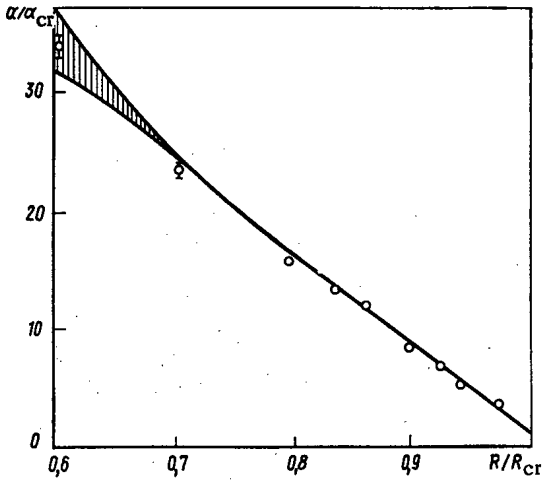


Fig. 1

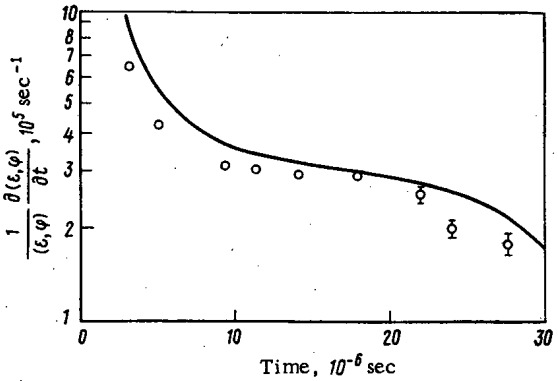


Fig. 2

Fig. 1. Dependence of $\alpha/\alpha_{cr}$ on radius for the BFS-32 assembly: solid line – from theory, points – from experiment.

Fig. 2. Relative derivative of the count rate as a function of time for an assembly containing natural uranium dioxide (symbols as in Fig. 1).

subject to boundary and initial conditions of the form

$$\hat{D}=\frac{\partial\bar{\varphi}}{\partial n}\Big|_{\gamma}=-\hat{l}\bar{\varphi};\ \bar{\varphi}(r,\ t)|_{t=0}=\bar{\varphi}_0(r),$$

where G is the number of energy groups, $\bar{\varphi}(r, t)=\{\varphi^{(1)}(r, t), \varphi^{(2)}(r, t), \ldots, \varphi^{G}(r, t)\}$; $\hat{S}$ is a lower triangular matrix of order G with nonnegative coefficients, T is the complete matrix of that type, and $\hat{v}^{-1}$, $\hat{D}$, $\hat{\Sigma}$, and $\hat{l}$ are diagonal matrices. There is always an asymptotic solution to (1), but the asymptotic distribution may occur after excessive time following the pulse, whereas we are interested in time intervals such that the neutron flux is still above the limit of detection of the instrument or above the background.

We solve (1) by a difference method. The stationary-state approximation has been examined in some detail [2], so we pass at once to the differential-difference equation

$$\hat{v}_h^{-1}\frac{\partial\bar{\varphi}_h}{\partial t}=\hat{\Lambda}_h\bar{\varphi}_h+\hat{T}_h\bar{\varphi}_h, \tag{2}$$

where $\hat{\Lambda}_h$, $\hat{v}_h^{-1}$, $\hat{T}_h$ are difference approximations for the operators div $\hat{D}$ grad $-\hat{\Sigma}+\hat{S}$, $\hat{v}^{-1}$, $\hat{T}$; then $\bar{\varphi}_h(r, t)\approx\bar{\varphi}_{ha}(r)\exp(-\alpha_0 t)$ for large times. It is necessary to follow the behavior of the flux from the start of the pulse to the steady-state value, so the difference scheme must be asymptotically stable [2]. Only a purely inexplicit scheme is unconditionally asymptotically stable amongst the various two-layer schemes for a parabolic equation, so we apply the operator $\hat{\Lambda}_h$ to the upper t layer. The $\hat{T}$ matrix is complete, and this is more convenient to apply to the lower layer. The error in the asymptotic or quasiasymptotic state is reduced by introducing corrections in terms of solutions exponential in t. As a result

$$\hat{v}_h^{-1}\varkappa\left[\bar{\varphi}_{h\tau}(r,\ t)-\bar{\varphi}_{h\tau}(r,\ t-\tau)\right]/\tau=\hat{\Lambda}_h\bar{\varphi}_{h\tau}(r,\ t)+\hat{T}_h\beta\bar{\varphi}_{h\tau}(r,\ t-\tau), \tag{3}$$

where $\tau$ is the time step and

$$\beta=\exp(-\alpha\tau);\ \varkappa=-d\tau/[1-\exp(\alpha\tau)];\qquad \alpha=\frac{1}{-\tau}\ln\left(\frac{\|\bar{\varphi}_{h\tau}(r,\ t-2\tau)\|}{\|\bar{\varphi}_{h\tau}(r,\ t-\tau)\|}\right). \tag{4}$$

The solution to (3) is found for each value of t by one-dimensional fitting for each group in sequence beginning with the first. The scheme of (3) has unconditional asymptotic stability and convergence, and calculations show that the corrections of (4) greatly improve the accuracy. It has been shown [3] for some simple cases (e.g., for $\hat{T}_h=0$) that $\alpha\to\alpha_a$, $\bar{\varphi}_{h\tau}\exp(\alpha t)\to\bar{\varphi}_{ha}$ const for $t\to\infty$ for any $\tau$. In practice these conditions are met for any $\hat{T}_h$ even in the more general case where the corrections of (4) are introduced separately for each group.



Declassified and Approved For Release 2013/02/15 : CIA-RDP10-02196R000800020001-4

Declassified and Approved For Release 2013/02/15 : CIA-RDP10-02196R000800020001-4

The scheme of (3) was implemented as the NESTOR program (nonstationary one-dimensional calculation) in Algol for the M-220; the experimental results were made comparable with the calculations by the use of data for assemblies of two types. The first type was composed of a series of single-zone multiplication systems whose composition was close to the core composition used in fast power reactors (the BFS-32 assembly [4]). A characteristic of such a system is the presence of a quasiasymptotic neutron-flux distribution. Assemblies of the second type corresponded to continuous variation of the neutron spectrum in time. We used an assembly containing natural uranium oxide, which is the blanket material used in fast reactors. The methods of measurement and the parameters of the apparatus corresponded with those of [4] (Figs. 1 and 2).

In the first case, $\alpha$ was calculated for detectors differing in spectral sensitivity $\varepsilon(E)$; the decrement $\alpha$ remained virtually constant after a transient period of about 1.5 $\mu$sec for assemblies of radius from $R_{cr}$ down to 0.7 $R_{cr}$. Smaller assemblies gave $\alpha$ that varied appreciably with time and depended on the type of detector. Figure 1 shows data for a detector having $\varepsilon(E) = \Sigma_f^5(E)$, and in that case the relation $\alpha(t) = [1/(\bar{\varepsilon}, \bar{\varphi})]\,\partial(\bar{\varepsilon}, \bar{\varphi})/\partial t$ after the transient period showed a part with very little slope (plateau). The maximum and minimum values of $\alpha$ given in Fig. 1 correspond to the initial and final instants as taken symmetrically about the middle of the plateau for falls in neutron flux by a factor $10^2$. In the second case, the calculations and experiments were performed for a detector having $\varepsilon(E) = \Sigma_f^5(E)$ and placed at the center of the assembly. A 26-group system of BNAB constants was used.

The experiments and calculations confirmed that these approximations are applicable on calculations on the prompt-neutron kinetics in assemblies (down to $K_{ef} = 0.7$ or less).

## LITERATURE CITED

1. B. I. Kolosov, FÉI-275 preprint, Obninsk (1971).
2. A. A. Samarskii and A. V. Gulin, Stability in Different Schemes [in Russian], Nauka, Moscow (1973).
3. V. E. Kolesov and O. I. Makarov, FÉI-822 preprint, Obninsk (1978).
4. I. P. Matveenko et al., At. Énerg., 44, No. 3, 262 (1978).

# EFFECTS OF ION-BOMBARDMENT DOSE AND PREVIOUS SURFACE TREATMENT ON THE EROSION OF MOLYBDENUM

B. A. Kalin, D. M. Skorov, and V. L. Yakushin

UDC 539.12.04:621.039.616

Blistering under ion bombardment for some considerable time was considered [1-2] as the most important form of erosion of the first wall in a thermonuclear reactor [3, 4]. However, subsequent study showed that blistering in fact falls at high radiation doses [5, 6].

When neobium was bombarded by helium ions of energy 15 keV at 2 mA/cm$^2$, the blistering vanished at doses of $(6.25\text{-}18.75)\cdot 10^{18}$ ions/cm$^2$ [5]. It was suggested that this was due to alteration in the distribution of the implanted gas when the tops of the blisters lift and that there is also an effect from cathode sputtering of the surface layer [5, 6]. The final topography is very much dependent on the irradiation conditions, including target temperature. It is therefore of interest to examine the effects of dose and previous treatment on the irradiation erosion of molybdenum, which is one of the promising materials for these discharge chambers.

Vacuum-melted molybdenum of MChVP grade and TsM10VD alloy were polished mechanically before irradiation, with final finishing with diamond paste type ASM 1/0. Some specimens of the TsM10VD alloy were additionally polished electrolytically. The state of the treated surface was monitored with a 201 PS profilograph.

The specimens were bombarded with helium ions of energy 20 keV at a beam current density of 660 $\mu$A/cm$^2$; the MChVB molybdenum was irradiated at 650°C to doses of $(5\text{-}500)\cdot 10^{17}$ ions/cm$^2$, while the TsM10VD

Translated from Atomnaya Énergiya, Vol. 47, No. 1, pp. 53-54, July, 1979. Original article submitted December 28, 1978.



0038-531X/79/4701-0562$07.50 © 1980 Plenum Publishing Corporation

Declassified and Approved For Release 2013/02/15 : CIA-RDP10-02196R000800020001-4

Declassified and Approved For Release 2013/02/15 : CIA-RDP10-02196R000800020001-4

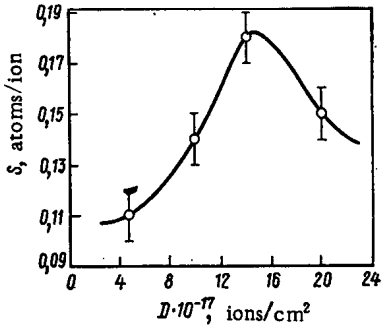


Fig. 1. Erosion coefficient of TsM10VD alloy in relation to dose.

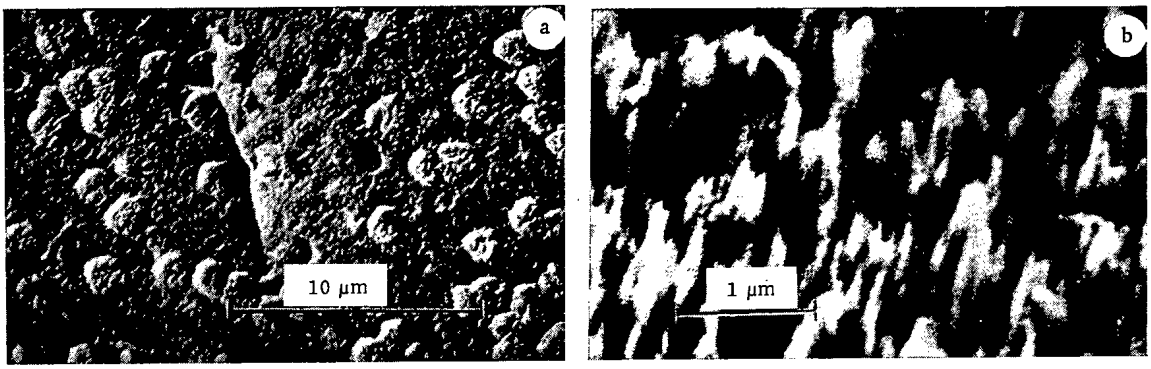


Fig. 2. Surfaces of specimens of TsM10VD alloy after dose of $1 \cdot 10^{18}$ ions/cm$^2$ (a) and of vacuum melted MChVP molybdenum after a dose of $5 \cdot 10^{19}$ ions/cm$^2$ (b).

was irradiated at 700°C with doses of $(4.8\text{-}20) \cdot 10^{17}$ ions/cm$^2$. See [7] for more details of the bombardment conditions. The surface topography was examined with an ÉMV-100L electron microscope by means of carbon replicas shadowed with chromium and also with a Kwikscan-50 scanning microscope. The erosion coefficient was deduced from the electron micrographs via the geometrical dimensions of the tops of the blisters, for which the numbers of atoms were calculated.

Figure 1 shows the observed dependence of the erosion coefficient for TsM10VD in relation to dose; at first, the coefficient increases, but there is a peak in the range $1.4 \cdot 10^{18}$ to $2 \cdot 10^{18}$ ions/cm$^2$. Figure 2a shows a typical electron micrograph of TsM10VD after a dose of $1 \cdot 10^{18}$ ions/cm$^2$. The surface has been substantially eroded, and most of the blisters have burst, with many of the tops leaving the surface of the material.

It was found that mechanical polishing greatly reduced the tendency of the material to produce blisters that fail, especially by comparison with the electropolished material, at all doses in the range from $5 \cdot 10^{17}$ to $5 \cdot 10^{19}$ ions/cm$^2$. For example, a mechanically polished surface showed no broken blisters, whereas electropolished specimens under analogous bombardment conditions showed considerable erosion arising from broken blisters (Fig. 2a). The suppression of blistering appears to be related to microscopic roughness of height 0.04-0.18 μm produced by mechanical polishing. This roughness prevents the gas from forming coplanar layers and thus hinders the union of helium bubbles into gas cavities, which represent the first stage of blistering. Electropolishing also hydrogenates and embrittles the surface layers of molybdenum, and this appears to favor erosion under irradiation.

Doses between $5 \cdot 10^{17}$ and $2 \cdot 10^{18}$ ions/cm$^2$ to MChVP molybdenum produced blisters; the blisters vanished on raising the dose to $5 \cdot 10^{18}$ ions/cm$^2$, but the surface of the material was etched, and cones of height about 0.7 μm were produced on further increase in the dose (Fig. 2b). Blistering is therefore a transient effect.

## LITERATURE CITED

1. W. Primak, Y. Dayal, and E. Edwards, J. Appl. Phys., 34, No. 4, 827 (1963).
2. W. Primak and J. Luthraf, ibid., 37, No. 6, 2287 (1966).
3. R. Behrisch, Nucl. Fusion, 12, No. 2, 695 (1972).
4. E. Kemp, ibid., 14, No. 2, 277 (1974).
5. J. Martel and S. Jacques, in: Proceedings of the Conference on Surface Effects in Controlled Thermonuclear Fusion Devices and Reactors, Argonne, Jan. 10-15, 1974.



Declassified and Approved For Release 2013/02/15 : CIA-RDP10-02196R000800020001-4

Declassified and Approved For Release 2013/02/15 : CIA-RDP10-02196R000800020001-4

6. J. Roth and R. Behrisch, J. Nucl. Mater., 57, No. 3, 365 (1975).
7. D. M. Skorov et al., in: Proceedings of the All-Union Conference on Engineering Problems of Thermonuclear Reactors [in Russian], Vol. 3, NIIÉFA, Leningrad (1977), p. 226.

# A CADMIUM-SULFIDE $\gamma$-RAY DOSIMETER WITH ELEVATED STABILITY UNDER IRRADIATION

V. K. Dubovoi

UDC 53.07/08+53.001.89

A major disadvantage of semiconductor $\gamma$-ray dosimeters is that the irradiation resistance is poor, which hinders their use in high-power irradiation systems, where the exposure dose may be many kR/sec.

In the present dosimeter, high radiation resistance is provided by the use of CdS crystals exposed to fast reactor neutrons. The radiation defects make these crystals homogeneous in bulk properties, while they have good sensitivity to $\gamma$ radiation and a specific resistance of $10^6$-$10^7$ ohm · cm, and the voltage–current response is linear up to fields of 300 V/cm. Ohmic contacts were formed with indium. The dimensions of the detectors were $0.5 \times 0.1 \times 1$ cm, so the $\gamma$-ray distribution at the point of measurement is altered only slightly. The current $I_\gamma$ is measured with a constant voltage applied to the detector. Shunting by the ionized air is eliminated by sealing the transducer and fitting special microconnectors that eliminate current liakage. Figure 1 shows the dosimeter characteristic, where $I_\gamma$ is proportional to the square root of the exposure dose. There is an increase in $I_\gamma$ with temperature, and therefore in the sensitivity of the $\gamma$-ray detector. Measurements were made of the current at a fixed exposure-dose rate of 50 R/sec for various photon energies $E_\gamma$; it was found that the CdS dosimeters had only a slight hardness trend for $\gamma$ radiation. We used $^{60}$Co ($E_\gamma$ = 1.17 and 1.33 MeV) and $^{137}$Cs (0.66 MeV) sources together with the $\gamma$ rays from a reactor, which are strongest at $E_\gamma$ = 0.3 MeV [1]. The radiation resistance in a $\gamma$-ray field was determined from the $I_\gamma$ curves in relation to $^{60}$Co $\gamma$-ray dose at a dose rate of 6000 R/sec, the result being the value of $\sim 10^9$ (Fig. 2).

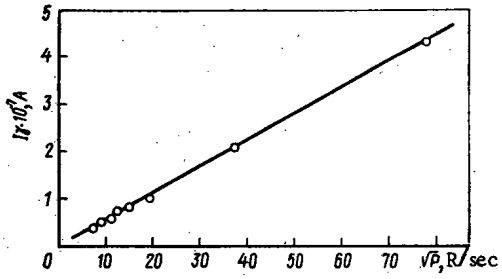


Fig. 1

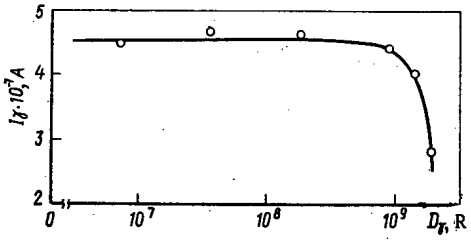


Fig. 2

Fig. 1. Relation of $I_\gamma$ to exposure dose for $^{60}$Co $\gamma$ rays at U = 5 V and T = 30°C.

Fig. 2. Dependence of $I_\gamma$ on $^{60}$Co exposure dose at U = 5 V, T = 30°C, and $P_\gamma$ = 6000 R/sec.

## LITERATURE CITED

1. V. M. Kolyada and V. S. Karasev, At. Énerg., 19, No. 6, 532 (1965).

Translated from Atomnaya Énergiya, Vol. 47, No. 1, p. 54, July, 1979. Original article submitted August 30, 1978.



0038-531X/79/4701-0564$07.50 © 1980 Plenum Publishing Corporation

Declassified and Approved For Release 2013/02/15 : CIA-RDP10-02196R000800020001-4

Declassified and Approved For Release 2013/02/15 : CIA-RDP10-02196R000800020001-4

# THE THERMAL-NEUTRON FISSION CROSS SECTION AND THE FISSION-RESONANCE INTEGRAL FOR $^{243}$Cm

K. D. Zhuravlev and N. I. Kroshkin

UDC 539.172.4

Thermal-neutron fission cross sections $\sigma_f$ and the resonant-fission integral $I_f$ for $^{243}$Cm have been measured in determining nuclear constants for the actinides by the cadmium difference method; the standard was a $^{235}$U target, for which the thermal-neutron fission cross section was taken as 582.2 ±1.3 barn, while the resonant-fission integral was taken as 275 ±5 barn [1]. Measurements were made in a horizontal channel in the SM-2 high-flux reactor. The cadmium ratio for $^{235}$U was 40 when the neutron beam was filtered with 1 mm of cadmium.

The uranium and curium targets were deposited on aluminum substrates of thickness 0.1 mm. The amount of substance in the target was about 1 $\mu$g in each case, while the diameter of the target spot was about 10 mm. The curium target had the following percent isotope composition: $^{242}$Cm 0.15 ± 0.07, $^{243}$Cm 37.29 ± 1.34, $^{244}$Cm 61.61 ±1.34, $^{245}$Cm 0.94 ±0.10. The number of nuclei in the curium target was determined from the spontaneous fission rates of $^{244}$Cm and $^{242}$Cm. The spontaneous-fission half-life of $^{244}$Cm was taken as $(1.270 \pm 0.007) \cdot 10^7$ yr, andthat for $^{242}$Cm was taken as $(6.09 \pm 0.18) \cdot 10^6$ yr [2]. The number of nuclei in the uranium target was determined by $\alpha$ counting in $2\pi$ geometry. The isotope composition of the uranium target and the method of use have been described in detail [3, 4].

The measurements led to correction of $\sigma_f$ and $I_f$ for $^{243}$Cm ($K_\sigma^{244} = 0.998$, $K_I^{244} = 0.987$ and $K_\sigma^{245} = 0.937$, $K_I^{245} = 0.987$), on account of the contents of $^{244}$Cm and $^{245}$Cm, which relate respectively to the thermal-neutron fission cross section and the resonant-fission integral.

The temperature of the neutrons at the reactor exit having a Maxwellian spectrum was 353°K [4], and the g(T) correction incorporated the fact that the fission cross section of uranium does not follow $1/\sqrt{E}$ so the value was 0.965 [5]. It was assumed for curium that the fission cross section follows $1/\sqrt{E}$ and g(T) = 1.

Table 1 gives the fission cross section and resonance integral, which are in agreement within the error of measurement. The spread in the values is probably due to the lack of data on the behavior of the fission cross section of $^{243}$Cm in the thermal range.

TABLE 1. Thermal-Neutron Fission Cross Section and Resonant Fission Integral for $^{243}$Cm in barn

| Parameter | Our results | Data of [1] | Data of [6] |
|---|---|---|---|
| $\sigma_f$ | 672±60 | 600±50 | 609,6±25,9 |
| $I_f$ | 1480±150 | 1860±400 | 1575±136 |

## LITERATURE CITED

1. Neutron Cross Sections, BNL-325, Third Edition, Vol. 1 (1973).
2. Yu. S. Zamyatnin, in: Nuclear Constants [in Russian], No. 14, Atomizdat, Moscow (1974), p. 22.
3. K. D. Zhuravlev, N. I. Kroshkin, and A. P. Chetverikov, At. Énerg., 39, No. 4, 285 (1975).
4. K. D. Zhuravlev and N. I. Kroshkin, in: Atomic Science and Engineering, Nuclear Constants Series [in Russian], No. 19, Atomizdat, Moscow (1975), p. 3.
5. P. É. Égel'staff, in: Handbook on Nuclear Physics [in Russian], Fizmatgiz, Moscow (1963), p. 268.
6. C. Bemis et al., Sci. Eng., 63, 413 (1977).

Translated from Atomnaya Énergiya, Vol. 47, No. 1, p. 55, July, 1979. Original article submitted August 7, 1978.

0038-531X/79/4701-0565$07.50 © 1980 Plenum Publishing Corporation



Declassified and Approved For Release 2013/02/15 : CIA-RDP10-02196R000800020001-4

Declassified and Approved For Release 2013/02/15 : CIA-RDP10-02196R000800020001-4

# ABSOLUTE MEASUREMENT OF THE BRANCHING RATIO FOR THE 277.6-keV LINE OF $^{239}$Np

V. K. Mozhaev, V. A. Dulin, and Yu. A. Kazanskii

UDC 661.039.51

It is common to measure the intensity of the $^{239}$Np $\gamma$ rays in order to determine the accumulation of $^{239}$Pu in breeder reactors; in some cases it is necessary to know the branching ratio of the 277.6-keV $\gamma$-ray line in the decay of $^{239}$Np. Also, it has been suggested that the set of standard calibrated radioactive preparations (from the IAEA) should contain $^{243}$Am instead of $^{203}$Hg. In that case it is also necessary to know the absolute yield of the $\gamma$ line of $^{239}$Np, as this is formed by the $\alpha$ decay of $^{243}$Am.

We have measured the absolute intensity of the $\gamma$ line of $^{239}$Np ($E_\gamma$ = 277.6 keV) by means of an $\alpha$ particle calibrated $^{243}$Am source and the $^{203}$Hg source from the OSGI set of standard radioactive sources. The $^{243}$Am was calibrated in precisely known geometry from the $\alpha$-particle counting rate provided by a silicon detector [1].

The $\gamma$ rays from the $^{243}$Am and $^{203}$Hg preparations were recorded with a germanium detector having a sensitive volume of about 35 cm$^3$.

The absolute yield of the $\gamma$ line of $^{239}$Np ($J_{\gamma Np}$) was determined from

$$J_{\gamma Np} = \frac{N_{\gamma Np} Q_{Hg} \varepsilon_{\gamma Hg}}{N_{\gamma Hg} Q_{Am} \varepsilon_{\gamma Np}} J_{\gamma Hg},$$

where $N_{\gamma Np}$ and $N_{\gamma Hg}$ are the count rates produced by $\gamma$ rays of energy 277.6 for $^{243}$Am and 279.1 keV for $^{203}$Hg; $Q_{Am}$ and $Q_{Hg}$ are activities of those isotopes; $\varepsilon_{\gamma Np}$, $\varepsilon_{\gamma Hg}$ are the efficiencies for $\gamma$ rays of energies 277.6 and 279.1 keV, respectively, in the germanium detector; and $J_{\gamma Hg}$ is the branching ratio for the $\gamma$ line ($E_\gamma$ = 291.1 keV) in the decay of $^{203}$Hg (0.8155 ± 0.0015 [2]).

The ratio of the $\gamma$-ray efficiencies ($\varepsilon_{\gamma Hg}/\varepsilon_{\gamma Np}$) is dependent on the slope of the efficiency curve for $\gamma$ rays in the total-absorption peak. The trend with energy is governed by the size of the sensitive volume and the counting geometry. The ratio of the efficiencies for $\gamma$ rays of energies of 279.1 and 277.6 keV was measured with the OSGI set as 0.995 ±0.004.

We give below the components of the error that determine the overall error in measuring the branching ratio of the $\gamma$ line of $^{239}$Np having $E_\gamma$ = 277.6 keV, %:

| | |
|---|---|
| Statistical error | 0.40 |
| Activity of $^{203}$Hg [3] | 1.50 |
| Activity of $^{243}$Am [1] | 0.33 |
| Ratio of efficiencies for $\gamma$ rays of $^{203}$Hg and $^{243}$Am. | 0.40 |
| Self-absorption of the $\gamma$ rays in $^{243}$Am | 0.001 |
| Branching ratio for $\gamma$ line of $^{203}$Hg ($E_\gamma$ =279.1 keV) | 0.20 |
| Total error of measurement for the branching ratio for the $\gamma$ line of $^{239}$Np ($E_\gamma$ = 277.6 keV) | 1.65 |

The overall error of measurement is clearly governed by the error in the calibrated $^{203}$Hg source from the OSGI set.

We give below the branching ratios for the $\gamma$ line of $^{239}$Np with $E_\gamma$ = 277.6 keV as measured here and quoted elsewhere:

Translated from Atomnaya Énergiya, Vol. 47, No. 1, pp. 55-56, July, 1979. Original article submitted September 1, 1978.



0038-531X/79/4701-0566$07.50 © 1980 Plenum Publishing Corporation

Declassified and Approved For Release 2013/02/15 : CIA-RDP10-02196R000800020001-4

Declassified and Approved For Release 2013/02/15 : CIA-RDP10-02196R000800020001-4

| | |
|---|---|
| [4] | 0.145 ±0.004 |
| [2] | 0.1450 ±0.0015 |
| [5] | 0.141 ±0.004 |
| [6] | 0.152 ±1.005 |
| Our result | 0.1430 ±0.0024 |

We are indebted to S. E. Lavrov and V. I. Ivanov for preparing the $^{243}Am$ source and determining the isotope composition.

## LITERATURE CITED

1. V. A. Dulin and V. K. Mozhaev, At. Energ., 44, No. 6, 528 (1978).
2. C. Bowman, Reports US Nuclear Data Committee, USNDC-9 (1973), p. 225.
3. Certificate Nos. 227 and 228, OSGI (1975).
4. J. Ahmad and M. Wahlgren, Nucl. Instrum. Methods, 99, No. 2, 333 (1972).
5. L. N. Yurova et al., At. Energ., 36, No. 1, 51 (1974).
6. C. Bowman, Reports US Nuclear Data Committee, USNDC-11 (1974), p. 274.

# CALCULATION OF THE TRUE VOLUME PROPORTION OF STEAM IN THE DRIVING SECTION OF A NATURAL-CIRCULATION LOOP

L. N. Polyanin and A. L. Putov

UDC 621.039.52.44

Here we calculate the true volume proportion of steam in the driving section of a natural-convection loop operating at low pressures.

The true volume content of steam $\varphi$ is related to the mass flow X and the steam breakthrough factor $\omega$ by

$$\varphi = 1\Big/\left(1+\omega\frac{\rho''}{\rho'}\frac{1-X}{X}\right), \tag{1}$$

where $\rho'$ and $\rho''$ are the densities of water and steam, respectively. The coefficient $\omega = W_V/W_W$ appearing in (1) varies over the height of the driving section, where $W_W$ and $W_V$ are the true speeds of the water and steam, on account of increase in the group rate of rise of the steam bubbles $W_{ris}^{gr}$ as the steam content increases.

By definition

$$\omega = \frac{W_V}{W_W} = 1+\frac{W_{ris}^{gr}}{W_W} = 1+\frac{1-\varphi}{1-X}\frac{W_{ris}^{gr}}{W_0^{ds}}, \tag{2}$$

where $W_0^{ds} = G/\rho' S_{ds}$ is the circulation rate, $S_{ds}$ is the area of cross section of the driving section, and G is the mass flow rate upon the heat carrier in the driving section.

Measurements [1, 2] for $\varphi \le 0.5$ show that $W_{ris}^{gr}$ is related to the rate of rise of a single bubble $W_{ris}^{0}$ by

$$W_{ris}^{gr} = W_{ris}^{0}/(1-\varphi). \tag{3}$$

We substitute (3) into (2) to get

$$\omega = (1+K_W)(1-\varphi)\Big/\left[1-\left(1+K_W\frac{\rho''}{\rho'}\right)\varphi\right], \tag{4}$$

where $K_W = W_{ris}^{0}/W_0^{ds}$.

Translated from Atomnaya Énergiya, Vol. 47, No. 1, pp. 56-57, July, 1979. Original article submitted September 1, 1978; revision submitted November 10, 1978.

0038-531X/79/4701-0567$07.50 © 1980 Plenum Publishing Corporation



Declassified and Approved For Release 2013/02/15 : CIA-RDP10-02196R000800020001-4

Declassified and Approved For Release 2013/02/15 : CIA-RDP10-02196R000800020001-4

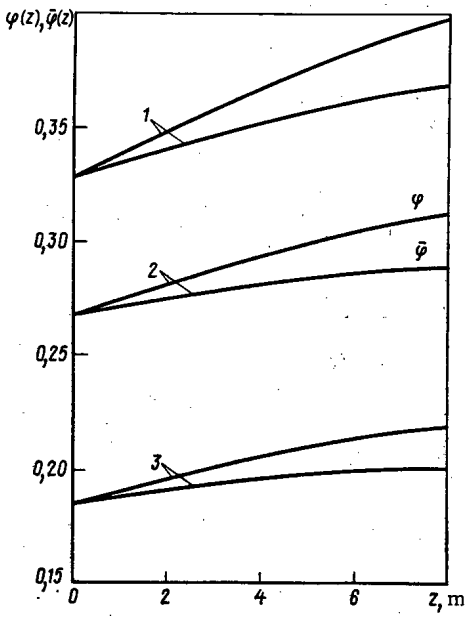


Fig. 1. Height variation of $\varphi$ (z) calculated from (15) and the mean value $\bar{\varphi}$ (z) for pressures (kgf/cm$^2$) of: 1) 12; 2) 16; 3) 25; for $X_0 = 0.01$.

The variation of X over the height z of the driving section is as follows for quasiequilibrium flow conditions:

$$\frac{dX}{dz} = -\frac{1}{r}\frac{di'}{dz} = -\frac{1}{r}\frac{di'}{dp}\frac{dp}{dz}, \tag{5}$$

where

$$\frac{dp}{dz} = -g[\rho'(1-\varphi)+\rho''\varphi], \tag{6}$$

because the pressure loss due to friction and acceleration of the flow can be neglected under these conditions. Here i' is the enthalpy of the water on the saturation line, p is pressure, r is the latent heat of vaporization, and g is acceleration due to gravity. As di'/dp is comparatively small in the driving section, it can be taken as constant.

From (1) and (4)-(6) we get an equation for the true volume steam content:

$$\frac{d\varphi}{dz} = \left[1-\left(1-\frac{\rho''}{\rho'}\right)\varphi\right]^3 \Big/ D(1+K_W), \tag{7}$$

where

$$D = r\rho''/g\left(\frac{di'}{dp}\right)(\rho')^2. \tag{8}$$

The effect from boiling in the carrier (which causes $\varphi$ to rise in the driving section) is important only in the region of comparatively low pressures, where $\rho''/\rho' \ll 1$, and then (7) has the solution

$$\varphi = 1 - 1\Big/\sqrt{\frac{1}{(1-\varphi_0)^2}+\frac{2z}{D(1+K_W)}}. \tag{9}$$

The value $\varphi_0$ at the inlet to the driving section (z = 0) is given by

$$\varphi_0 = 1\Big/\left[1+(1+K_W)\frac{\rho''}{\rho'}\frac{1-X_0}{X_0}+K_W\frac{\rho''}{\rho'}\right], \tag{10}$$

which is equivalent [1, 3] to the generally accepted formula

$$\varphi_0 = W_0''/(W_0''+W_0'+a), \tag{11}$$

where $W_0'$ and $W_0''$ are the reduced velocities of the water and steam respectively, while $a$ is the characteristic velocity of single-bubble rise $W_{ris}^0$ appearing in (3). It is recommended [1, 4] that this speed should be derived from



Declassified and Approved For Release 2013/02/15 : CIA-RDP10-02196R000800020001-4

Declassified and Approved For Release 2013/02/15 : CIA-RDP10-02196R000800020001-4

$$a=\begin{cases}(0{,}65-0{,}0039p)\sqrt[4]{\frac{d_{ds}}{63}}, & d_{ds}<200 \text{ mm},\\ 0{,}86-0{,}0052p, & d_{ds}\geqslant 200 \text{ mm},\end{cases} \quad (12)$$

where $d_{ds}$ is the diameter of the driving section in mm and p is pressure in kgf/cm$^2$ ($11 \leq p \leq 125$ kgf/cm$^2$).

It has been found by experiment [5] that the deformation of the steam-content curve at the inlet to the driving section has virtually no effect on the mean value $\bar{\varphi}$ and therefore on the flow rate of the carrier in this natural-circulation loop. Measurements on the VK-50 boiling-water reactor [6] provided an analogous conclusion, namely that the total flow rate in the natural-circulation loop is independent of the energy generation in the individual cassettes in the core. Therefore, $\varphi_0$ can be calculated from (10) with $X_0$ taken as the mean mass steam content over the section at the outlet from the core.

Figure 1 illustrates the solution by reference to theoretical $\varphi(z, p)$ and $\bar{\varphi}(z, p) = \frac{1}{z}\int_0^z \varphi(z', p)\,dz'$ for the case $X_0 = 0.01$ and $K_W = 2$; clearly, the change in the true volume content of steam over the height arising from the boiling in the carrier is considerable at low pressures in an extended driving section, and this should therefore be incorporated into the calculations on the driving head and the steam available in the loop.

## LITERATURE CITED


1. A. I. Filimonov et al., Teploenergetika, No. 10, 22 (1957).
2. G. B. Wallis, One-Dimensional Two-Phase Flow, McGraw-Hill (1969).
3. A. Ya. Kramerov and Ya. V. Shevelev, Engineering Calculations on Nuclear Reactors [in Russian], Atomizdat, Moscow (1964).
4. G. G. Bartolomei, V. A. Suvorov, and S. A. Tevlin, in: Water Preparation and Processes in Boilers [in Russian], No. 1, Gosénergoizdat, Moscow (1963).
5. I. S. Dubrovskii, Teploenergetika, No. 2, 31 (1974).
6. A. P. Sarygin et al., At. Energ., 30, No. 4, 350 (1971).


# A LOCAL APPROACH TO DETERMINATION OF THE COORDINATES OF AN INTERFACE

F. L. Gerchikov and V. D. Kosarev

UDC 539.171:539.12

X rays are used to considerable advantage at the present time in automatic-control systems [1]; this requires an optimum apparatus design and also definition of the working conditions in the radiation fields, so it is necessary to know the parameters of the direct beam and of the scattered radiation, including the fields arising from backscattering at interfaces with air.

Much of the information on scattered-radiation characteristics for interfaces has been derived either by Monte Carlo techniques or by integrating the distributions for point unidirectional sources over the surface of the scatterer or over the volume of the air [2-4]. However, the methods and apparatus available for integral evaluation of the scattered radiation and for determining the coordinates of the interface when one of the media is air are subject to substantial limitations on account of the marked effect of the component scattered by the air [2, 3]. Measurements show that the backscattered flux decreases away from the scatterer, whereas the flux scattered by the air increases. These two fluxes become comparable at a certain distance. The point where the fluxes are equal is the critical value $R_{cr}$ as regards determination of the upper limit to the boundary position.

It has been pointed out [2] that the $\gamma$ rays from $^{137}$Cs show a detectable effect in the air at a distance of 10 m, while $R_{cr} = 22$ m; our measurements have also shown that $R_{cr} = 12$-15 m for x rays of effective quantum energy 60 keV [4].

Translated from Atomnaya Énergiya, Vol. 47, No. 1, pp. 57-58, July, 1979. Original article submitted December 4, 1978.

0038-531X/79/4701-0569$07.50 © 1980 Plenum Publishing Corporation



Declassified and Approved For Release 2013/02/15 : CIA-RDP10-02196R000800020001-4

Declassified and Approved For Release 2013/02/15 : CIA-RDP10-02196R000800020001-4

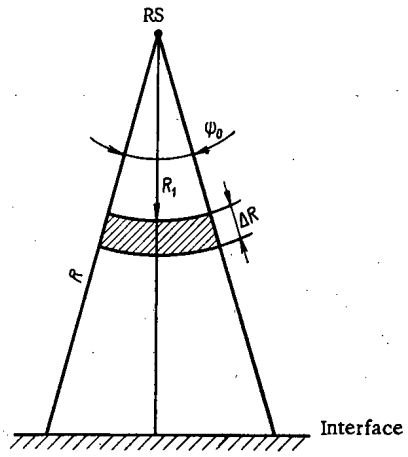


Fig. 1. Working geometry.

Therefore, on the whole, the integral approach to the identification of interfaces and the parameters of the backscattering pattern in the presence of air show marked effects from the distance to the interface, and these effects are extremely important in determining the upper limit to the coordinates of the interface.

Consider an air medium at a distance R from a scatterer exposed to point isotropic pulsed x-ray source RS which is combined with a total-absorption detector in conditions of good geometry, in which an energy flux $E_0$ is emitted into an angle $\Psi_0$ (Fig. 1). We estimate the air component of the scattering on the assumption that the interface is a hemisphere at the center of which lie the detector and source, which are at a distance $R_1$ in vacuum from the hemisphere. The backscattered energy flux is [2] as follows in the air–vacuum geometry:

$$E_a(E_1) = E_0 A_e \Psi_0 / 2\pi R_1^2, \tag{1}$$

where $A_e$ is the energy albedo.

We increase $R_1$ by a certain amount $\Delta R$ and then have by analogy with (1) that

$$E_a(R_1+\Delta R) = E_0 A_e \Psi_0 / 2\pi (R_1+\Delta R)^2. \tag{2}$$

The energy flux backscattered by the air layer at a distance $\Delta R$ from the detector is

$$E_a(\Delta R) = E_a(R_1+\Delta R) - E_a(R_1).$$

If a layer $\Delta R$ of air is placed at a distance R from the source, a survey [2] indicates that the backscattered energy flux arising from the localized area of air as corrected for attenuation is

$$E_a(\Delta R) = E_0 A_e \Psi_0 \exp(-2\mu_0 R)[1-\exp(-2\mu_0 \Delta R)](2\pi R^2)^{-1}. \tag{3}$$

The density of the energy flux backscattered by the material is affected by the attenuation of the primary beam $\mu_0$ and that of the scattered beam $\mu_1$, the result being [2]

$$E_r = E_0 A_e \Psi_0 \exp[-(\mu_0+\mu_1) R](2\pi R^2)^{-1}. \tag{4}$$

We use (3) and (4) with suitable steps to get

$$\frac{E_a(\Delta R)}{E_r} = \frac{1-\exp(-2\mu_0 \Delta R)}{\exp[-(\mu_1-\mu_0) R]}. \tag{5}$$

As $\mu_0 \Delta R \ll 1$ and $(\mu_1-\mu_0)R \ll 1$ in (5) for soft x rays, we put

$$\frac{E_a(\Delta R)}{E_r} = \frac{2\mu_0 \Delta R}{1-(\mu_1-\mu_0) R}. \tag{6}$$

We determine $R_{cr}$ by equating (6) to 1 and allow $\Delta R$ to tend to zero (the localized air volume is minimal). Then we have

$$R_{cr} = (\mu_1-\mu_0)^{-1}. \tag{7}$$



Declassified and Approved For Release 2013/02/15 : CIA-RDP10-02196R000800020001-4

Declassified and Approved For Release 2013/02/15 : CIA-RDP10-02196R000800020001-4

Comparison of (7) with the analogous expression $R_{cr} = (3\mu_0 + \mu_1)^{-1}$ of [2] shows that local estimates of the backscattered radiation and determination of the position of the interface when one of the media is air can allow one to identify the backscattering from the air and the material over a range of coordinates of the interface broader than that for the integral method. Engineering implementation of the local-evaluation method can be provided by dynamic strobing of the detector; a narrow strobe $\Delta t$ ($\Delta R$) is used with a synchronized source to scan localized volumes of air in accordance with a set program, as well as the surface of the scatterer in order to identify the quanta scattered by the material and the air.

In experiments, $\Delta t = 10$ nsec ($\Delta R = 1.5$ m), and the radiation sources were ones developed in collaboration with I. P. Karpinskii et al. [5] and Kalinin Polytechnical Institute in Leningrad, which have been used in determining the coordinates of air–concrete interfaces for $R \leq 80$ m. The detector was a plastic scintillator (polystyrene containing P-terphenyl and POPOP) working with an FÉU-87 [6].

## LITERATURE CITED

1. Apparatus and Methods for X-Ray Analysis [in Russian], Nos. 19-21, Mashinostroenie, Leningrad (1978).
2. B. P. Bulatov and N. F. Andryushin, Backscattered Gamma Radiation in Radiation Engineering [in Russian], Atomizdat, Moscow (1971), p. 201.
3. Radiation Technology, Issue 3, Papers from the All-Union Radiation Engineering Research Institute [in Russian], Atomizdat, Moscow (1969), p. 117.
4. F. L. Gerchikov, At. Energ., 40, No. 6, 487 (1976); 41, No. 6, 414 (1976).
5. I. D. Ivanov et al., in: Nuclear Instrumentation [in Russian], Nos. 34-35, Atomizdat, Moscow (1977), p. 126.
6. A. P. Karmanova and E. E. Stepanov, in: Papers from the All-Union Instrumentation Research Institute [in Russian], Nos. 30-31 (1976), p. 69.



Declassified and Approved For Release 2013/02/15 : CIA-RDP10-02196R000800020001-4

Declassified and Approved For Release 2013/02/15 : CIA-RDP10-02196R000800020001-4



# ACADEMICIAN PAVEL ALEKSEEVICH CHERENKOV

## (ON HIS 75th BIRTHDAY ANNIVERSARY)

E. I. Tamm and B. B. Govorkov

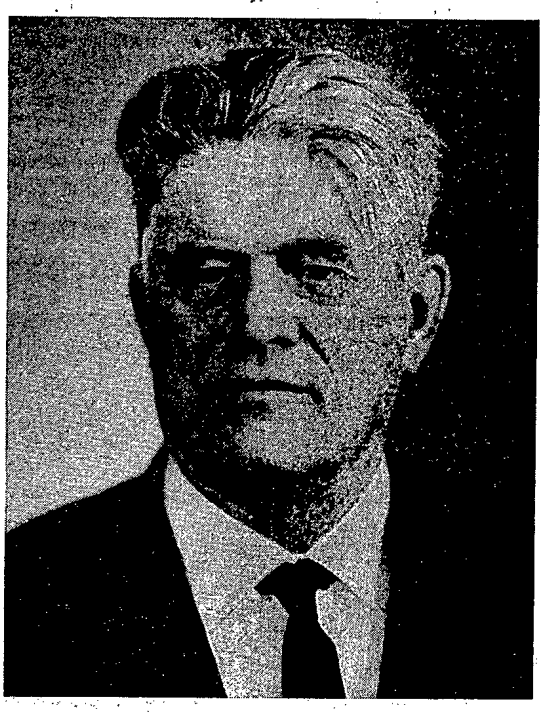

On July 28, 1979, Pavel Alekseevich Cherenkov, the eminent physicist-experimenter, whose name is associated with one of the most outstanding scientific discoveries of our time, was 75 years old. He greeted his anniversary full of creative plans, and his energy and enthusiasm are to be envied by many young scientists. During recent years, by the initiative of Pavel Alekseevich, many new, interesting, and promising investigations have been initiated, covering broad problems of contemporary physics. These include questions of the structure of elementary particles and the investigation of new nuclear structures (hypernuclei) and, at first sight far removed from these questions, problems of the generation and utilization in different fields of science and technology of new forms of electromagnetic radiation, like the so-called synchrotron and undulatory radiation. This is far from a complete list of the problems, on the solution of which P. A. Cherenkov is now working, as Director of one of the most prominent laboratories of the P. N. Lebedev Institute of Physics of the Academy of Sciences of the USSR. The creative life of Pavel Alekseevich is associated with this Institute. In 1932 he became a graduate of the Institute of Physics of the Academy of Sciences (FIAN) and, on the initiative of S. I. Vavilov, he started to investigate the luminescence of solutions of uranium salts under the action of $\gamma$ radiation. These investigations also led Pavel Alekseevich to the discovery of a new, remarkably beautiful physical phenomenon. He discovered that $\gamma$ radiation creates a weak luminescence of the solution, which differs sharply from normal luminescence. In extremely time-consuming experiments, in which the method of photometry at the threshold of vision was used, Pavel Alekseevich studied certain characteristic features of the emission discovered by him. In the investigations the main traits of P. A. Cherenkov's nature were displayed – enthusiasm, unusual tenacity in achieving the designated goal, ability to find the simplest solution to the problems arising, and the knack of paying attention to the "trifles" of the experiment.

After 2 years it already had become clear that the fluorescence discovered had no relation with luminescence, its polarization was measured, and an increase of energy in the emission spectrum with a reduction of

Translated from Atomnaya Énergiya, Vol. 47, No. 1, pp. 59-60, July, 1979.



0038-531X/79/4701-0572$07.50 © 1980 Plenum Publishing Corporation

Declassified and Approved For Release 2013/02/15 : CIA-RDP10-02196R000800020001-4

Declassified and Approved For Release 2013/02/15 : CIA-RDP10-02196R000800020001-4

the wavelength of the primary $\gamma$ quanta was discovered. This allowed S. I. Vavilov in 1934 to arrive at the conclusion that the new form of luminescence was related with the electrons formed in the solutions by the Compton scattering of $\gamma$ radiation. For the next few years, Pavel Alekseevich studied experimentally all the fundamental characteristics of the new physical phenomenon, the nature of which was realized in 1936, after its theory was developed by I. E. Tamm and I. M. Frank. They showed that the luminescence discovered by P. A. Cherenkov is the emission of a charged particle, moving with a velocity exceeding the velocity of light in the substance. In 1936-1937, P. A. Cherenkov verified quantitatively the Tamm–Frank theory by measuring the characteristic angle of emission and its dependence on the refractive index of the medium, established the energy distribution in the emission spectrum, and the absolute brightness of the luminescence. These investigations brought P. A. Cherenkov world recognition. G. S. Landsberg called them the "decoration of Soviet physics." The new form of radiation is known now as "Cherenkov radiation."

In 1946, after this work, P. A. Cherenkov, S. I. Vavilov, E. I. Tamm, and I. M. Frank were honored with the State Prize of the Soviet Union.

The discovery by P. A. Cherenkov, in addition to the enormous scientific interest, has a great practical importance. Thus, in high-energy physics the most outstanding experimental research conducted over the period of the last decades has proved to be possible only because of the use of methods for recording particles based on the application of Cherenkov radiation, or as it is now customary to say, Cherenkov counters. Threshold and differential (gas) Cherenkov counters, shower Cherenkov spectrometers, various Cherenkov chambers – all these are the instruments without which it is impossible now to describe the experimental physics of elementary particles. The use of Cherenkov detectors in physics, astronomy, and other fresh fields of science has reached such scales that, without fear of being mistaken, it may be asserted that P. A. Cherenkov is now one of the world's most well-known physicists.

In 1958 P. A. Cherenkov, I. E. Tamm, and I. M. Frank were awarded the Nobel Prize for Physics "for the discovery and explanation of the Cherenkov effect."

In the years of the Great Patriotic War, Pavel Alekseevich was occupied with the development of an instrument of military designation, based on the use of certain methods of nuclear physics. Since 1946, Pavel Alekseevich participated in the development and construction of the first electron accelerators in the laboratory directed by V. I. Veksler. After his participation in work on the construction of a 250-MeV electron synchrotron, Pavel Alekseevich, together with the team of authors, was awarded the State Prize of the Soviet Union.

From 1959 Pavel Alekseevich directed the Laboratory of Photomeson Processes of FIAN, investigating the electromagnetic interactions of elementary particles. For a start, Pavel Alekseevich carried out fundamental research of photon – nucleon interactions, in particular the photoscattering of the lightest nuclei at an energy of 250 MeV. After this work, in 1977 P. A. Cherenkov with co-authors was honored for the third time with the State Prize of the Soviet Union.

Pavel Alekseevich headed the work on the creation of the FIAN scientific group for the investigation of electromagnetic interactions, including the high-intensity "Pakhra" accelerator, operating at 1.3 GeV, and the modern measurement–recording center. Without waiting for the completion of construction of this complex, P. A. Cherenkov in the laboratory started to work on a study of high-energy electromagnetic processes, creating jointly with the Institute of High-Energy Physics (IFVÉ) and the Erevan Institute of Physics (ErFI) the electron beam on the Serpukhov proton accelerator.

P. A. Cherenkov was one of the first physicists who paid attention to the abundant possibilities opened up by the use of synchrotron radiation. Even in the 1950s synchrotron radiation was the principal proposed and applied method, proposed by him together with Yu. M. Ado, for the storage of electrons and for the production of colliding electron–positron beams in synchrotrons. Subsequently, Pavel Alekseevich and authors addressed a paper in which the possibilities were considered of using synchrotron radiation in science and technology. Now, synchrotron radiation is being widely used everywhere where there are electron synchrotrons and storage devices, and in some countries sources of synchrotron radiation have been specially constructed.

P. A. Cherenkov, with young colleagues, has done much for the theoretical and experimental study of undulatory radiation on the undulator, built by them for the first time and operating in the rectilinear gap of the "Pakhra" synchrotron.

Pavel Alekseevich Cherenkov is widely known not only to the world scientific community. He devotes much effort and energy to the struggle for peace and to the expansion of scientific relations between the scientists of different countries. For many years he has been a Member of the Presidium of the Soviet Committee for



Declassified and Approved For Release 2013/02/15 : CIA-RDP10-02196R000800020001-4

Declassified and Approved For Release 2013/02/15 : CIA-RDP10-02196R000800020001-4

World Protection, a Member of the Soviet Committee for European Safety and Collaboration, and a participant of the Pugwash movement of scientists.

Pavel Alekseevich Cherenkov has been rewarded with two Orders of Lenin, two Orders of the Red Banner, the Order of the "Badge of Honor," and medals of the Soviet Union. The high merits of P. A. Cherenkov have been marked also with orders of foreign countries.

The friends and colleagues of Pavel Alekseevich warmly wish him good health, success, and new creative happiness.

## THE 50th BIRTHDAY ANNIVERSARY OF EVGENII VLADIMIROVICH KULOV

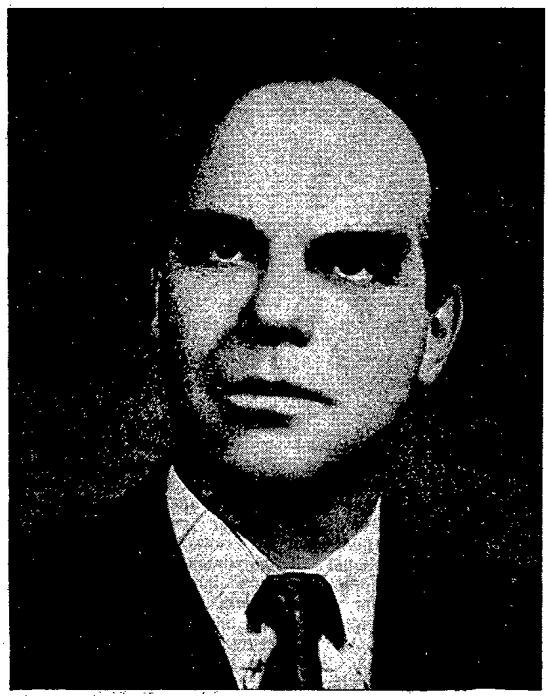

The editorial staff of the Journal heartily congratulate Evgenii Vladimirovich Kulov, Member of the Editorial Board of the Head of the Central Administration of the State Committee for the Utilization of Atomic Energy, on his 50th birthday, and wish him good health and new creative successes.

Translated from Atomnaya Énergiya, Vol. 47, No. 1, p. 60, July, 1979.


0038-531X/79/4701-0574$07.50© 1980 Plenum Publishing Corporation

Declassified and Approved For Release 2013/02/15 : CIA-RDP10-02196R000800020001-4

Declassified and Approved For Release 2013/02/15 : CIA-RDP10-02196R000800020001-4

INFORMATION

# THE ACCIDENT AT THE THREE MILE ISLAND NUCLEAR POWER PLANT

As is known, on March 28, 1979, there was an accident at the Three Mile Island nuclear power plant which attracted the close attention of the world for several days. At that power station there is a Babcock and Wilcox pressurized water reactor with a power of 956 MW (gross). The reactor was first brought to criticality on March 9, 1978, and produced its first electricity on March 15, and was in commercial operation since December 30.

There were many sensational and contradictory reports about the accident. In some of them the danger of the accident was unjustifiably exaggerated. Recently publications have appeared which are used as the basis of this report.* It makes it possible to follow the causes, development, and resolution of the accident and to evaluate its consequences.

## Chronology of the Development and Resolution of the Accident

0 sec (4:00:0 local time). At a power of 98% of nominal, all three feed pumps shut off. The cause of the shutting off was said to be either a cutting off of the supply of condensate to the condensate cleaning system due to a fault in a valve on a connecting pipe or an obstruction in the ion exchange filters. Similar shutoffs of the feed pumps had been noticed previously (at least eight times since October, 1978). When the main feed water system fails the emergency supply system is supposed to be turned on automatically. However, this time, although the emergency feed pumps were turned on, water did not come into the loop since the gates in this system had been left closed after earlier tests. As a result, the steam generators ceased to be supplied with feed water which caused the turbines to be shut off. According to a statement by the NRC, operation of a nuclear power plant with closed gates on the emergency feed water supply system is forbidden.

3-6 sec. Because heat removal had ceased the temperature and pressure in the reactor began to rise. At a pressure of 158 kg/cm$^2$ in the primary loop the relief valve 7 (see Fig. 1) on the volume compensator 8 operated and part of the coolant went into the overflow tank 3.

9-12 sec. When the pressure in the loop reached 166 kg/cm$^2$ the reactor was automatically stopped.

15 sec. The pressure in the loop fell to 155 kg/cm$^2$ and reached roughly an atmosphere below the value at which valve 7 should close; however, this did not occur. Evidently, the operators did not know that the valve had not closed since at that time the apparatus which indicated the water level in the volume compensator was out of order and gave high readings (the apparatus went off scale).

30 sec. Sensors indicated that the emergency feed water supply pumps were working but fruitlessly since, as noted, the gates in this system were closed.

60 sec. The water level in the volume compensator 8 rose sharply and reached a minimum in both steam generators.

2 min. When the pressure in the loop fell to 112 kg/cm$^2$ the emergency core cooling system (ECCS) turned on automatically, sending water directly into the primary loop. It is intended to operate as well if the water level in the volume compensator is reduced or the pressure in the containment vessel rises.

3 min. The pressure in the overflow tank 3 reached 7 kg/cm$^2$.

4 min 30 sec. Since the ECCS supplied more water than had flowed out of the volume compensator, the operator manually turned off one of the pumps supplying water to this system in order to avoid completely filling the volume compensator, at which time it would become impossible (under normal conditions) to regulate the pressure in the primary loop.

*This report is compiled from material published in: Nuclear Engineering International, 24, No. 285, p. 10 (1979); RUN-Actualites, No. 2, p. 190 (1979); Nuclear News, Special Report, April 6, 1979; Atomwirtschaft, 24, No. 5, p. 222 (1979); and SVA-Bulletin, No. 7, p. 11 (1979).

Translated from Atomnaya Énergiya, Vol. 47, No. 1, pp. 61-63, July, 1979.

0038-531X/79/4701-0575$07.50 © 1980 Plenum Publishing Corporation



Declassified and Approved For Release 2013/02/15 : CIA-RDP10-02196R000800020001-4

Declassified and Approved For Release 2013/02/15 : CIA-RDP10-02196R000800020001-4

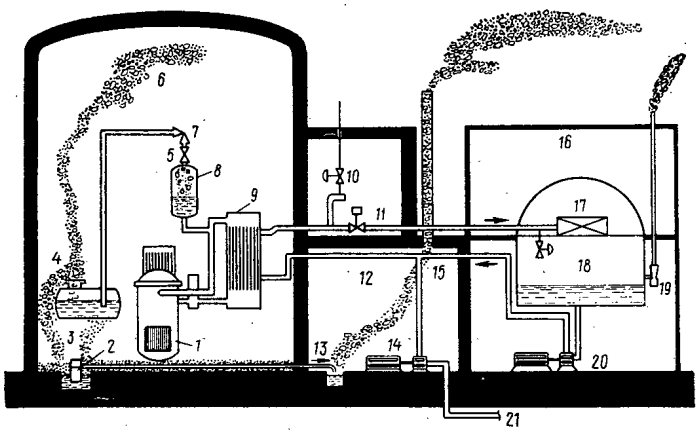


Fig. 1. Schematic longitudinal cross section of the Three Mile Island nuclear power station: 1) reactor; 2) waste water (sump) pump; 3) overflow tank; 4) relief diaphragm; 5) shutoff valve; 6) containment vessel; 7) relief valve; 8) volume compensator (surge chamber); 9) steam generator; 10) valve for release of steam to the atmosphere; 11) main steam pipe; 12) auxiliary building; 13) waste (drainage) water; 14) emergency feed (makeup) water system pump; 15) feed water pipe; 16) machine room; 17) turbine; 18) condenser; 19) ejector; 20) feed pump; 21) pipe from emergency feed water supply.

6 min. The pressure at the output of the reactor fell to 94 kg/cm$^2$, that is, to saturation at a temperature of 307°C.

7 min 30 sec. When the pressure in the overflow tank rose to 10.5 kg/cm$^2$, in accordance with the design a system was automatically turned on to pump water from this tank to a reservoir in the auxiliary building 12.

8 min. The gates in the emergency feed water supply system were opened manually. The thermal shock of the cold water entering the almost dry steam generators resulted in the rupture of the seal on one of them. Next the damaged steam generator was shut off. Starting the steam generators sped up the drop in pressure in the primary loop.

10 min. The second pump which supplies water to the ECCS was turned off manually.

11-12 min. For the first time since 7 minutes after the accident began, the readings of the water level in the volume compensator indicated a level in the operating range, evidently due to turning off the last ECCS pump.

15 min. Despite the fact that water was pumped out of the overflow tank, the pressure in it rose to 13.3 kg/cm$^2$, the relief diaphragm on the tank ruptured, and about 40 tons of water poured out onto the floor of the reactor building.

20-60 min. Attempts were made to stabilize the reactor at a pressure of 71 kg/cm$^2$ and a temperature of 288°C. A steam bubble began to form in the upper part of the reactor.

1 h 15 min. Both circulation pumps in one loop of the reactor were turned off because noise and vibration in the pumps created a fear that cavitation would set in.

1 h. 40 min. Both circulation pumps in the other loop were turned off.

1 h 45 min-2 h. The water temperature at the inlet to the reactor was 65°C and at the outlet 327°C. This jump indicated the absence of natural circulation of water and heat removal through the steam generators. The steam bubble expanded and covered the top of the core. The fuel elements were thus damaged and part of the fission products fell into the coolant. Because of the reaction of the zirconium in the jackets on the fuel elements with steam, hydrogen formed which collected in the upper part of the reactor vessel. However, because there was no operational method of analysis, the operators did not suspect its existence in the steam bubble at this time.



Declassified and Approved For Release 2013/02/15 : CIA-RDP10-02196R000800020001-4

Declassified and Approved For Release 2013/02/15 : CIA-RDP10-02196R000800020001-4

2 h 18 min. The volume compensator was closed by the shut off valve 5 (evidently, up to this time the operators did not know that valve 7 had been jammed in an open position). However, the pressure in the reactor continued to fall and the steam-hydrogen bubble continued to expand.

2 h 30 min. The pressure in the reactor fell to 49 kg/cm$^2$.

3 h 00 min. The pressure in the reactor rose to 148 kg/cm$^2$.

3 h 15 min. A pressure rise of 0.35 kg/cm$^2$ was noticed in the overflow tank 3.

3 h 48 min. A pressure rise of 0.77 kg/cm$^2$ was noticed in the overflow tank. Both these rises could have been caused by escape of steam since the pressure in the reactor again fell to 123 kg/cm$^2$ (evidently, in the preceding 1-2 h the operators, trying to stabilize the reactor, opened and closed the volume compensator and turned the ECCS off and on). The excess pressure in the containment vessel rose from 0.07 to 0.21 kg/cm$^2$.

5 h 00 min. The pressure in the containment vessel reached 0.32 kg/cm$^2$. It was isolated at the design pressure of 0.28 kg/cm$^2$ with the waste water pipe being closed. Thus, direct escape of radioactivity from the vessel was stopped. Nevertheless, it took place from the auxiliary building to which some of the water from the overflow tank had been pumped previously when it had fallen on the floor because of overflow or breakage of the seal in that loop. Then krypton and xenon entered the atmosphere but iodine was mainly retained in the ventilation system. Somewhat earlier there was an escape of radioactivity during a release of steam, which had been slightly contaminated during leaks in the steam generators, through valve 10.

7 h 30 min. In more than 2 h the pressure changed from 87 to 147 kg/cm$^2$ with a large jump in the temperature between the inlet and outlet of the reactor. In order to reduce this jump, as is necessary for cooling the reactor with a low-pressure system, the operator opened valve 5. As a result there was a further discharge of coolant.

8-9 h. The pressure in the reactor fell to 35 kg/cm$^2$. At 42 kg/cm$^2$ a system for sending borated water into the core operated.

10 h. In the containment vessel there was an abrupt rise in the pressure to 2 kg/cm$^2$, probably due to an explosion of detonating gas. The system went into operation and 19 m$^3$ of sodium hydroxide solution was scattered into the vessel. (The containment vessel had been designed and tested for a pressure of 4.2 kg/cm$^2$.)

13 h 30 min. Valve 5 on the volume compensator was closed. The circulation pump in the loop with the undamaged steam generator was turned on. Over the next 3 h the pressure in the reactor again rose from 46 to 162 kg/cm$^2$. The reactor was cooled by the undamaged steam generator at an inlet temperature of 200°C and an outlet temperature of 293°C. The rapid cooling prevented a gas bubble under the reactor cover. If the pressure were reduced it could expand and cover the core which would in turn cause additional damage to the fuel elements. The size of the bubble was calculated using actual data on the pressure, temperature, and location of the water level in the volume compensator.

The hydrogen bubble was eliminated after several days with the aid of the coolant cleanup system as well as by removal of water at the inlet to the reactor and injection into the steam cavity of the volume compensator. Thus, by using the variable solubility of hydrogen at different pressures, it was possible to transfer the hydrogen to the volume compensator and then remove it to the inner volume of the containment vessel.

## Radiation Situation

The radioactive releases from the nuclear power station consisted mainly of noble gases which were separated from the overflow water in the auxiliary building and then entered the atmosphere. They were too small to have any effect on the population. True, there is a report that the maximum dose rate measured outside the power plant must have been (apparently at the moment the cloud passed by) 20-25 mrem/h, while in the Harrisburg region (roughly 16 km from the plant) it was 0.3 mrem/h. However, on April 7, observers from the NRC determined that the maximum dose 1.5 km from the plant was 0.05 mrem·h. The natural irradiation dose to a resident of Harrisburg is estimated to be 88 mrem/yr. According to data from the NRC and the Environmental Protection Agency, the dose due to the accident is roughly the same. For comparison, it is noted that the natural irradiation dose to residents of Denver, Colorado, is about 147 mrem/yr because of the high altitude of the city.

In the neighborhood of the power plant various organizations made analyses of many samples of milk, air, water, soil, and plants. The content of radioiodine in those samples where it was observed corresponded



Declassified and Approved For Release 2013/02/15 : CIA-RDP10-02196R000800020001-4

Declassified and Approved For Release 2013/02/15 : CIA-RDP10-02196R000800020001-4

to a specific activity of 10-20 pCi/liter (in one sample 31 pCi/liter), which is much less than the amount, 12,000 pCi/liter, allowed by the public health authorities when domestic cattle have to be transferred to stored feed. Radioiodine was observed in only 8 out of 152 air samples taken outside the plant. The highest activity was $2.4 \cdot 10^{-14}$ Ci/liter. The concentration of radioactive inert gases which was observed in the air a distance of up to 65 km from the plant was less than a quarter of the allowed value. Radioactive iodine was not observed in a single one of 130 water samples. Based on the amount of radioiodine which went beyond the confines of the plant, the calculated irradiation dose to the thyroid gland of any user of the water was estimated to be less than 0.2 mrem. Radioiodine was not observed in a single one of 147 soil samples or of 171 plant samples.

The radiation situation at the power plant is worse. At the site the dose rate on April 7 was 85 mrem/h and increased somewhat in later days. In the state of March 31, three employees of the power plant received a dose of from 3.1 to 3.8 rem during an attempt to drain and close the auxiliary building, that is, a dose larger than the allowed quarterly dose (3 rem). Twelve other employees received enhanced doses; however, the doses they received were much less than 3 rem. Access to the containment vessel is closed.

MAIN CHARACTERISTICS OF THE PWR REACTOR

| | |
|---|---|
| Power, MW: | |
| electrical | 959 (gross) |
| thermal | 2770 |
| Uranium load, tons | 82 |
| Number of fuel assemblies | 177 |
| Number of fuel elements per assembly | 208 |
| Specific energy density in the core, kW/liter | 90 |
| Uranium enrichment, % | 2.57 |
| Pellet diameter, cm | 1.09 |
| Maximum fuel temperature, °C | 2299 |
| Fuel-element shell: | |
| material | Zircalloy-4 |
| thickness, mm | 0.67 |
| Parameters of the water in the primary loop: | |
| pressure, kg/cm$^2$ | 154.7 |
| inlet temperature, °C | 292 |
| outlet temperature, °C | 320 |
| Parameters of the water in the secondary loop: | |
| pressure, kg/cm$^2$ | 63 |
| temperature, °C | 297 |

The reactor has two loops, each with two main circulation pumps with a capacity of 16,000 tons/h; the steam generator is a vertical type with a capacity of 2760 tons/h.



Declassified and Approved For Release 2013/02/15 : CIA-RDP10-02196R000800020001-4

Declassified and Approved For Release 2013/02/15 : CIA-RDP10-02196R000800020001-4



# SECOND ALL-UNION CONFERENCE ON THE CHEMISTRY OF URANIUM

É. A. Semenova

The conference took place in October, 1978, in Moscow. Work on increasing the efficiency of all stages of the nuclear power fuel cycle was discussed.

More than 500 experts took part in the conference. In conveying greetings to the participants from the President of the USSR Academy of Sciences, Academician A. P. Aleksandrov, Academician I. V. Tanaev noted the achievements of Soviet science in the field of uranium chemistry and the need to expand their work in view of the planned expansion of nuclear power.

One hundred six talks were heard in two plenary sessions and five sections. Review talks by B. N. Laskorin, A. G. Samoilov, N. P. Galkin, and G. B. Naumov dealt with the mechanism for formation of uranium deposits, new natural uranium compounds, and the physical and chemical basis for extracting it from mineral slurries, underground leachate solutions, and natural waters. The following were mentioned: the efficient use of autoclave processes for processing difficult and complex ores, the extensive use of sorption and extraction methods in the fuel complex, the creation of efficient extractants and sorbents of new types (sorbents impregnated with organic solvents, organophosphorus superextractants, amphoteric cation exchange-solvating complexing agents, cyclic ethers, etc.), and the use of laser techniques in different stages of the fuel cycle. Chemical and physical–chemical methods of separating uranium isotopes were discussed and information was presented on a large class of uranium fluoride compounds which are important in the development of the scientific and technical foundations for dealing with nuclear-pure materials and for the regeneration of spent fuel. Considerable attention was devoted to materials problems which arise in the development of designs and technology for manufacturing fuel elements.

In talks in the section entitled "Natural uranium compounds," data were presented on structural studies, the composition and properties of natural and synthetic uranium oxides, uranyl phosphates, and mourite, and on the formation and dissolving of uranium oxides in natural processes and during underground leaching. It was noted that oxidation–reduction and acid–base conditions in the water and the class of the geochemical barrier determine the existence of the many geochemical types of uranium concentrations. A classification was proposed in the form of a table and matrix with which it is possible to predict new geochemical types of hydrogeneous deposits.

The talks in the section "Physical–chemical foundations of uranium extraction" reflected deeper study of the extraction and sorption processes employing different types of ionites and extractants (research on the kinetics and chemistry of sorption and extraction, the effects of anions, the determination of the thermodynamical characteristics of the processes), the extraction of uranium in the form of a uranyl halogen acetate as one promising approach, and the wider use of modern instrumental techniques in research on uranium extraction processes and the use of computers for analyzing the results.

A large fraction of the talks in the section "Coordination compounds of uranium in solutions" was devoted to the thermal stability of uranium salts (uranium and sodium fluorides, uranium trioxide dihydride, ammonium-uranyl tricarbonate, hexahydrauranyl nitrate, the carboxylates, etc.) with the use of high resolving power devices (the MTV-10-8 microthermal balances and others) and to studies of the structure and properties of synthetic uranyl sulphate complexes with bivalent metals, with uranyl molybdates and tungstates of the alkali metals, and with the uranyl perbromates.

Many of the talks given in the section "Behavior of uranium in melts and solid phase reactions" touched on more detailed studies of the chemical processes which occur in halide melts of uranium and the alkali metals. Complexing and the diffusion of uranium in halide melts were examined; the physical–chemical conditions for formation of solid phases based on the phosphates of uranium and ruthenium in melts of the alkali

Translated from Atomnaya Énergiya, Vol. 47, No. 1, pp. 63-64, July, 1979.

0038-531X/79/4701-0579$07.50 © 1980 Plenum Publishing Corporation



Declassified and Approved For Release 2013/02/15 : CIA-RDP10-02196R000800020001-4

Declassified and Approved For Release 2013/02/15 : CIA-RDP10-02196R000800020001-4

metal chlorides and the kinetics of its removal by gaseous fluorination were investigated; and results were presented on the volatility of $UCl_4$ and $ThCl_4$ from melts with alkali metal chlorides. The precipitation of uranium from fluoride melts by the oxides of Ca or Al was considered. The theoretical requirements for electrorefining of uranium in molten halides with liquid metal electrodes were presented. The results of a study of thermal dissociation and synthesis of the uranium oxides were presented. New results on the pyrohydrolysis of uranium hexafluoride, on the effect of an external force field on dissociation reactions, and on the recovery and conversion of uranium fluorides were discussed. Reports were given on studies of the complex ternary silicides of uranium with transition metals, of mixed chalcogenides of uranium, and of the lanthanoids which are new magnetic and semiconducting materials.

At the conference talks were also heard on methods of determining uranium, impurities in it, and the quality of nuclear fuel. V. K. Makarov noted the possibility of, limits of application of, and errors of gravi- and titrimetric, electrochemical, chemical–spectral, atomic absorption, mass and $\gamma$ spectroscopic, neutron measurement, and x-ray fluorescence analytic techniques. Volume, mass spectrometric, spectrophotometric, and other methods were proposed for determining the uranium in spent fuel, which permit a measurement error of about 0.3%. In other talks remote automatic or nondestructive methods of determining uranium were shown as possibilities with less accuracy (roughly 5-10%) but greater convenience for monitoring the production of pure uranium compounds. An automatic rapid method for determining the nonstoichiometry of nuclear fuel was proposed that was based on the emf of a high-temperature solid-electrolyte galvanic cell which makes it possible to determine the ratio of oxygen to uranium to a high accuracy not attainable with other methods.

The problem of environmental protection was examined in connection with the possible disposal of uranium in the form of solid and liquid wastes in the nuclear power fuel cycle. In this regard, the talk by D. I. Gusev was of interest. In it he presented data on the uranium content in various environmental objects, including human tissues, and demonstrated the effect of uranium on aqueous organisms when it is in a reservoir for a long time. Ways in which uranium enters the human body were examined. In one of the talks the ecological parameters for monitoring the uranium level in the hydrosphere and the biochemical parameters for natural water reservoirs were cited.

At the conference attention was turned to research on quantum chemistry that is needed for a scientific basis for the synthesis of uranium compounds with an unusual valence for this element and for a choice of ligands which stabilize the coordination compounds of uranium with different degrees of oxidation of its atoms.

The participants in the conference noted its high scientific level.

## SYMPOSIUM ON THE SCIENTIFIC FOUNDATIONS OF RADIOACTIVE WASTE HANDLING

V. I. Spitsyn and A. S. Polyakov

The symposium took place in November-December 1978, in Boston (USA). Seventy-seven talks were presented there. Experts working on the treatment of highly active liquid wastes hold to the view that before final burial the wastes must be embedded in stable solid materials. In Great Britain, Belgium, France, and West Germany the technology of solidifying wastes to obtain borosilicate glasses is most developed. In France a two-stage process of vitrification at the AVM installation in Marcoule was developed and first carried out in 1978. In West Germany and Belgium they are planning to build similar installations. In these countries a process for embedding glass granules in metallic matrices has been developed. In Great Britain work is continuing on the development of calcination with subsequent vitrification in a single crucible device.

The idea of creating "barriers" which are meant to provide a better guarantee of protection of the biosphere than glass alone was discussed in many talks. The first barrier is to be a solid chemically and thermally stable composition (core) which includes the highly active wastes. The material in the inner core is expected to be a baked ceramic supercalcinate and glass granules. The second barrier is a layer of pyrolytic carbon and aluminum oxide which coats the core. The third barrier is a metallic matrix (Pb+Sn; Cu; Ti, etc.)

Translated from Atomnaya Énergiya, Vol. 47, No. 1, pp. 64-65, July, 1979.

 0038-531X/79/4701-0580$07.50 © 1980 Plenum Publishing Corporation

Declassified and Approved For Release 2013/02/15 : CIA-RDP10-02196R000800020001-4

Declassified and Approved For Release 2013/02/15 : CIA-RDP10-02196R000800020001-4

which is highly thermally conducting and resistant to corrosion and mechanical action. The container and, finally, an appropriate geological medium can serve as subsequent barriers.

The embedding of highly active wastes in minerals known to be stable over millions of years was discussed. Fixation of radionuclides by titanate (inorganic) ionites followed by hot isostatic pressing was reported (Sweden, USA, and others). Embedding of wastes in a glass ceramic based on fresnoite $Ba_2TiSi_2O_8$ (West Germany), in synthetic rock ("synrock") containing silicate products and titanates such as $BaAl_2Ti_6O_{16}$, $ZrO_2$–Ca, Ti, $CaTiO_3$, $BaAl_2Si_2O_8$, $KAlSiO_4$, $KAlSi_2O_6$ (Australia), and in polludite (USA and others) was studied.

In many talks the properties of the hardened materials were introduced. Thus, in the Hahn-Meitner Institute (West Berlin) the behavior of He formed in glasses due to alpha decay of actinides in it (the nuclear reaction $^{10}B(n, \alpha)^7Li$ was used to simulate alpha decay) has been studied.

H. Healey and others (USA) used a scanning electron microscope to study the microstructure of solidified wastes, a pycnometer to determine the fraction of pores in the ceramic that were connected to the surface, and an ion beam spectrochemical analyzer to study leaching and determine the content of Si, Al, alkali, alkali-metal, and transition elements Fe, Zr, and Mo (W. Houser and others, USA).

The possibility of obtaining more certain data on the kinetics of the transfer of radioactivity into the environment from solidified wastes by means of relatively short-term experiments was analyzed in detail (USA). The solidification of the longest lived and one of the most volatile radioisotopes $^{129}I$ is being worked out. It is proposed to embed up to 18% iodine in the form of barium iodate in concrete. It is considered that constant isolation for the immense length of time required for $^{129}I$ cannot be guaranteed but the combination of isolation and dilution will prevent danger to the present and future generations. Natural analogs are being sought for determining the possible changes in solidified wastes over a prolonged retention period with limited-duration laboratory experiments, the stability of natural glasses (the oldest volcanic glasses are about 40 million years old but most of them are much younger) is being studied, and the rates of hydration of volcanic glasses are being determined as functions of the composition, temperature, and climate.

In the talk by G. MacCarthy (USA) the feasibility of hydrothermal contact of solidified wastes with rock as a result of which some radionuclides (and possibly the majority of them) will interact with alumosilicate rocks (but not with salt formations) was examined. Such contact may lead to formation of new thermodynamically stable and low-solubility mineral-like phases.

The interaction of vitrified simulated wastes with rocks is being studied in the USA. A system was kept in a heated state for a month, after which x-ray structural and electron micrographical analyses were carried out on 17 elements. Salt formations were discussed in detail as a medium for burial of solidified wastes. It was noted that although these formations contain less than 1% water on the average, locally the water content may be higher by a factor of five or more. Under the action of various forces the liquid migrates in salt with a speed of from several millimeters to 1 m/yr. In addition a solution of chlorides may accumulate near waste containers and cause them to corrode (USA).

The action of radiation on natural and artificial rock salt and the hydrothermal action of salt brine on glasses at 350°C were discussed at the symposium. Tufa (a material with high sorption properties because of its high (up to 70%) zeolite content; clinoptilolite is the main zeolite mineral in deep laying tufas and is stable up to 700°C) and $CaSO_4$ (low solubility, high thermal conductivity, and insignificant liquid content characterize this material as a medium more suitable for wastes than rock salt) have been proposed as geological media for permanent burial of solidified wastes. The importance of organizing a "bank" of experimental results for models which would make it possible to predict the behavior, including migration, of radionuclides over a long period of time, as well as the extent of extrapolation of laboratory investigation, was noted. In this regard the observations made at the site of the natural nuclear reactor in Oklahoma may yield interesting results.

Talks by experts from the USA, Sweden, and West Germany were devoted to an examination of the thermodynamics of radionuclide migration in the geosphere and to a study of the sorption properties of clay and rock. Pumping bentonite into crushed rocks is an effective means of inhibiting migration of radionuclides from a waste reservoir into the environment (Sweden).

At the symposium it was reported that the chemical interaction between wastes and the nearby geosphere may play a controlling role in their migration. Thus, corrosion of a metal container may lead to entry of polyvalent metal ions into the ground water in an amount sufficient to inhibit ion exchange retention of radionuclides in nearby minerals, and sorption on silicate materials may lead to separation and creation of



Declassified and Approved For Release 2013/02/15 : CIA-RDP10-02196R000800020001-4

Declassified and Approved For Release 2013/02/15 : CIA-RDP10-02196R000800020001-4

zones of enhanced concentration of certain radionuclides within the depository. The required lifetime for the canisters (one of the barriers against entry of radionuclides into the biosphere) will be determined either by a systematic analysis of the degree of risk or by legislated requirements (USA). Solidified waste canisters made of titanium (Sweden) and canisters for spent fuel elements made of copper or $\alpha$-$Al_2O_3$ (Sweden) or of glass-ceramic $\beta$-spodumene (USA) are planned. Presentations on the corrosion of eleven samples of material for bottles for long-term containment of $^{85}Kr$, on concrete and other low-temperature binders for solidifying radioactive wastes, and on the development of mathematical models for evaluating the main aspects of treating highly active wastes were of interest.

## CONFERENCE OF EXPERTS ON THE EFFECT OF NUCLEAR POWER ON THE ENVIRONMENT

L. A. Il'in and V. I. Karpov

Specialists from Australia, Austria, Great Britain, Argentina, Spain, Canada, China, Poland, the USSR, Turkey, France, Switzerland, Sweden, and Japan, as well as representatives of international organizations (UNEP, IAEA, ICRP, SCRD, WHO, EEC, and the World Council of Churches), participated in the conference which took place in November, 1978, in Geneva, Switzerland. The chairman of the meeting was the prominent Swedish scientist and director of the Institute of Radiation Protection, B. Lindell.

A draft of the talk, "The effect of nuclear power on the environment," prepared by a group of specialists headed by El-Hinnawi, chairman of the energy program and director of the council on the state of the environment at UNEP, was discussed at the conference. This meeting was one of a series on evaluating the effect of various energy sources (organic, nuclear, etc.) on man and the environment.

In this draft talk, data were presented on the present state and predicted estimates of the development of traditional and nuclear energy in the world through the year 2000, on dosage due to various forms of radiation on people in the USA, Great Britain, and Canada, and on the types of nuclear reactors and their use through the year 2000. Special attention was devoted to the sources of and ways that radioactive and chemical substances and heat enter the environment, the possible effects on man and the environment, and the human dose levels due to all operations in the nuclear fuel cycle, from the mining of uranium ore to reprocessing of spent nuclear fuel. The vital operations in the nuclear fuel cycle of burial of highly radioactive wastes and disassembly of nuclear power stations at the end of their operating life were discussed.

According to IAEA estimates, which agree with the data of other organizations, nuclear power will provide 11-13% of the total electrical power needs of the world in 1985 and about 17-20% in 2000. The installed power of nuclear power plants is 350-400 GW(e) in 1985 and will be 1500-1800 GW(e) in 2000. The world production of uranium in 1972-1975 was 19,000-20,000 tons/yr, in 1977 it was 30,000 tons/yr, in 1990 it is estimated that it will be about 0.8-1 million tons/yr, and toward the year 2000 it will be 2-3 million tons/yr. The water cooled–water-moderated reactor will be the main commercial reactor for electrical-power generation.

According to the data presented in the UNEP talk the main factors in the effect of the nuclear fuel cycle on man and the environment and the possible criteria for comparing the fuel cycles for electrical-power generation could be the following:

the amount of fatal accidents and illnesses among workers involved in power production;

the specific (per GW(e)/yr) yields of harmful substances and heat into the environment and their effect on man and the biosphere;

the cost of reducing the release of harmful substances from dumps and tailings accumulations to established norms;

destroyed and nonreclaimable land;

the unit values of the natural resources used (land, water, organic fuel, air).

Translated from Atomnaya Énergiya, Vol. 47, No. 1, pp. 65-66, July, 1979.

 0038-531X/79/4701-0582$07.50© 1980 Plenum Publishing Corporation

Declassified and Approved For Release 2013/02/15 : CIA-RDP10-02196R000800020001-4

Declassified and Approved For Release 2013/02/15 : CIA-RDP10-02196R000800020001-4

We now consider some quantitative data according to these factors on the effect of the nuclear fuel cycle on man and the environment.

Among uranium miners the number of fatal accidents is 0.1-0.5 per GW(e)/yr and the number of lung cancer cases is $1.5 \cdot 10^{-4}$ man/yr. Several experts stated that similar data could be presented for other stages of the nuclear fuel cycle as well.

In the talk the characteristic waste products and numerical estimates of their amounts were given for operations in the nuclear fuel cycle. Thus, in mining the main environmental effects are the destruction of land, dumps, mine drainage water, and contamination of the air with dust and radionuclides. The annual release of radon from the surface of a mine which provides for the operation of a 1 GW(e) nuclear power station is 100 Ci. In processing, about 70% of the activity of the ore remains undissolved in tailings. Storage of the tailings requires an area of 120 ha for 1 GW(e). Tailings accumulations can be a source of atmospheric pollution and pollution of ground water by radionuclides. Thus, special effort must be made to reduce their entry into the environment to established norms. Similar data are given for other operations in the nuclear fuel cycle.

An estimate was given in the talk of the population irradiation dose when the nuclear fuel cycle is operating. It appears that at present the irradiation dose to the population due to nuclear power is small (0.003-0.25 mrem/yr with an overall dose to individuals of 160-180 mrem/yr due to natural radiation, medical procedures, etc.). The development of nuclear power through the year 2000 will not cause significant change in these numbers.

The talk is a summary and reference on the sources and amount of wastes produced and entering the environment in all phases of the nuclear fuel cycle and on the possible dose burdens on man through the year 2000. Because of the comments by these experts the talk will be further improved and used for comparing the effects of various energy sources on man and the environment. It is presumed that the concluding conference on comparing the effect of different forms of energy production will take place in October-November, 1979.

## SCIENTIFIC-TECHNICAL CONFERENCE "ENERGY AND ENVIRONMENTAL PROTECTION"

B. M. Stolyarov

This conference, which took place at the Exhibition of Achievements of the National Economy (VDNKh) of the USSR in November, 1978, dealt with the problems of protecting the air and water supply from the wastes of thermal and nuclear power stations. Three sections were working at the conference, including one on the protection of the environment during energy extraction at nuclear power stations, in the work of which representatives of scientific-research, construction, and design organizations and nuclear power stations participated.

Considerable attention was devoted to the hygiene aspects of protecting the environment from the wastes of nuclear power stations. In evaluating the level of possible radioactive contamination of objects in the environment, the main criteria are the industrial hygiene standards which regulate the limit of the annual dose to a critical population group due to external and internal exposure and the operational limits on the amount of individual radionuclides and their mixtures in the atmosphere and water. The talk by N. G. Gusev examined the basic assumptions of the new draft regulation "Hygiene rules for the design and operation of nuclear power stations" (SP-AÉS-78). These rules will replace "Hygiene rules for the design of nuclear power stations," No. 38/3-68. The main topic of the talk was the physical basis of the dosage quotas, accidental irradiation dosages, gaseous aerosol wastes, etc. Stricter standards are proposed for the allowable normalized emission (ANE) per 1000 MW(e) of nominal power and the maximum allowable emission (MAE) at a nuclear power station as a whole (Table 1). There RNG denotes any mixture of radioactive noble gases of artificial origin. The long-lived nuclides are aerosols deposited in a filter during 1 (24 h) day and measured 1 day after the sample has been taken. They include aerosols of all radionuclides remaining on the filter two days after

Translated from Atomnaya Énergiya, Vol. 47, No. 1, pp. 66-67, July, 1979.

0038-531X/79/4701-0583$07.50 © 1980 Plenum Publishing Corporation 

Declassified and Approved For Release 2013/02/15 : CIA-RDP10-02196R000800020001-4

Declassified and Approved For Release 2013/02/15 : CIA-RDP10-02196R000800020001-4

TABLE 1. Norms for Gaseous Emissions, Ci/day

| Nuclide | ANE | MAE | Nuclide | ANE | MAE |
|---|---|---|---|---|---|
| RNG | 500 | 3000 | Long-lived | 0,015 | 0,090 |
| $^{131}I$ (gaseous and aerosol phases) | 0,01 | 0,06 | Short-lived | 0,1 | 0,6 |

TABLE 2. Normalized Emissions, Ci/day

| Nuclear power station | Year | RNG | $^{131}I$ |
|---|---|---|---|
| Kolskaya | 1976—1977 | 5 | 0 |
| Armyanskaya | 1977 | 4 | $1,7 \cdot 10^{-4}$ |
| Kurskaya | 1977 | 180 | $\sim 0$ |
| Chernobylskaya | XI.77—IV.78 | 220 | $\sim 0$ |

deposition began. Short-lived nuclides refer to radioactive aerosols deposited on a filter over a period of 2 h and measured 1 h after the sample has been removed. They include aerosols of radionuclides remaining on the filter 3 h after deposition began. A single (or daily) release of radionuclides 5 times in excess of the daily mean value is allowed provided the total emission for the week does not exceed the corresponding calculated value.

In the new rules, ANE and MAE for $^{90}Sr$, $^{89}Sr$, $^{137}Cs$, $^{69}Co$, $^{54}Mn$, $^{51}Cr$ are introduced. Experience in the operation of nuclear power stations has shown that the releases of radionuclides are considerably less than these provisions (Table 2). The same may be said of the long-lived aerosols.

Scrubbing of air in recirculating ventilation systems at nuclear power stations to remove radioactive aerosols and iodine by means of sprinkler systems was the topic of E. M. Klement'eva's talk (F. É. Dzherzhinskii All-Union Heat Engineering Institute). The essence of the method is that the flow of recirculating air is washed in special chambers by water that is sprayed from a jet. Water is a solvent for iodine and its compounds. Studies of the properties of aerosols at a nuclear power station with a water-cooled—water-moderated power reactor (VVER) reported by S. S. Chernyi and V. P. Grigorov (F. É. Dzherzhinskii All-Union Heat Engineering Institute) showed that the concentration of radioactive aerosols in rooms and air ducts at a nuclear power station is usually small and does not exceed $5 \cdot 10^{-13}$ Ci/liter. During reloading of fuel it may reach $10^{-11}$ Ci/liter in isolated places. It was found that the bulk of the radioactive aerosols have much larger size than previously assumed. Thus, the parameters of the logarithmically normal distributions of particle activity averaged in terms of their aerodynamic dimensions in different ventilation systems vary and during normal use the aerodynamic median diameter for the long-lived nuclides is 0.9-4.5 $\mu$m with a standard deviation of 1.9-2.6. During reloading and repair work the median diameter of the aerosols in certain rooms and ventilation systems increases and may reach 8-10 $\mu$m. These results suggest the use of a filter material that is coarser than FPP-15 cloth and therefore more retentive of dust.

G. V. Matskevich (F. É. Dzherzhinskii All-Union Heat Engineering Institute) examined the prevention of contamination of the environment by liquid waste from nuclear power stations. It was noted that most water and chemical systems in a nuclear power station have no outlet. Water that is contaminated by radionuclides is cleaned in special reprocessing systems and returned to the cycle. The reprocessing wastes stay on the reactor site under constant dosimetric monitoring. Only balanced amounts of water are released to the environment after cleanup, storage in monitored tanks, and dilution to an extent that the concentration of radionuclides meets the standard for drinking water.

Part of the talks dealt with the experience in designing equipment for ventilation systems and cleanup systems for special gases and water.

Representatives of the NVAÉS and Kurskaya nuclear power stations spoke at the conference and shared their experience in adjusting and operating gas cleanup and ventilation systems.

Recommendations were adopted for further improving the means and methods of preventing environmental effects of nuclear power stations.



Declassified and Approved For Release 2013/02/15 : CIA-RDP10-02196R000800020001-4

Declassified and Approved For Release 2013/02/15 : CIA-RDP10-02196R000800020001-4

# INTERNATIONAL SEMINAR ON THE PRACTICAL SIGNIFICANCE OF THE ICRP RECOMMENDATIONS

Yu. V. Sivintsev

The seminar, which took place in Vienna in March, 1979, was organized by the ICRP, the IAEA, and international public health and labor organizations. More than 250 experts discussed 42 talks. The reports of the prominent scientists, the members of the ICRP, in which the idea of the ICRP was described and its difference from previous recommendations was explained in detail, were grouped separately. Previously the ICRP supported numerical values of the maximum allowable radiation dosage of 5 rem/yr for professional workers and 0.5 rem/yr for individuals in the general population. The radiation environment was regarded as acceptable if the irradiation dose did not exceed the appropriate maximum allowable values. In Publication No. 26 this principle and the numerical values of the basic dose limits (this new term has replaced the previous maximum allowable dose) are retained but only without stochastic effects. The dose limit for nonstochastic effects is set at 50 rem/yr. In order to prevent nonstochastic effects of radiation, the ICRP has accepted a lower limit (30 rem/yr) for the lens of the eye.

Another task of radiation protection was declared to be to limit stochastic effects to an acceptable level. The ICRP relates the introduction of the concept of acceptable risk to the assumption of a nonthreshold linear dependence of radiobiological effect on dose and to the principle of "justification of practice." The use of sources of ionizing radiation is justified only when the benefit gained by using them exceeds the harm to personnel and limited groups of the population due to chronic low-intensity irradiation. B. Lindell noted in his talk that the justification procedure was identical to a "risk–benefit" analysis.

The resulting new principle, the optimization of protection, represents, in the opinion of the ICRP, a practical means of applying the recommendation to keep the dose at as low a level as is reasonably acceptable (the ALARA principle). In the same talk by Lindell, it was shown that optimization is identical to applying estimates of the "cost-effectiveness of protective measures." In such calculations the dominant factor is the estimate of the monetary value per unit collective dose (man-rem). As noted in the talks by D. Beninson, C. Jamme, and E. Pochin, the limits must be regarded as marking the region of unacceptable irradiation. In arguing this position, E. Pochin noted that according to present estimates a radiation dose of 5 rem/yr corresponds to a risk level of about $10^{-4}$/yr (or 100 fatal cases per year per million radiation workers). This is equivalent to the mean frequency of fatal accidents in industry in the developed countries. Nowadays people consider work conditions with a risk of about $10^{-5}$/yr as "safe" and for the general population a risk of $10^{-6}$/yr. Based on these initial data, the ICRP considers that the average radiation dose for personnel and individuals in the population must not exceed 1/10 the corresponding dose limit.

There was considerable interest in a talk reviewing previously published data on lung-cancer fatalities among uranium miners. The seminar participants took into consideration that a group of experts from the IAEA is completing a numerical analysis of dosimetric data, which were possibly higher in previous work, and noted information on the dust content in air from other hazardous substances.

The ICRP recommendation that the mean annual dose to personnel not exceed 0.5 rem/yr signifies a need to greatly strengthen radiation protection at almost all stages of the nuclear fuel cycle. Thus, according to data in a talk by a group of staff members from the Trombay nuclear center (India), the mean annual radiation dose to personnel (rem/yr) is: 1 for uranium extraction in France (lung irradiation 1.5-2); 0.4-0.5 in Great Britain and 0.47-0.59 in the USA for nuclear fuel manufacture; 0.74-1.2 in the USA (1969-1975), 0.16-0.55 in France (1964-1974), 0.89-1.15 in West Germany, and 0.98 (2.07 for personnel involved in repairs) in Canada for nuclear power plant operation; and 1.25 in Great Britain and 3.15 in the USA for reprocessing of spent fuel at a radiochemical plant. As French trade union representatives noted, the sharp increase in the price of nuclear fuel in recent years has not been accompanied by greater expenditure on protection. As a result the irradiation dose to personnel has not been reduced, but has increased to 1.2-2.8 rem/yr (0.46 at

Translated from Atomnaya Énergiya, Vol. 47, No. 1, pp. 67-68, July, 1979.

0038-531X/79/4701-0585$07.50© 1980 Plenum Publishing Corporation



Declassified and Approved For Release 2013/02/15 : CIA-RDP10-02196R000800020001-4

Declassified and Approved For Release 2013/02/15 : CIA-RDP10-02196R000800020001-4
uranium mines; 0.32-0.85 at nuclear power plants; and 0.4-1.5 at radiochemical plants). Thus, the benefits and costs associated with the use of nuclear energy go to different professional groups and this is an additional circumstance which complicates the practical application of the principle of optimizing radiation protection.

Part of the talks were devoted to optimization of protection in the medical use of ionizing radiation. The experience with applying this principle in Danish radiotherapy centers is of interest. In that country, with its population of 5 million, there is a relatively high incidence of cancer. It is the cause of 23% of deaths: 18,500 per year; 390 and 350 per 100,000 men and women, respectively. Nevertheless, radiotherapy has a positive effect. Thus, there were 1250 cases of uterine cancer (7%); as a result of treatment of 1100 cases, the fatality rate was reduced to 500 women/yr (4%). According to the estimates of K. Ennou and K. Jensen, for several years the irradiation dose to personnel, due mainly to hand-operated irradiation of patients, has been considerably greater than 0.5 rem/yr and in some cases exceeded 5 rem/yr. Application of the principle of optimization, however, has led to the conclusion that the use of the technically complex method of gradual introduction, which is distinguished by a sharp reduction in the radiation danger, is economically unjustified.

Of the talks devoted to evaluating the value of 1 man-rem, considerable attention was drawn to work according to which the estimates published previously by the ICRP (100-250 dollars/man-rem) are too low. Thus, in the just-mentioned Danish talk, the value was taken to be 2000 dollars/man-rem. Among the data cited by Beninson, a set of numbers was published which characterize the growth in the value of the coefficient $\alpha$ as a function of the extent of protection of the population of the region next to a reactor with gaseous radioactive material releases. An analysis was made for the B3000 reactor of the ASEA-atom firm assuming 0.1% defective fuel elements in the core for four different methods of cleaning up the refuse: a gas holder in the form of a tank filled with sand of the type used at the Oskarshamn nuclear power station; the same type of gas holder supplemented with an apparatus for recombining radioactive gases of the type used at the Barsebeck nuclear power station; a gas holder with a recombiner with an adsorbent based on activated carbon of the type used at the Forsmarkt nuclear power station; and three stage cleanup with a system for pumping the gases into hermetically sealed vessels. On going from the first to the last version, the coefficient $\alpha$ rises from 79,000 to 1,165,000 dollars/man-rem. A group of investigators from West Germany showed that for collecting long-lived gaseous-phase nuclides at radiochemical plants with a production of 1500 tons/yr at an $\alpha$ of 100-200 dollars/man-rem the cost for clean up of emissions of $^{3}H$ is 1-2.5; $^{14}C$, 1-2; $^{85}Kr$, 25; $^{129}I$, 2.5-4.5; and aerosols, 1.5-2.5 million dollars.

At round-table discussions the members of the ICRP and representatives of the leading nuclear centers discussed the problems of justified risk and the practical significance of the ICRP recommendations. The IAEA plans to publish the proceedings of the symposium in 1979.

## CONFERENCE ON THE DISRUPTIVE INSTABILITY IN CLOSED SYSTEMS

V. G. Merezhkin

About 50 experts from Great Britain, the USSR, the USA, France, and Japan participated in the conference which was organized by the IAEA in February, 1979, in Garching (West Germany).

As is known, the disruptive instability determines the maximum attainable current and plasma density in tokamaks. The problem was the topic of this conference, where the results of theoretical and experimental research from the past few years were discussed. Experiments on stelarators and tokamaks were discussed, the possibility of stabilizing the disruptive instability was analyzed, and the rates of loss of energy and current drop as disruptions develop in planned large machines were evaluated.

Up to the present time four types of disruptive instabilities in tokamaks have been identified and are being studied: internal, during current rise, minor, and major. The internal disruption, which causes sawtooth oscillations in the temperature in the center of the plasma column, was observed in 1974 in the ST tokamaks with a peaked electron temperature and current density profile. The first investigations showed that the

Translated from Atomnaya Énergiya, Vol. 47, No. 1, pp. 68-69, July, 1979.


0038-531X/79/4701-0586$07.50© 1980 Plenum Publishing Corporation

Declassified and Approved For Release 2013/02/15 : CIA-RDP10-02196R000800020001-4

Declassified and Approved For Release 2013/02/15 : CIA-RDP10-02196R000800020001-4

disruption is initiated by the development of a helical mode (m = 1, n = 1). B. B. Kadomtsev proposed a model of the internal instability which explained the rapid drop in the temperature and current density in the plasma region near the axis by recrossing of magnetic field lines near the resonance surface at q = 1. Recent experiments on the PLT (USA) have shown that this model needs refinement since in some cases the field line recrossing effect is manifested weakly or is absent. In the theoretical work of A. Ware presented at the conference, an explanation for the internal disruption was proposed based on an instability in the poloidal rotation of the plasma.

Disruptive instabilities during the current rise have been studied on the TFR (France), PULSATOR (West Germany), and ALCATOR-A (USA) machines. Experiments on ALCATOR-A showed that in the disruptions which occur during the current rise the number of periods of the perturbations in the poloidal field, m, is related to the parameter $q_L$ (calculated for a plasma boundary at the limiter radius) by the roughly constant relation $q_L \sim 1.6$ m. Analyzing these results, the experimenters concluded that the peculiarities in the behavior of the disruptive instability during the current rise are related to the skin effect distribution of the current during this stage of the discharge and can be avoided by increasing the plasma density and reducing the rate of rise of the current in the initial stage.

In the stationary stage of a tokamak discharge a minor disruption, in which one of the harmonics m = 4, m = 3, or m = 2 remains isolated throughout the entire disruption, may occur or a major disruption may occur, developing in two stages. In a typical major disruption a harmonic with m = 2 appears at first and a harmonic with m = 3 or m = 4 occurs in the middle. During the transition between the first and second stages and at the end of a major disruption, harmonics with m = 1 and m = 0 occur. The structure and dynamics of development of the instability in minor disruptions have been studied in many experiments in terms of external perturbations of the magnetic field and perturbations of the x-ray emission from the central region of the plasma column. Experiments have established that in a minor disruption with an isolated m = 2 harmonic the harmonic with m = 1 also appears, rigidly coupled to the m = 2 mode. Coupled perturbations appear in the initial stage of a major disruption as well. As experiments on the T-3, T-4, ORMAK (USA) and DITE (Great Britain) have shown, a major disruption occurs due to a narrowing of the current channel in the plasma because its periphery has been cooled by impurities. This explains the appearance of the m = 2 mode at the beginning of a disruption in the case of a fairly large value of $q_L \sim 4$-5 when a disruption usually occurs with a large amount of impurities in the plasma. Recently it has been demonstrated on several tokamaks that the amount of light impurities can be sharply reduced and that highly stable discharges are observed with a low value of $q_L = 2$-2.5. In experiments on DITE, JIPP, JFT-2, and DIVA (Japan) it was noted that the perturbations in the poloidal field in this stability window are reduced to about $5 \cdot 10^{-4}$.

The report by K. Odayama on the possibility of obtaining stable regimes in a tokamak at low values of $q_L \sim 1.3$-1.7 without a disruptive instability attracted great interest at the conference. Such regimes were obtained in the DIVA machine with a shell placed close to the plasma. Despite the regular instability in regimes with small $q_L$ and significant losses associated with this instability, the energy lifetime of the plasma was $\tau_E \sim 2.1$-5.7 msec, about twice that predicted by the dependence observed on ALCATOR, $\tau_E \sim n\sqrt{q_L}$ (where n is the mean plasma density).

In studies of the instability of the plasma in the W VII-A (West Germany) and Uragan stellarators in Ohmic heating regimes a close correspondence was observed in the behavior of disruptions and helical perturbations of the plasma in stellarators and tokamaks. The perturbation in the W VII-A occurred primarily near the q = 1 and q = 2 rational surfaces. For small values of the rotational transform angle, about 0.5, coupled m/n = 1/1 and m/n = 2/1 modes were observed in this stellarator as well as isolated m/n = 1/1 and m/n = 3/2 perturbations.

H. Furth proposed an "economical" theory of disruptive instabilities which starts from the assumption of "competition" among tearing modes. B. Careras presented the results of a numerical simulation of the tearing instability and noted the possibility of a sharp increase in the amplitude of the m/n = 3/2 mode during the nonlinear stage of development of the m = 2 mode. The presence of magnetic islands near the q = 3 resonant surface in a minor disruption, which agrees with the tearing instability model, was demonstrated in experiments on the TOSCA machine (Great Britain).



Declassified and Approved For Release 2013/02/15 : CIA-RDP10-02196R000800020001-4

Declassified and Approved For Release 2013/02/15 : CIA-RDP10-02196R000800020001-4

## NEW BOOKS

V. L. Blinkin and V. M. Novikov

### LIQUID-SALT NUCLEAR REACTORS*

Reviewed by Yu. I. Koryakin

Current developments in nuclear power, the success of which is well known, often overshadow the essence of the assumptions behind its development. In the meantime there is sufficient justification for formation of opinions or doubts about the correctness of the operating principles in practice in the nuclear power economy. This is the sort of critical evaluation which is made by the authors of the book reviewed here. Despite the fact that the book is mainly based on foreign materials and is thus a review, the authors' position appears rather clearly and definitely. The authors see and prove that liquid salt nuclear reactors, which make possible a compact and promising fuel cycle, can be regarded as reactors of the future and as an alternative to the liquid metal fast breeder reactors presently in existence and under construction.

The authors correctly focus attention on the problem of the external fuel cycle rather than on the problem of producing energy. It can be said directly that the scale and effectiveness of nuclear power generation even in the distant future depends ultimately on the solution of this problem.

The approximately ninety references enabled the authors both to make a scrupulous examination of the main features of liquid salt reactors and their external fuel cycle and to assemble the material in the book in monograph form.

Of course, the authors' bias becomes noticeable upon acquaintance with the book. It appears, as is usual and as a rule, in a veiling of the negative sides of the reactor concepts being described and in an emphasis on the positive sides. But, even understanding this, it is impossible to refuse the authors their due: Their great merit is that they have systematically and in detail illuminated a little-known but possibly very promising approach to the development of nuclear power. Of no less value is the fact that the book leads one to reflection and, thus, stimulates new research.

V. V. Fisenko

### CRITICAL TWO-PHASE FLOWS†

Reviewed by V. N. Smolin

Interest in two-phase flows has been dictated by the practical needs on new branches of industry such as nuclear power, cryogenics, and rocket technology. Over the last decade a huge amount of experimental and theoretical material has been accumulated on the structure and flow regimes of two-phase systems, on heat exchange and hydraulic resistance in two-phase flows, on the thermodynamic and acoustic properties of tow-phase systems, etc. However, most of the material is unrelated and has not been systematized, which makes it difficult to use for practical purposes. Thus, the appearance of a monograph which analyzes and generalizes research on two-phase flows is extremely necessary for engineering and technical workers at research and design institutes as well as at construction offices specializing in power production, particularly nuclear.

In the first chapter the physical features of the critical flow of a two-phase system are described on the basis of the general assumptions of molecular kinetic theory and continuum mechanics. The conditions for

* Atomizdat, Moscow (1978), 112 pp., 1.10 rubles.
† Atomizdat, Moscow (1978), 160 pp., 1.50 rubles.

Translated from Atomnaya Énergiya, Vol. 47, No. 1, pp. 69-70, July, 1979.

 0038-531X/79/4701-0588$07.50 © 1980 Plenum Publishing Corporation

Declassified and Approved For Release 2013/02/15 : CIA-RDP10-02196R000800020001-4

Declassified and Approved For Release 2013/02/15 : CIA-RDP10-02196R000800020001-4

formation of a flow crisis in single-phase compressible flows are examined and the theoretical models for determining the critical flow rate of a two-phase flow are analyzed. Later, the propagation speeds of perturbation waves in a two-phase medium and the adiabatic index of two-phase mixtures are examined together with the validity of using this index for establishing the coupling between various parameters of two-phase media in an isentropic process in the range of gas contents from 0 to 1.

In the second chapter a dependence is proposed for the adiabatic index on the critical flow parameters of two-phase single- and multicomponent mixtures of chemically nonreacting substances. This dependence makes it possible to determine the critical outflow velocity and critical flow rate of a mixture for known parameters of a retarded flow, assuming that the medium is homogeneous at the critical cross section of the channel, as well as to determine the propagation of small perturbations in a homogeneous two-phase medium.

In the third chapter the peculiarities of formation of a critical flow of a two-phase medium in the case of boiling water flowing out through channels with various geometries are discussed. The phenomena accompanying formation of a critical flow in various self evaporating fluids are analyzed. Conclusions are drawn about general effects for materials with different physical properties. An expression is proposed for the isentrope index in a dimensionless form for calculating the critical flow rate and the critical outflow velocity of various materials. The method for calculating critical two-phase flows is based on the assumption that irreversible losses do not occur as the heat transfer fluid moves toward the critical cross section.

The fourth chapter is devoted to solving the problem of safety in nuclear power plants when the circulation loop seal is broken, leading ultimately to ensuring core cooling under conditions of falling pressure and disruption of the coolant circulation regime, as well as to taking the necessary steps to localize the consequences of an accident. The interrelations between a change in pressure in the first loop and the rate it is emptied due to critical outflow of a single-component two-phase mixture are analyzed. It is concluded that the compressibility of the coolant during critical outflow of the two-phase mixture has a controlling effect on the nature of this process. For this case the hydrodynamics of the flow of the medium is determined by the propagation speed of sound, which is close to the thermodynamical equilibrium speed of the flow. Based on an analysis of experimental data, a quantitative estimate is made of the effect of the Mach criterion on the dissipative component of the pressure losses. As an example an algorithm is given for calculating the change in the coolant parameters when the loop is depressurized.

In the fifth chapter flows of highly humid two-phase systems in variable cross section channels are described. Such flows must be studied in order to solve problems associated with the efficient use of the energy in the gaseous component to increase the kinetic energy of the condensed phase in special apparatus and components of modern technology.

In the concluding sixth chapter the appearance of nonstationarity in two-phase critical flows is examined. The theoretical study of this problem is still in a developmental stage. Various methods of solving nonlinear differential equations for the behavior of the medium under nonstationary conditions are used in this case. In particular, the author examines the solution of the nonstationary problem by the method of characteristics taking several peculiarities of two-phase flows into account and by a numerical difference method based on the equations for the directions and conditions for compatibility of the characteristic curves. In the latter case some approximations are determined for the parameters of state at the vertices of a grid.

One may argue with individual conclusions and assumptions, such as those about the reasons for the hydrodynamic instability and the heat transfer crisis in steam generator channels. It is possible, naturally, to propose other methods and computational algorithms; however, there is no doubt that this book will be useful to design engineers and scientific workers in institutes involved in the design of reactors as well as to the engineering and technical staff at nuclear power stations.



Declassified and Approved For Release 2013/02/15 : CIA-RDP10-02196R000800020001-4

Declassified and Approved For Release 2013/02/15 : CIA-RDP10-02196R000800020001-4

# TRITIUM MEASUREMENT TECHNIQUES *

Reviewed by B. P. Maksimenko

Tritium is presently used on a rapidly expanding scale both in various areas of science and technology and in industry. Progress in thermonuclear research in recent years is opening the way to production of thermonuclear power based on the D–T reaction, which will require working with a substantial amount of tritium. In this regard, the appearance of a book which examines, discusses, and systematizes the modern techniques for measuring tritium in various media, including atmospheric air, water, soil, and biological objects, is most topical and useful.

Considerable attention is devoted to selection of representative samples for measuring tritium and to their preparation for quantitative analysis. In the case of liquid and solid samples the problem is complicated by the fact that the beta particles from the tritium are mostly absorbed in the sample material because of their small energy and it is thus difficult to use nondestructive monitoring techniques. It becomes necessary to initially prepare the samples chemically or physically.

In the discussion of measurement techniques the criteria for choosing the most appropriate of them are examined: sensitivity, accuracy, and duration of the measurements, the particular way in which the tritium is released or its specific chemical or physical form, the commercial availability of equipment and apparatus, and the need to process isolated samples or to carry out continuous detection. In the section devoted to the measurement of surface activity, the methods of using gas discharge and scintillation counters and photographic emulsion for this purpose are described, along with a method for taking samples by wiping followed by a measurement of activity. Less used methods which are discussed include mass spectrometry, gas chromatography, avalanche semiconductor detectors, bremsstrahlung detection, electron multipliers, photographic film dosimetry, calorimetry, and thermal stimulation of exoelectron emission. The book also describes the calibration of standard emitters (tritiated water, tritiated toluene, etc.) by microcalorimetry and activity radiometry with the aid of proportional counters with internal filling, as well as the use of standard emitters for calibrating liquid scintillation counters (with the aid of internal or external standard emitters) and gaseous counters. Underground water which has been in low ground levels for a long time compared to the half life of tritium is recommended as a material which is free of tritium for determining the background counting rate of measurement systems. Another possible such substance might be deep sea water which is not in contact with subsurface currents. Two techniques are analyzed from the standpoint of estimating the errors in the corresponding calibration of the measurement system.

Among the definite merits of this book are its great informativeness and the large number of practical recommendations based on a deep understanding of the advantages and disadvantages of the methods discussed there and which can be called upon to help the researcher in choosing the appropriate method for solving a given problem. The good translation and high level of scientific editing of the material should also be noted. There is no doubt that this book will be useful as a systematic handbook for measurements of tritium.

* Atomizdat, Moscow (1978), 96 pp., 0.90 ruble.

Translated from Atomnaya Énergiya, Vol. 47, No. 1, p. 70, July, 1979.



0038-531X/79/4701-0590$07.50 © 1980 Plenum Publishing Corporation

Declassified and Approved For Release 2013/02/15 : CIA-RDP10-02196R000800020001-4

Declassified and Approved For Release 2013/02/15 : CIA-RDP10-02196R000800020001-4

from
CONSULTANTS BUREAU
A NEW JOURNAL

# Soviet Microelectronics

A cover-to-cover translation of *Mikroélektronika*

Editor: **A. V. Rzhanov**
*Academy of Sciences of the USSR, Moscow*

Associate Editors: **K. A. Valiev** and **M. I. Elinson**
Secretary: **P. I. Perov**

Microelectronics is one of the most critical areas of modern technology. Filling the need for a primary research journal in this important area, this bimonthly journal contains articles on new advances in the solution of fundamental problems of microelectronics. Noted scientists discuss new physical principles, materials, and methods for creating components, especially in large systems. Among the topics emphasized are:

- component and functional integration
- techniques for producing thin layer materials
- designs for integrating circuits and systems analysis
- methods for producing and testing devices
- classification and terminology.

*Soviet Microelectronics* provides an on-going up-to-date review of the field for electronics and electrical engineers, solid-state physicists, materials scientists, and computer and information systems engineers.

Subscription: Volume 9, 1980 (6 issues) $160.00

## *Random Titles from this Journal*

Optical Image Recording and Charge Spreading in an MIS (Metal-Insulator-Semiconductor) Structure—V. V. Pospelov, V. N. Ryabokon', K. K. Svidzinskii, and V. A. Kholodnov

Diffraction of Light at an Amplitude—Phase Grating Induced by Light in a Metal-Insulator-Semiconductor-Metal Structure—L. A. Avdeeva, P. I. Perov, V. I. Polyakov, M. I. Elinson, and B. G. Ignatov

Electrical Properties of Gallium-Phosphide Displays—Yu. N. Nikolaev and V. M. Tarasov

Epitaxial Gallium Arsenide Films for Microelectronics—L. N. Aleksandrov, Yu. G. Sidorov, V. M. Zaletin, and E. A. Krivorotov

Effect of Conditions of Formation of Aluminum Oxide Films on the Properties of MOS Structures Based on Them—B. Ya. Aivazov, Yu. P. Medvedev, and B. O. Bertush

Effect of Strong Electric Fields on the Charge Distribution in the Oxide in the System Electrolyte-$SiO_2$-Si—V. A. Tyagai, O. V. Snitko, A. M. Evstigneev, N. A. Petrova, Yu. M. Shirshov, and O. S. Frolov

**SEND FOR FREE EXAMINATION COPY**

**PLENUM PUBLISHING CORPORATION**
227 West 17th Street, New York, N.Y. 10011

In United Kingdom: Black Arrow House
2 Chandos Road, London NW10 6NR England

Declassified and Approved For Release 2013/02/15 : CIA-RDP10-02196R000800020001-4

Declassified and Approved For Release 2013/02/15 : CIA-RDP10-02196R000800020001-4

# NEW RUSSIAN JOURNALS

## IN ENGLISH TRANSLATION

### BIOLOGY BULLETIN
*Izvestiya Akademii Nauk SSSR, Seriya Biologicheskaya*

The biological proceedings of the Academy of Sciences of the USSR, this prestigious new bimonthly presents the work of the leading academicians on every aspect of the life sciences—from micro- and molecular biology to zoology, physiology, and space medicine.
Volume 7, 1980 (6 issues) . . . . . $195.00

### SOVIET JOURNAL OF MARINE BIOLOGY
*Biologiya Morya*

Devoted solely to research on marine organisms and their activity, practical considerations for their preservation, and reproduction of the biological resources of the seas and oceans.
Volume 6, 1980 (6 issues) . . . . . $115.00

### WATER RESOURCES
*Vodnye Resursy*

Evaluates the water resources of specific geographical areas throughout the world and reviews regularities of water resources formation as well as scientific principles of their optimal use.
Volume 7, 1980 (6 issues) . . . . . $215.00

### HUMAN PHYSIOLOGY
*Fiziologiya Cheloveka*

A new, innovative journal concerned *exclusively* with theoretical and applied aspects of the expanding field of human physiology.
Volume 6, 1980 (6 issues) . . . . . $195.00

### SOVIET JOURNAL OF BIOORGANIC CHEMISTRY
*Bioorganicheskaya Khimiya*

Features articles on isolation and purification of naturally occurring, biologically active compounds; the establishment of their structure, methods of synthesis, and determination of the relation between structure and biological function.
Volume 6, 1980 (12 issues) . . . . . $245.00

### SOVIET JOURNAL OF COORDINATION CHEMISTRY
*Koordinatsionnaya Khimiya*

Describes the achievements of modern theoretical and applied coordination chemistry. Topics include the synthesis and properties of new coordination compounds; reactions involving intraspheral substitution and transformation of ligands; complexes with polyfunctional and macromolecular ligands; complexing in solutions; and kinetics and mechanisms of reactions involving the participation of coordination compounds.
Volume 6, 1980 (12 issues) . . . . . $255.00

### THE SOVIET JOURNAL OF GLASS PHYSICS AND CHEMISTRY
*Fizika i Khimiya Stekla*

Devoted to current theoretical and applied research on three interlinked problems in glass technology; the nature of the chemical bonds in a vitrifying melt and in glass; the structure-statistical principle; and the macroscopic properties of glass.
Volume 6, 1980 (6 issues) . . . . . $145.00

### LITHUANIAN MATHEMATICAL JOURNAL
*Litovskii Matematicheskii Sbornik*

An international medium for the rapid publication of the latest developments in mathematics, this quarterly keeps western scientists abreast of both practical and theoretical configurations. Among the many areas reported on in depth are the generalized Green's function, the Monte Carlo method, the "innovation theorem," and the Martingale problem.
Volume 20, 1980 (4 issues) . . . . . $175.00

### PROGRAMMING AND COMPUTER SOFTWARE
*Programmirovanie*

Reports on current progress in programming and the use of computers. Topics covered include logical problems of programming; applied theory of algorithms; control of computational processes; program organization; programming methods connected with the idiosyncracies of input languages, hardware, and problem classes; parallel programming; operating systems; programming systems; programmer aids; software systems; data-control systems; IO systems; and subroutine libraries.
Volume 6, 1980 (6 issues) . . . . . $115.00

### SOVIET MICROELECTRONICS
*Mikroelektronika*

Reports on the latest advances in solutions of fundamental problems of microelectronics. Discusses new physical principles, materials, and methods for creating components, especially in large systems.
Volume 9, 1980 (6 issues) . . . . . $160.00

**Send for Your Free Examination Copy**

**PLENUM PUBLISHING CORPORATION,** 227 West 17th Street, New York, N.Y. 10011
In United Kingdom: Black Arrow House, 2 Chandos Road, London NW10 6NR, England
Prices slightly higher outside the U.S. Prices subject to change without notice.

Declassified and Approved For Release 2013/02/15 : CIA-RDP10-02196R000800020001-4